Raman Spectroscopic Investigations on Monomeric Deltahedral Nanogermanide Clusters and their Condensed Oligomeric and Polymeric Derivatives

by

Aslıhan Kırcalı

A Thesis Submitted to the
Graduate School of Sciences & Engineering
in Partial Fulfillment of the Requirements for
the Degree of

Master of Science
in
Material Science and Engineering

Koç University

July 2007

Koç University

Graduate School of Sciences and Engineering

This is to certify that I have examined this copy of a master's thesis by

Aslıhan Kırcalı

and have found that it is complete and satisfactory in all respects,
and that any and all revisions required by the final
examining committee have been made.

Committee Members:

_____

Mehmet Somer, Ph. D. (Advisor)

_____

Michael Baytinger, Ph. D.

_____

H. Funda Yağcı Acar, Ph. D.

Date: _____

ABSTRACT

The present study consists of two related parts. The first part is focused on Raman spectroscopic characterization of neat, *en* solvated (*en = ethylenediamine*) or sequestered (sequestering agents: *cryptand 2, 2, 2,* and *18-crown-6*) alkali metal germanium compounds including the well-known monomer deltahedral cluster anions $[Ge_9]^{n-}$ (n = 2, 3, 4), as well as the condensed oligomer and polymer derivatives of $[Ge_9]^{4-}$; $[Ge_9\text{-}Ge_9]^{6-}$ [45], $[Ge_9{=}Ge_9{=}Ge_9]^{6-}$ [48] and $_\infty[\text{-}(Ge_9)\text{-}]^{2-}$ [51], respectively. The assignment of the vibrational spectra was confirmed by quantum chemical calculations. The monomer $[Ge_9]^{n-}$(n = 2, 3, 4) moieties exhibit very specific band patterns in their Raman spectra, with one very strong and characteristic "breathing mode" at 221 cm^{-1} (n = 4), 224 cm^{-1} (n = 2) and 219 cm^{-1} (n = 3), which may be used as identification sonde, both in solids and liquids. The spectra of the condensed cluster are characterized by two well-separated frequency groups, located at **268** cm^{-1} (**inter**) / 220 cm^{-1} (intra) (dimer), **240** cm^{-1} / 200 cm^{-1} (trimer) and **269** cm^{-1} / 200 cm^{-1} (polimer), respectively. The key for the distinction between inter and intra cluster vibrations are the intercluster (–Ge_9–Ge_9–) exobonds which are considerably shorter than those within the cluster. Accordingly, the vibrations of the exobonds in all three cluster anions are significantly higher than those of the intracluster modes. Also, the downshift of the $\upsilon(trimer)_{inter}$ with respect to the dimer and polymer species is in best agreement with the reported intercluster bond lengths: 2.488 (dimer), 2.579-2.601(trimer) and 2.486 Å (polimer).

The cluster compounds and moieties investigated in the present thesis are very sensitive to air and moisture, so that they can only be handled under inert conditions. On the other hand, their pronounced reactivity makes them potential precursors for the synthesis of new materials. For this purpose, several oxidative coupling reactions of $[Ge_9]^{4-}$ (precursor K_4Ge_9) have been accomplished utilizing elemental Ge, $E15(Ph)_3$ (E15 = P, As, Sb, Bi; Ph

= phenyl), *DMF*, dodecyltrimetyl ammonium bromide *[DoDe]Br*, air, water, aqueous *HCl* solution and *NH_4Cl* in *liquid ammonia* as oxidizing agents. The reaction products and the step-growth condensation process were followed by Raman spectroscopy, using the measured characteristic frequencies as identification sonde for the different cluster moieties, and powder XRD. Two results are worth mentioning. The Raman spectra have proved that the green coloration in solutions associated with the oligomerization of the Ge_9 cluster originates from the presence of the dimer species $[Ge_9–Ge_9]^{6–}$. This means that trimer, tetramer and polymer cluster anions exist only in the compounds in the solid state. Additionally, both the decomposition of the precursor K_4Ge_9 in air, as well its oxidation (protonation) with deoxygenated water and aqueous solution of *HCl* yields as main product $K_3HGe_7O_{16} \cdot 4H_2O$. Only when the oxidation takes place in absence of air and water - e.g. with *NH_4Cl* in *liquid ammonia* - the product obtained is the well-known clathrate compound K_8Ge_{46} [18]. This is important, since clathrates are known as potential candidates for materials with thermoelectric, HT super conducting and electro optical properties.

The second part of the thesis includes the synthesis, crystal structure, Raman and EPR spectra of the novel cluster compound $[Na(cp)]_3Ge_9$. The crystal structure (mnkl., Space group: *P*21/*n*, a = 22.870(2) Å, b = 14.435(1) Å, c = 24.178(2) Å, β = 107.69(1), Z = 4) contains two topologically very similar $[Ge_9]^{3–}$ moieties with slightly distorted C_{4v} symmetry. The paramagnetic properties of the cluster ions $[Ge_9]^{3–}$ were confirmed by EPR spectroscopy.

ÖZET

Bu çalışma temelde birbiriyle ilişkili iki bölümden oluşur. Birinci bölümde, bilinen ve yeni sentezlenen katkısız, *en* çözünmeli ve katyonu *cryptand 2, 2, 2,* veya *18-crown-6* ile stabilize edilmiş dokuz atomlu germanyum gruplarının tekli; $[Ge_9]^{n-}$ (n = 2, 3, 4), çoklu $[Ge_9\text{-}Ge_9]^{6-}$ [45], $[Ge_9{=}Ge_9{=}Ge_9]^{6-}$ [48] ve polimer $_{\infty}[\text{-}(Ge_9)\text{-}]^{2-}$ formları Raman spektroskopi yöntemiyle karakterize edildi. Titreşim spektrumlarının verileri kuantum kimyası hesaplarıyla doğrulandı. Tekiz gruplarının $[Ge_9]^{n-}$ (n = 2, 3, 4) Raman spektrumlarında çok güçlü ve karakteristik nefes modları 221 cm^{-1} (n = 4), 224 cm^{-1} (n = 2) ve 219 cm^{-1} (n = 3) dalga numaralarında gözlendi. Bu dalga numaraları katı ve solüsyon içindeki diğer grupların incelenmesinde ayıraç olarak kullanılabilir.

Çoklu ve polimer gruplarının Raman spektrumları iki tane karakteristik bant gösterdi. Bunlar ; sırasıyla ikili yapılar için **268** cm^{-1} (**moleküller arası**) / 220 cm^{-1} (molekül içi), üçlü yapılar için **240** cm^{-1} / 200 cm^{-1} ve polimer yapısı için **269** cm^{-1} / 200 cm^{-1} dalga numaralarında gözlenmiştir. Moleküller arası ve molekül içi bağlarının titreşimleri arasındaki fark, dokuz atomlu molekül arası bağ uzunluklarının, molekül içi bağ uzunluklarından daha kısa olmasıyla açıklanabilir. Bu nedenle, moleküller arasındaki bağlarının titreşimleri, molekül içindeki bağlarının titreşimlerinden daha büyük dalga numaralarında tespit edilmiştir. Bunun yanı sıra, ikili ve polimer grupları göz önünde bulundurulduğunda, üçlü yapıların moleküller arası bağ titreşimlerinin dalga numaralarındaki sapma, bu grupların yayınlanan moleküller arası bağ uzunluklarıyla (2.488 (ikili), 2.579-2.601 (üçlü) ve 2.486 Å (polimer)) uyum içerisindedir.

Bu tür grupların bileşikleri hava ve neme karşı duyarlı olduklarından, bütün reaksiyon aşamaları nitrojen atmosferi altında gerçekleştirildi. Diğer taraftan, bu grupların belirgin reaktiflikleri, onların yeni maddelerin sentezinde başlangıç materyali olarak kullanılmasını sağlar. Bu sebepten dolayı, $[Ge_9]^{4-}$ (başlangıç materyali: K_4Ge_9) grubunun çeşitli

oksidasyon reaksiyonları yapılmış ve bu reaksiyonlarda saf germanyum elementi, *E15(Ph)$_3$* (E15 = P, As, Sb, Bi; Ph = fenil), *DMF*, *[DoDe]Br*, hava, su, sulu *HCl* solüsyonu ve sıvı amonyak içinde *NH_4Cl* oksidasyon etmenleri olarak kullanılmıştır. Reaksiyon ürünleri ve reaksiyon sırasındaki ara basamaktaki ürünler, daha önce ölçülen karakteristik titreşim bantlarına göre Raman spektroskopisiyle ve toz XRD ölçümleriyle incelendi. Elde edilen sonuçlar birbiriyle uyum içindedir. Raman spektroskopi incelemeleri solüsyonlardaki yeşil renge Ge_9 gruplarının çoklu yapıları oluşturmasının sebep olduğunu gösterdi. Bunun anlamı üçlü, dörtlü ve polimer yapılarının ancak katı fazdaki bileşiklerde bulunabileceğidir. Bunlara ilaveten, K_4Ge_9 bileşiğinin hava altındaki dekompozisyonu, oksijensiz su ve *HCl*'in sulu çözeltisi ile oksidasyonu $K_3HGe_7O_{16} \cdot 4H_2O$ bileşiğini vermiştir. Sadece, *NH_4Cl* 'in saf sıvı amonyak çözeltisi oksidasyon etmeni olarak kullanıldığında bilinen K_8Ge_{46} [18] kafes bileşiği elde edilmiştir. Bu kafes bileşikleri termoelektrik, elektro optik ve süper iletken maddeler olması açısından çok önemlidir.

Bu çalışmanın ikinci bölümü, yeni bileşik olan $[Na(cp)]_3Ge_9$ sentez yöntemini, kristal yapısını, Raman ve EPR spektrumlarını içerir. Bu bileşiğin kristal yapısı (mnkl., uzay grup: $P2_1/n$ a = 22.870 (2) Å, b = 14.435 (1) Å, c = 24.178 (2) Å, β = 107.96(1)° ve Z = 4) topolojik olarak birbiriyle aynı olan, düzensiz C_{4v} simetrisine sahip iki grup $[Ge_9]^{3-}$ içerir. $[Ge_9]^{3-}$ grubunun paramanyetik özellikleri EPR ölçümleriyle desteklendirilmiştir.

ACKNOWLEDGEMENTS

I sincerely thank my advisor, Prof. Dr. Mehmet Suat Somer for giving me a chance to work in his research group and his help during my study. I was lucky to start my academic career with him and grateful to him for his kindly support and friendly advices.

I would like to thank all instructors of Materials Science and Engineering master program in Koç University and members of my thesis jury. I, in particular, to Dr. Durata Haciu for helping me in editing my thesis and her friendship.

My gratitude goes to Prof. Dr. Thomas Fässler and Dr. Stephan Hoffman from Technical University of Munich for allowing me to use their facilities for the single crystal X-ray diffraction measurements of $[Na(cp)]_3Ge_9$.

I thank Dr. Emre Erdem from Darmstadt Technical University for his friendship and Electron Paramagnetic Resonance measurements.

I also appreciate Olcay Bolükbaşi from Istanbul University for her contribution in quantum chemical calculations.

I would like to thank all members of Inorganic research group in Koc University for their help and their good friendship, especially, Burcu Uslu for her help during the synthesis process and Selçuk Acar for DTA/TG measurements. I am also grateful to our glassblower, Muharrem Güler for blowing all the special glassware equipment.

I thank all people who directly and indirectly supported me during this research, not only with their useful comments but also with their friendship.

Finally, I would like to thank my parents; Pervin Kırcalı, Mehmet Ali Kırcalı, and, my brother Gürkan Kırcalı and my grandparents; Meliha and Mehmet Biçer for their sensibility and their endless love. I couldn't have achieved anything without them.

TABLE OF CONTENTS

LIST OF TABLES

LIST OF FIGURES

NOMENCLATURE

cp	4, 7, 13, 16, 21, 24-hexaoxa-1, 10-diazabicyclo-[8.8.8] hexacosane
18-cr-6	1, 4, 7, 10, 13, 16-hexaoxacyclooctadecane
en	ethylenediamine
DMF	dimethylformamide
[DoDe]Br	didodecyl dimethylammonium bromide($C_{26}H_{56}NBr$)
HCl	*hydrochloric acid*
v	frequency
E	energy
n	order of diffraction
λ	wavelength
d	spacing of layers
hkl	Miller indices
θ	incident angle of photon
φ	phase of wave
R	residual or agreement index
GooF (S)	goodness of fit
n	number of reflection
p	total number of refined parameters
g	gyromagnetic ratio
μ_B	Bohr magneton
B	Field strength of magnetic field

CHAPTER 1
INTRODUCTION

The first manifestation of homoatomic clusters was reported by Joannis in 1891 [1] who observed that lead can be dissolved in *liquid ammonia* in the presence of sodium and obtained green colored solution. In the following years, several investigations have been done by Kraus, Smyth, and Zintl [2,3] to interpret the structure of homoatomic clusters of metals. Especially Zintl is the first user of extraction chemistry on intermetallic phases in *liquid ammonia*. The precursor for these experiments were "alloys" obtained from the reaction of alkali or earth alkaline metals with - i.e. E1, E2 - metallic or semi-metallic post transition elements, such as Tl, Ge, Sn, Pb, Sb and Bi (E13, E14, E15)[4, 5, 6]. Zintl's major achievement was, however, to recognize that these intermetallic phases were salt-like - i.e. built up by isolated cations and anions -, formed by complete electron transfer from the more electropositive alkali or earth alkaline metal to the more electronegative element - i.e. metal or semi-metal of E13, 14 or 15-. Zintl applied this idea to rationalize the connectivity and electronic structure of NaTl and stated: "On 1:1 combination of Na and Tl, each sodium atom will readily give away its one valence electron to a thallium atom. Each Tl^- possesses now four valence electrons and forms polyanions with the diamond-like tetrahedral frame work structure whose cavities are filled by the sodium cations". Klemm and Busmann developed this idea into the so called 'pseudo-element' concept, meaning that bonding behavior and the connectivity of e.g. a single negatively charged ion would be similar to the corresponding "valence isolectronic" neutral element of the next group to its right. The anionic partial structures obey the (8-N) rule of Hume-Rothery [7] and the rule of Grimm and Sommerfeld [8] (N = actual VEC (valence electron count)). The consequent

use of these rules result in the well-known series of valence isoelectronic species, such as $P^{2-} \equiv S^{-} \equiv Cl^{0} \equiv -CH_3$ and $Si^{2-} \equiv P^{-} \equiv S^{0} \equiv -CH_2- \equiv Tl^{2-} \equiv Si^{-} \equiv P^{0} \equiv =CH-$, with the connectivity one (–), two (=) or three (≡), respectively. Hereby, the bonds between the homoatomic constituents of the anionic partial structures are assumed to be covalent, thus localized. The Zintl-Klemm concept, is not only a very powerful tool correlating the structures of the polar intermetallic phases with their stoichiometries but allowing also synthesis plans for designing and tailoring new "Zintl phases" with the well-know properties such as, shiny metallic or gray appearance, electrovalent, semi- or poor conducting, brittleness and diamagnetism.

It is important to note that the prominent cluster moieties - the so called "Zintl ions" named after the discoverer - such as Pb_9^{4-}, Pb_7^{4-} Sn_9^{4-}, Bi_5^{3-}etc. formed by dissolution of the polar intermetallic alkali metal binaries, contain delocalized electrons and therefore do not obey the Zintl-Klemm conception. But their formation occurs according to the electron transfer principles required by the rules of Zintl-Busmann-Klemm.

From the preparative point of view, the isolation of the crystalline compounds containing the classical Zintl anions in *liquid ammonia* created always serious problems, because the solid residue obtained after the solvent evaporation was usually an amorphous ammoniate or the starting intermetallic phase. In this sense, the introduction of the new solvent *ethylenediamine* (*en*) by Kummer and Diehl was an important step towards isolation of stable solvates and their structural characterization by single crystal X-ray diffraction method.

Indeed, Na_4Sn_9 $[en]_7$ is the first solvate of a Zintl phase whose crystal structure was proved to comprehend homoatomic nine-atom polyhedron of Sn_9^{4-} and *en* solvated Na cations [9]. However, the first systematic advancement for the isolation and stabilization of the homoatomic anions has been done by Corbett in 1977 using *cryptand 2, 2, 2* [Fig. 1] as a sequestering agent [10].

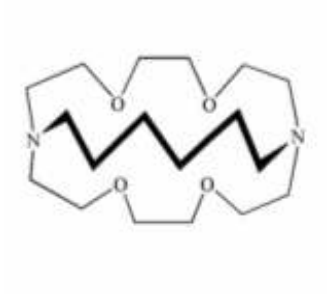

Figure 1*:* *Cryptand 2, 2, 2* = 4, 7, 13, 16, 21, 24-hexaoxa-1, 10-diazabicyclo-[8.8.8]hexacosane.

The ligand *cp* does not only enhance the solubility of alkali metals but also prohibits the cation-anion electron delocalization in the alloy phase. Especially, *cp 2, 2, 2* with its cavity radius of 1.35-1.40Å, is not only a perfectly appropriate cage for K^+ ions ($r(K^+)$ = 1.33-1.44 Å), but also suitable for Na^+ ($r(Na^+)$ = 0.95-1.12Å) and Rb^+ ($r(Rb^+)$ = 1.40-1.50Å). Another widely used sequestering agent is *18-crown-6* ether [Fig. 2]. Its cavity radius, 1.34-1.43 Å, is suitable for both K^+ and Rb^+, and to some extend for Cs^+ as well. The latter is known to form also stable complexes with *18-crown-6* ether in ratio 2:1, in which Cs^+ is sandwiched between two microcyclic molecules [11]. An important detail is that crown ether doesn't act as a cage and can

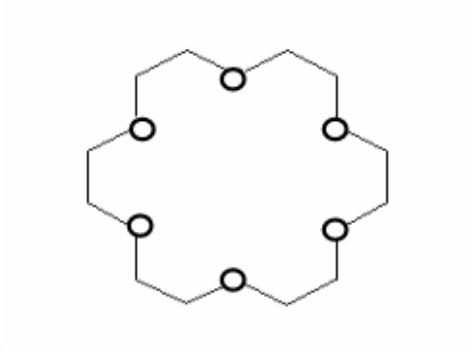

Figure 2: *18-crown-6* = 1, 4, 7, 10, 13, 16-hexaoxacyclooctadecane.

coordinate cations only from one side. Another remarkable difference between crown ethers and cryptands is that the cation confined in cryptand can't interact with the ionic part of the structure, while in the case of crown ethers, the cation can undergo additional interactions with anions or solvent molecules.

Up to now, many polyatomic anions with or without sequestering agents have been characterized by using single X-ray diffraction method. In general, group 14 atoms have some distinctive properties related to their simplicity and the high reactivity from Si to Pb due to non-metallic character at the top of the group to metallic at the bottom. Carbon is a non-metal, silicon and germanium are metalloids, and tin and lead are metals. The physical properties of group 14 alter one element to another according to their metallic character. Melting point, boiling point, heat of atomization, and first ionization energy decrease due to the change in bonding from covalent to metallic down the group. At the same time, density and conductivity increase the increasing metallic character.

Combined with alkali metals, elements in group 14 form well- known binaries with the compositions M_4E_4, $M_{12}E_{17}$, M_4E_9, $M_8E_{44/46}$ and Na_xSi_{136} (M = Na, K, Rb, Cs ; E = Si, Ge, Sn, Pb) [12-19]. Dominant units in M_4E_4 phases are slightly distorted M_4E_4 heterocubanes *(stallae quadrangulae)* formed by tetrahedral $[E_4]^{4-}$ anions and completed by 4 μ^3 bridging M^+ cations [20]. $M_{8-x}E_{46}$ [21] and $Na_{24-x}Si_{136}$ [22] belong to the class of compounds called clathrates. The cubic clathrate I phases ($M_{8-x}E_{46}$) are built up by 3D network of tetrahedrally coordinated E14 atoms forming two types of polyhedra: 20-atom pentagonal dodecahedron and 24-atom tetrakaidecahedron. The alkali metal atoms are encapsulated in the cages if their radii are compatible with the size of the cage cavity. The crystal structure of type-II clathrates ($Na_{24-x}Si_{136}$) is similar, comprehending pentagonal dodecahedral Si_{20} and hexakaidecahedral Si_{28} cages, centered by Na atoms. While the M_4E_4 and the clathrate phases are known for more than 50 years, the 4:9 and 12:17 binaries were not discovered and structurally and vibrational spectroscopically characterized before 1997. According to

the results of X-ray single crystal diffraction measurements M_4E_9 and $M_{12}E_{17}$ (M= Na, K, Rb, Cs; Ge, Sn) phases are built up by isolated nine-atom *nido* cluster anions $[E_9]^{4-}$ and the cluster moieties $[E_4]^{4-}$ and $[E_9]^{4-}$ in ratio 2:1, respectively. Even 10 years ago, the identification of $[E_9]^{4-}$ species in neat solids was quite surprising, since it was believed that $[E_9]^{n-}$ cluster anions were formed ONLY after the reaction of the binary precursors ME_x (M = E1; E = Ge, Sn; x = 1.4- 3) in appropriate solvents. Both M_4E_9 and $M_{12}E_{17}$ can be obtained from the high temperature reactions of stoichiometric mixtures. The phases are soluble or partially soluble ($M_{12}E_{17}$) in *liquid ammonia* and *ethylenediamine*. The formation of $[E_9]^{4-}$ cluster in M_4Ge_9 binaries can be rationalized by the Zintl-Klemm-Busmann rules, according to which electropositive alkali metals transfer the electrons to the group 14 elements [23, 24]. The ionic charge 4– indicates that four of the nine E atoms in (E_9) are receiving a single negative charge each and becoming formal E^-, while the remaining five E atoms maintain their neutrality (E^0). From 8-N rule one obtains for the E^- and E^0 atoms the connectivity 4 and 3, respectively, meaning that each of the nine E atoms in $[E_9]^{4-}$ should be connected by three or four localized bonds to their next neighbors. As can be seen in figure 3, the bonding situation in $[E_9]^{4-}$ is quite different than predicted by Zintl-Klemm theory. Herein, the Ge atoms are connected via 4 and 5 bonds each, respectively, which means that the bonding behavior of the (E_9) cluster does simply not fit into the Zintl concept. The quantum chemical calculations have confirmed that these types of species are electron deficient and stabilized by a delocalized electronic system.

a **b**

Figure 3: Structures of $[Ge_4]^{4-}$ tetrahedron (a) and mono-capped square-antiprismatic $[Ge_9]^{4-}$ with C_{4v} symmetry (b)

The bonding situation in deltahedral clusters was first rationalized by an empirical set of rules developed by Wade [25]. This approach - also called *Wade's rules* - is also known as *Polyhedral Skeletal Electron Theory (PSEPT)* [26]. The *Wade's rules* are basically used to declare a structure for a given chemical formula or to rationalize the number of cluster-bonding electrons in an experimentally determined cluster structure and can be summarized as follows [27]:

- A *closo*-deltahedral cluster cage with n vertices requires (n + 1) pairs of electrons to occupy (n + 1) cluster bonding MOs.
- If a *closo*-deltahedral cluster cage has n vertices, its related *nido*-cluster has (n-1) vertices and (n + 1) pairs of electrons.
- If a *closo*-deltahedral cluster cage has n vertices, its related *arachno*-cluster has (n - 2) vertices and (n + 1) pairs of electrons.
- If a *closo*-deltahedral cluster cage has n vertices, its related *hypho*-cluster has (n - 3) vertices and (n + 1) pairs of electrons.

According to Wade the starting point for the classification is related to *closo*-deltahedral cages depicted in [Fig. 4]. Removal of one vertex with respect to the parent skeleton composes *nido*-cluster while removing of two and three vertices will generate *arachno* and *hypho*-clusters.

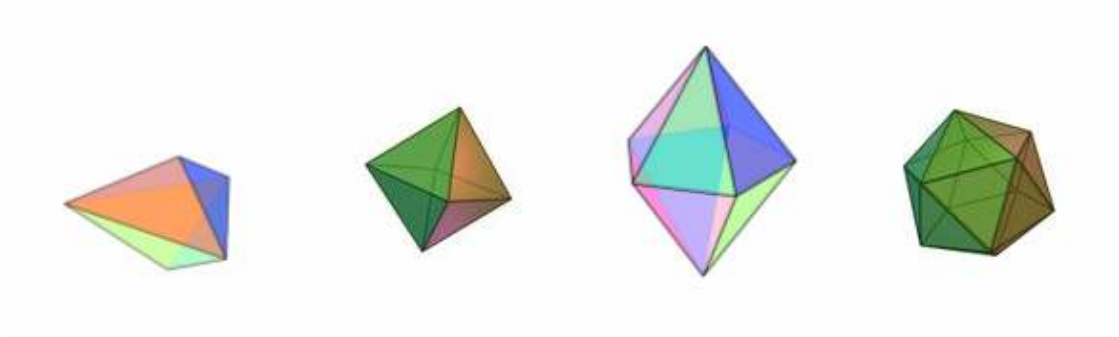

n= 5 (Trigonal bipyramid) | n=6 (Octahedron) | n=7 (Pentagonal bipyramid) | n=8 (Dodecahedron)

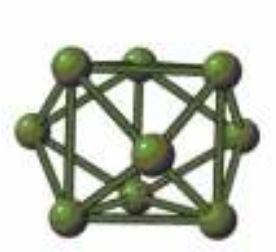

n=9
(Tricapped trigonal prism)

Figure 4: Scheme of the deltahedral cages with 5 to 12 vertices.

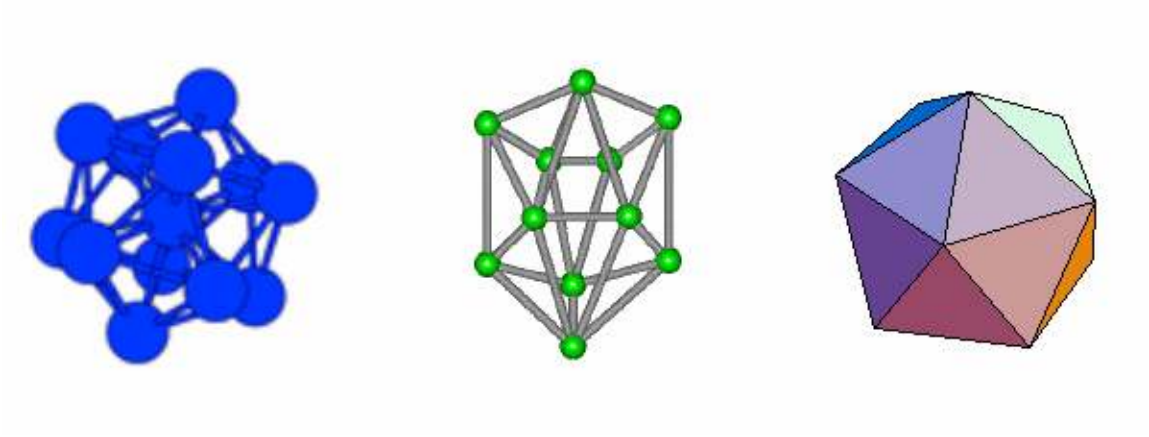

n=10	n=11	n=12
(Bicapped square-antiprism)	(Octadecahedron)	(Icosahedron)

Figure 4: Continued of scheme of deltahedral cages with 5 to 12 vertices.

The well-know boron hydrides species such as $[B_6H_6]^{2-}$ (hexahydrohexaborate), B_4H_{10} (*arachno*-tetraborane), neutral molecules P_4, As_4, Sb_4 and the tetrahedranides $[E_4]^{4-}$ (E= Si, Ge, Sn, Pb) [14, 15, 28-34], cationic $[Bi_5]^{3+}$ [35] and the isoelectronic moieties $[E_5]^{2-}$ (E= Si, Ge, Sn, Pb) [36-38], $[E_9]^{4-}$ (E= Si, Ge, Sn, Pb) [12-16], $[Ge_9]^{2-}$[39], paramagnetic $[Ge_9]^{3-}$[40, 41] and the mixed moiety $[Sn_9Tl]^{3-}$ [42] are the most prominent examples of "*Wade*-cluster".

According to *Wade's rules*, each group 14 atom provides two of its four valence electrons for cluster-bonding (skeleton electrons) while the remaining two are forming a localized lone pair. A $[Ge_9]^{4-}$ anion has 40 valence electrons, distributed as (9 x 2) + 4 = 22 skeletal electrons (i.e. 11 pairs) and 9 lone pairs. For n + 1 = 11, n will be 10, meaning that the structure of $[Ge_9]^{4-}$ is based on a deltahedron with 10 vertices, from which one vertex is to

be removed. As a result, the structure of a $[Ge_9]^{4-}$ cluster is *nido*-cage, a monocapped square antiprism with the point group symmetry C_{4v} [Fig. 5].

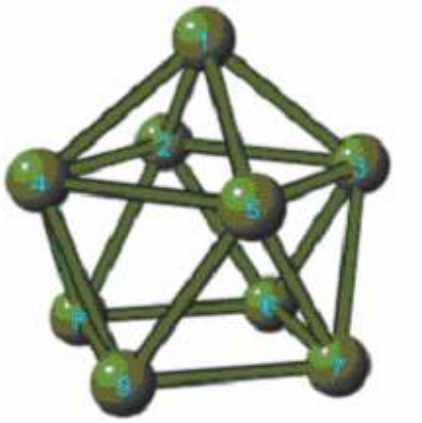

Figure 5: Scheme of nido-cage, a monocapped square antirprism, $[Ge_9]^{4-}$.

Other topologically related deltahedral cluster anions are $[Ge_9]^{2-}$ and $[Ge_9]^{3-}$ [Fig. 6], firstly reported in the compound $[K(cp)]_6Ge_{18}\cdot 2.5H_2O \equiv [K(cp)]_6\ [Ge_9^{2-}]\ [Ge_9^{4-}]$ by Corbett and et. al in 1977 [39].

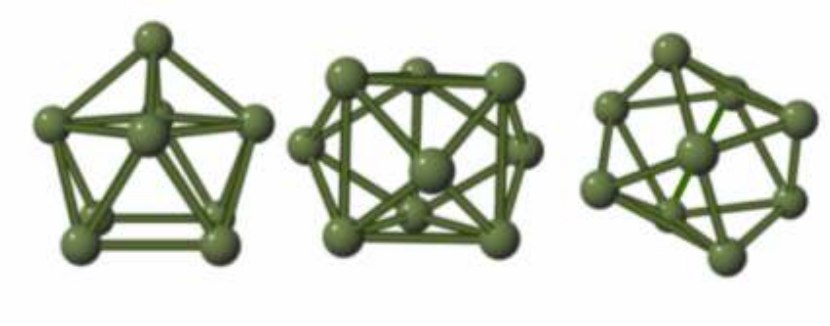

$[Ge_9]^{4-}$ $[Ge_9]^{2-}$ $[Ge_9]^{3-}$

Figure 6: Scheme of $[Ge_9]^{4-}$, $[Ge_9]^{2-}$, $[Ge_9]^{3-}$ clusters drawn using Jmol-9.

[$Ge_9]^{3-}$ moieties were found in [K(*cp*)$_3$] [Ge_9] P(C_6H_5)$_3$ [40] and [K(*cp*)]$_3Ge_9$ [41], but never as pure cluster phase and always in coexistence with $[Ge_9]^{4-}$and $[Ge_9]^{2-}$. The structures of $[Ge_9]^{2-}$and $[Ge_9]^{3-}$ can easily be rationalized using the *Wade's rules.* A $[Ge_9]^{2-}$ unit has 20 skeletal electrons ((2x9) + 2) - i.e. 10 electron pairs and 9 vertices - and its structure is tricapped trigonal prism with the symmetry D_{3h}. In the case of paramagnetic $[Ge_9]^{3-}$ the number of the skeletal electrons is odd equaling to 21 ((2x9) + 3), which means that the structure should be a variant between those of $[Ge_9]^{2-}$and $[Ge_9]^{4-}$. From this point of view, the geometry of $[Ge_9]^{3-}$ can be described as disordered tricapped trigonal prism of C_{2v} symmetry.

During the last six years different novel condensed polygermanides were synthesized and structurally characterized, containing deltahedral Ge_9 clusters as building blocks. Their formation can be rationalized as a radical-polymerization of the $[Ge_9]^{3-}$ moieties under emergence of 2c-2e covalent intercluster bonds. Recent oxidative coupling reactions of $[Ge_9]^{4-}$ brought new perspectives in the mechanism of the controlled growing of the Ge_9 species. The compound, Cs_4(K-*cp*)$_2$[(Ge_9)-(Ge_9)]·6*en* [44] was the first example comprehending the dimer units; $[Ge_9–Ge_9]^{6-}$. In the meanwhile several crystalline compounds have been synthesized and structurally characterized which include the dimer $[Ge_{18}]^{6-}$ groups, such as [M_6(Ge_9–Ge_9)] (*DMF*)$_{12}$ (M = K, Rb) [45] and [Cs_6(Ge_9–Ge_9)] ·4*NH*$_3$ [46]. The formation of the dimer units, $[(Ge_9)-(Ge_9)]^{6-}$ [Fig. 7], can be rationalized as coupling of two monomers $[Ge_9]^{4-}$ via an intercluster bond between two basis vertices of the Ge_9 units. Hereby, the monomers are oxidized, which means that the formation of dimers can take place only in the presence of suitable oxidizing agents, such as *P(Ph)*$_3$, *Cs[BrI*$_2$*]* etc.

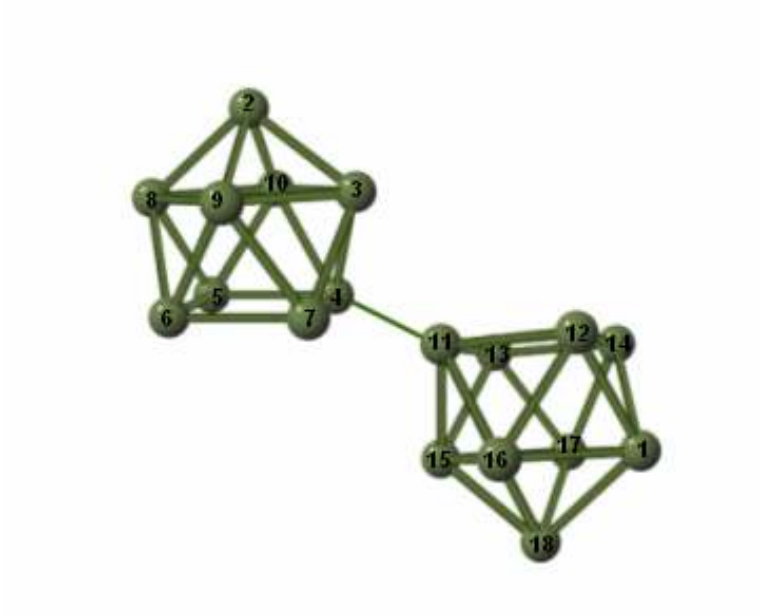

Figure 7: Scheme of a dimeric unit of deltahedral germanium cluster drawn by Jmol-9.

In a similar manner, trimer and tetramer; $[Ge_9{=}Ge_9{=}Ge_9]^{6-}$ and $[Ge_9{=}Ge_9{=}Ge_9{=}Ge_9]^{8-}$ [Fig. 8] were prepared as solvates – $[Rb(cp)]_6[Ge_9{=}Ge_9{=}Ge_9]\cdot 3$ *en* [47], $[K(18\text{-}cr\text{-}6)]_6[Ge_9{=}Ge_9{=}Ge_9]\cdot 3$ *en* [48]; $[Rb(18\text{-}cr\text{-}6)]_8$ $[Ge_9{=}Ge_9{=}Ge_9{=}Ge_9]\cdot 2$ *en* [49], $[K(18\text{-}cr\text{-}6)]_8$ $[Ge_9{=}Ge_9{=}Ge_9{=}Ge_9]\cdot 8$ *en* [50] and their crystal structures were determined using single crystal X-ray diffraction method. In these oligomers, the (Ge_9) polyhedra are connected via two intercluster bonds each, to generate the linear trimeric and tetrameric units. The charge of the trimer moiety is 6, the middle Ge_9 cluster employs four interclusture bonds and the other two Ge_9 have 2 intercluster bonds. The topology and the intercluster connectivities for the tetramers are similar. A common bonding aspect in all three condensed oligomeric clusters is that the intercluster bond lengths are considerably shorter than those measured for the intracluster bonds. Due to the presence of two and four-fold intercluster

connectivities, however, the related bond distances in the trimeric and tetrameric moieties are slightly but significantly longer than in dimers.

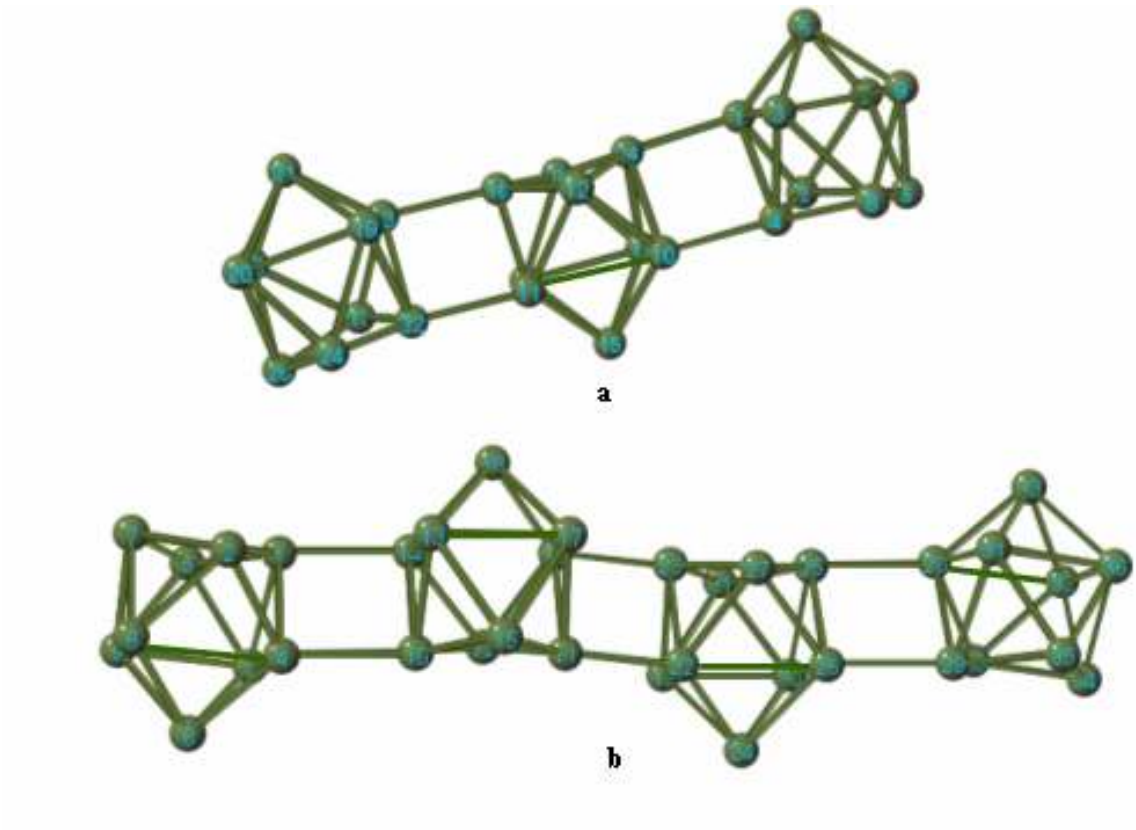

Figure 8: Structures of trimer (a) and tetramer (b) polygermanide anions.

For further structural and bonding details are depicted in Table 1.

Species	Compounds	Intercluster Bond Length	Intracluster Bond Length
Dimer $[(Ge_9–Ge_9)]^{6-}$	$Cs_4(K\text{-}cp)[(Ge_9–Ge_9)]\cdot 6en$ [44]	2.488Å	2.525 – 2.778 Å
	$M_6[(Ge_9–Ge_9)]\ (DMF)_{12}$ (M=K, Rb) [45]	2.420 / 2.471Å (K) 2.464 / 2467 Å (Rb)	2.488 / 2.887Å (K) 2.508 / 2.885 Å (Rb)
Trimer $[Ge_9=Ge_9=Ge_9]^{6-}$	$[Rb(cp)]_6[Ge_9=Ge_9=Ge_9]\cdot 3en$ [47]	2.579-2.601Å	2.523- 3.085 Å
	$[K(18cr6)]_6[Ge_9=Ge_9=Ge_9]\cdot 3en$[48]	2.581-2.640 Å	2.493-3.011 Å
Tetramer $[Ge_9=Ge_9=Ge_9=Ge_9]^{8-}$	$[Rb(18cr6)]_8[Ge_9=Ge_9=Ge_9=Ge_9]\cdot 2en$ [49] (x=2, 6)	2.546-2.673 Å	2.517-2.747Å
	$[K(18cr6)]_8[Ge_9=Ge_9=Ge_9=Ge_9]\cdot 8en$ [50]	2.554- 2.752Å	2.486-3.025Å
Polymer $_\infty[\text{-}(Ge_9)\text{-}]^{2-}$	$[K(18cr6)]_2[\text{-}(Ge_9)\text{-}]$ [51]	2.486 Å	2.552-2864 Å

Table 1: Inter- and intracluster bond length d (Ge-Ge) (Å) of the known oligomer and polymer Ge_9 clusters.

The existence of the polymeric $^1_\infty[(Ge_9)]^{2-}$ in $[K(18\text{-}cr\text{-}6)]_2[\text{-}(Ge_9)\text{-}]\cdot en$ was reported already in 2000 by Guloy et. al. [51], i.e. long before the identification of the trimer and tetramer species succeeded. According to the results of the X-ray diffraction measurements, the Ge_9 polyhedra are interconnected by two opposite basal atoms of neighboring clusters in trans position, to create a zigzag chain of $^1_\infty[(Ge_9)]^{2-}$ with up and down arrangement of the Ge_9 clusters. As for the oligomeric units, the intercluster bonds in the polymer are significantly shorter than the intracluster ones. With $d(Ge\text{-}Ge)_{inter}$ = 2.486 Å, the intercluster bond lengths vary only slightly from those in dimers $d(Ge\text{-}Ge)_{inter}$ = 2.420-2.488 Å and are directly comparable with (Ge-Ge) bond distance in elemental Ge (2.444 Å). These findings suggest that the intracluster bond order is very close to one.

A very recent application of the oxidative coupling reaction is the synthesis of the well-known clathrates $M_{8-x}Si_{46}$ (M = Na, K) [21] and $[]_{24}Ge_{136}$ [22] by oxidation of the precursors M_4Si_4 and Na_4Ge_9 with suitable oxidizing agents, such as *$AlCl_3$*, *DTAC* (Dodecyltrimethylammonium chloride), water vapor and gaseous *HCl*. During the formation of the empty clathrate $[]_{24}Ge_{136}$, the polymerization of $[Ge_9]^{4-}$ supports the formation of 3D network of four-bounded germanium atoms (Ge^0) [22]. In the case of the synthesis of crystalline $M_{8-x}Si_{46}$ (M = Na, K), the binaries M_4Si_4 (M = Na, K) were reacted with gaseous *HCl* at 400 ^{0}C (Na_4Si_4) and 450 ^{0}C (K_4Si_4), formed by thermal dissociation of NH_4Cl and the solid state reaction of $NaHSO_4$ with NaCl [21].

In the present study, the monomer $[Ge_9]^{n-}$ (n = 4, 3, 2)[13, 15, 40, 41, 39], oligomer $[Ge_9\text{-}Ge_9]^{6-}$[45], $[Ge_9{=}Ge_9{=}Ge_9]^{6-}$[47] and polymer $_\infty[\text{-}(Ge_9)\text{-}]^{2-}$ [51] nonagermanide anions in alkali metal their binaries, cryptates, *18-crown-6* salts, an in en solutions were synthesized and characterized by Raman spectroscopy. The assignments of the vibrational spectra were confirmed by quantum chemical calculations.

One of the most outstanding properties of the anionic (Ge_9) species is their extreme sensitivity toward oxidation, making them high reactive precursors in tailoring new materials. For this purpose, several oxidative coupling reactions of $[Ge_9]^{4-}$ (precursor K_4Ge_9) have been carried out using elemental Ge, *$E15(Ph)_3$* (E15 = P, As, Sb, Bi; Ph = phenyl), *DMF*, dodecyltrimetylammonium bromide *[DoDe]Br*, air, water, aqueous *HCl* solution and *NH_4Cl* in *liquid ammonia* as oxidizing agents. The reactions products were followed by Raman spectroscopy, utilizing the characteristic frequencies as identification probe and powder XRD. The results of these investigations are presented in the following chapters.

CHAPTER 2
EXPERIMENTAL SECTION

All manipulations were carried out in a glove- box with moisture and oxygen level below 1ppm. Elemental K (Alfa, 98%), Na (≥99%, pieces**,** Riedel-de Haën) , Rb(Aldrich, 98+%), Ge (Aldrich, 99.999%) and crown ethers (*cryptand 2, 2, 2* = 4, 7, 13, 16, 21, 24-hexaoxa-1, 10-diazabicyclo-[8.8.8] hexacosane (Aldrich, 98%), *18-crown-6* = 1,4,7,10,13,16-hexaoxacyclooctadecane (Fluka, 99.5%)) were used as received and the solvents (*ethylenediamine* (Aldrich, 99%), *toluene* (Aldrich, 99.8%)) used in the experiments were redistilled and handled under inert atmosphere.

2.1 Synthesis of Precursors

The precursors were synthesized from stoichiometric mixtures of the elements (i.e alkali metal pieces and well-grinded Ge powder) in a sealed niobium ampoule that was placed in an evacuated fused silica glass to prevent the oxidation of the niobium metal. The quantities used for a typical batch are given in parenthesis.

K_4Ge_9: was synthesized from stoichiometric mixtures of the elements (K = 0.400g and Ge = 1.671g). The sample was heated up to 750 ^{0}C (2 h), annealed at 750 ^{0}C (5 h) and cooled down to room temperature (2 h).

KGe_4: The ampoule containing the elements K (0.200g) and Ge (1.485g) in ratio 1 : 4 was heated up to 700 ^{0}C and annealed for 5 hours.

KGe_2: The precursor of KGe_2 was prepared in molar ratio 1:2 (0.200g K and 0.742 g Ge). The sample was heated in a sealed niobium ampoule up to 750 ^{0}C (2h), annealed at 750 ^{0}C (5 h) and then cooled down to room temperature (2 h).

$KGe_{1.8}$: The sample containing 0.400 g K and 1.336 g Ge was annealed at 750 ^{0}C for 5 hours and the furnace was turned off.

$KGe_{1.5}$: The appropriate mixture of the elements K (0.200 g) and Ge (0.557 g Ge) was heated up to 750 ^{0}C (4h), annealed at 750 ^{0}C (6h) and cooled down to room temperature (4h).

$K_{12}Ge_{17}$: $K_{12}Ge_{17}$ was obtained via a high temperature reaction of the stoichiometric mixture of the elements (0.300 g K and 0.789 g Ge). The mixture was heated up to 850 ^{0}C (2h), annealed at the same temperature for 6 hours and cooled down to room temperature (2h).

$NaGe_4$: 0.100g Na and 1.320g Ge were placed in a niobium ampoule and heated up to 750^0 C and annealed for 6 hours.

Rb_4Ge_9: Well grinded Rb_4G_4 (1.000 g) - synthesized according to [52] - and 0.574 g Ge powders were mixed and placed in niobium ampoule. The sample was heated up to 740 0C and annealed there for 6 hours.

2.2 Synthesis of Compounds

$[K(cp)]_2Ge_9$:

An H-reaction tube was used for all *ethylenediamine* solvated medium reactions [Fig. 9]. 130 mg of KGe_2 was placed in tube 1 and dissolved in 2ml *en*. After two hours of stirring, a dark red solution formed which was filtered to tube 2 that contained 208 mg of *cryptand 2, 2, 2*. The solution was stirred until all *cryptand* dissolved and layered with 2ml *toluene*. Finally, the H tube was sealed from both caps. 5 days later, red rod-like crystals of the compound, $[K(cp)]_2Ge_9$, were obtained [39].

Figure 9: Scheme of an H tube.

[K (*cp*)]$_2$Ge$_9$*:

$KGe_{1.5}$ (0.061 g) was dissolved in 2 ml *en* and stirred at 50 ^{0}C until all precursor dissolved. Afterwards, the clear dark red solution was filtered on *cryptand 2, 2, 2* (0.110 g) and stirred for another 10 min. The solution was layered with 2 ml *toluene*. After 10 days, red rod-like crystals of the compound formed.

[K-(*cp*)]$_3$ P(C$_6$H$_5$)$_3$Ge$_9$:

0.100 g of $KGe_{1.8}$ was placed in an H tube and dissolved in 2ml *en*. When 0.240 g *cryptand 2, 2, 2* was added on it a dark red solution was observed. The solution was stirred for 30 min. and filtered on 0,154 g of *P(Ph)$_3$*. 2 days later, red hexagonal crystals were obtained [40].

[K (*cp*)]$_3$Ge$_9$·(*NH$_3$*)$_x$:

0.060 g of $K_{12}Ge_{17}$ and 0.150 g of *cryptand 2, 2, 2* were placed on the filter and in the bulb of the soxhlet, respectively, depicted in Fig. 10. Using liquid N_2 as coolant, ammonia was then condensed in the reaction tube. After liquefaction of NH_3 in an ethanol-dry ice bath (-70 ^{0}C) and allowing the soxhlet to warm up slowly to room temperature, the extraction

started. During the extraction, all reactants were dissolved. Two days later, prismatic orange-red crystals of the compound [K (*cp*)]$_3$Ge$_9$ deposited from the red solution. The reaction was then stopped and the ammonia solution was decanted into the empty bulb. The latter was cooled with liq. N_2 until the solution was frozen and the bulb was sealed off.

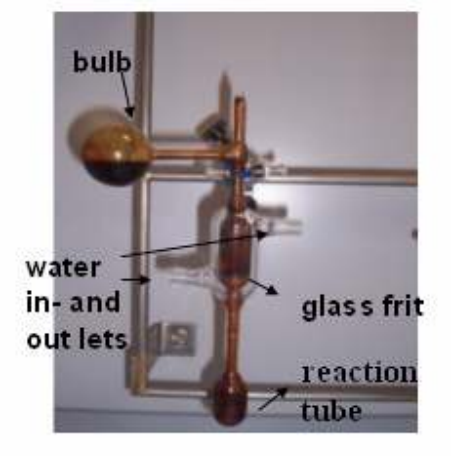

Figure 10: Scheme of a soxhlet.

[M$_6$ (Ge$_9$–Ge$_9$)] (*DMF*)$_{12}$ (M = K, Rb):

0.150 g K_4Ge_9 and 0.150 g Rb_4Ge_9 phases were separately placed in two H-tubes. 2ml *DMF* was added on each and the solutions were stirred until all precursors dissolved and filtered. The filtered solutions were cooled down – 36 ^{0}C. At the end of the reactions, ruby-red crystals of [K$_6$ (Ge$_9$–Ge$_9$)] (*DMF*)$_{12}$ and red crystals of [Rb$_6$ (Ge$_9$–Ge$_9$)] (*DMF*)$_{12}$ were obtained [45].

$Cs_6Ge_{18}(en)_x$:

KGe_4 (0.270 g) was dissolved in 3ml *en* yielding a dark green solution which was filtered on *CsI* (1.000 g). During 2 days of annealing at 100 ^{0} C, bluish-red needlelike crystals deposited at the wall of the reaction tube.

[Rb (*cp*)]$_6$[Ge_9=Ge_9=Ge_9]·3*en*:

0.108 g Rb_4Ge_9 was dissolved in 2 ml *en* and stirred for 10 min. 0.200 g of *cryptand 2, 2, 2* was added to enhance the solubility of Rb_4Ge_9 and brown-red color was observed. The solution was stirred for 30 min. and filtered on 0.600 g of *P(Ph)$_3$*. After the filtration, the solution was heated up to 70 ^{0}C and stood overnight at the same temperature. When the heating process finished, the brown-red color of the solution changed to dark-green. The dark green solution was filtered and layered with 2 ml of *toluene*. 5 days later, needle like dark green crystals were observed [47].

[*DoDe*]$_6$[Ge_9=Ge_9=Ge_9]:

0.200 g of K_4Ge_9 was dissolved in 2 ml *en* and mixed with 1.250 g. didodecyl dimethyl ammonium bromide. The dark green suspension was heated until all *[DoDe] Br* (Aldrich, 98%) dissolved and annealed at 70 ^{o}C overnight.

[M (*18-cr-6*)]$_6$[Ge_9=Ge_9=Ge_9] (M: K, Na):

The reaction was done in *liquid ammonia* solvated medium and soxhlet was used as a reaction vessel. For both reactions 0.150 g of the precursors KGe_4 and $NaGe_4$, respectively, and 0.120 g (for K) and 0.126 g (for Na) of *18- crown-6* were placed in the soxhlet. The system was connected to a vacuum line for condensation of liq. NH_3 (amount: ca. 5 mL; coolant liq. N_2). During the extraction, the precursor was dissolved and the solution poured through the filter onto 18-*crown*-6. After 4 days, the blue needle-like crystals of the compounds deposited on the wall of the reaction tubes.

[K (*18-cr-6*)]$_2$ [-(Ge$_9$)-]:

3 ml dark green *en* solution of 0.104 g KGe_4 was slowly filtered on 2 ml *toluene* solution of 0.052 g *18-crown-6*. After 10 days, blue-green rod-like crystals appeared on the wall of the glass tube [51].

[*DoDe*]$_2$[-(Ge$_9$)-]:

As mentioned above, K_4Ge_9 was reacted with *[DoDe]Br* in *DMF* solution to get the compound; [*DoDe*]$_6$[Ge_9=Ge_9=Ge_9]. Surprisingly, when *DMF* was used as a solvated medium instead of *en* and the reaction was done in the same conditions, the blue- green precipitation of the compound [*DoDe*]$_2$[-(Ge$_9$)$_\infty$-] was obtained. (0.200 g of K_4Ge_9 were dissolved in 2 ml *DMF* and filtered on 1.250 g. didodecyl dimethyl ammonium bromide. The dark green solution was stirred until all *[DoDe] Br* dissolved and stood overnight at 70 ^oC)

$K_3HGe_7O_{16}$·4(H_2O):

(a) Mixture of 1ml H_2O and 1ml *HCl* (conc.) solution was added drop wise to 0.150 g green crystalline powder of the compound [K(*18-cr-6*)]$_2$ [-(Ge$_9$)-] under nitrogen. The dark brown suspension was stored at 4 ^0C for 2 days. Afterwards, the mixture was filtered, the obtained black precipitate washed 2 times with water and dried at 70 ^0C.

(b) 100 mg K_4Ge_9 was exposed to air for 2 days and decomposed in the DTA instrument under purge of dry air (5 °C/min, T_{max} = 600 ^oC).

(c) 2 ml water was added to 100 mg of K_4Ge_9 under nitrogen. The black suspension was stored at 4 °C for 2 days, filtered and dried at 70 $^\circ C$.

K_8Ge_{46}:

1.000 g of K_4Ge_9 was reacted with 0.066 g of *NH_4Cl* in *liquid ammonia* at room temperature. The reactants were placed in a schlenk tube that was connected to the vacuum line equipped with a mercury column manometer and the ammonia gas cylinder. NH_3 was condensed onto the reactants at -196 ^{0}C. After liquefaction of ammonia at -70 ^{0}C, the schlenk tube was connected to the Hg manometer acting as a pressure relief valve for both hydrogen gas - formed during the reaction - and the NH_3 gas evaporated during the very slow warming up of the liquid ammonia phase, overnight. The residue is a black crystalline powder.

All reactions of the present study are summarized in the figures 11, 12, 13 and the characterization techniques in appendix B.

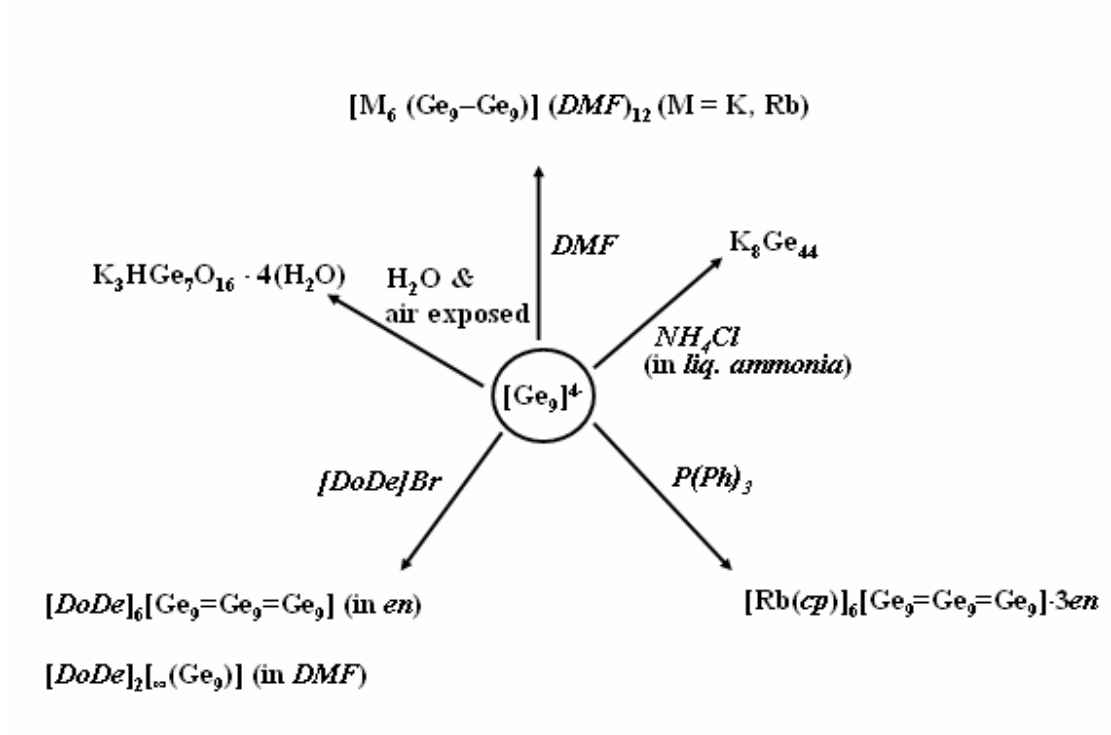

Figure 11: List of the reactions in which M_4Ge_9 was used as precursor.

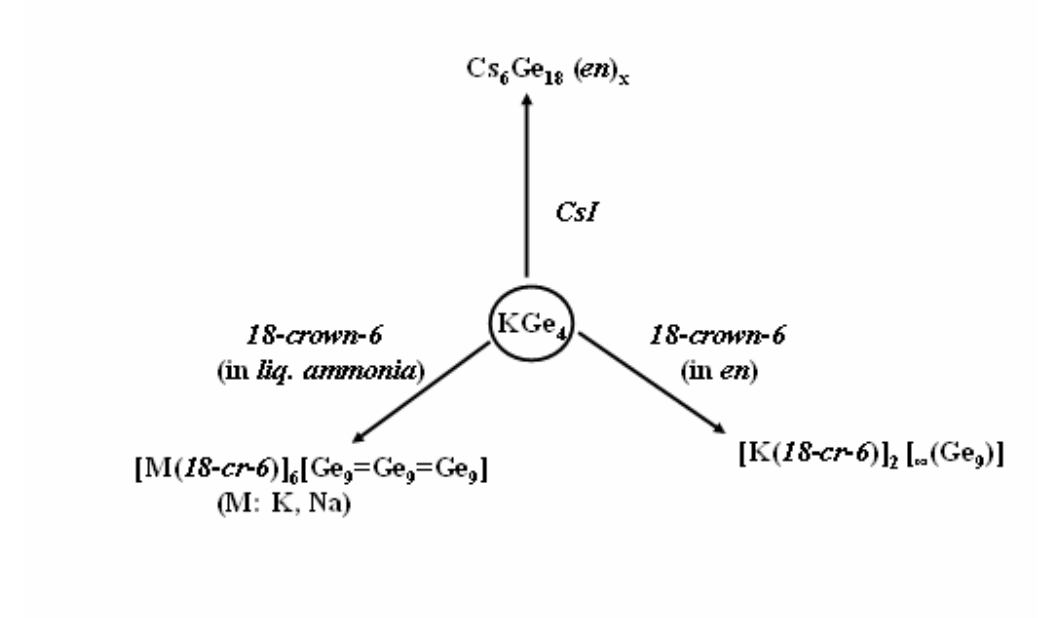

Figure 12: Reactions of the precursor KGe_4.

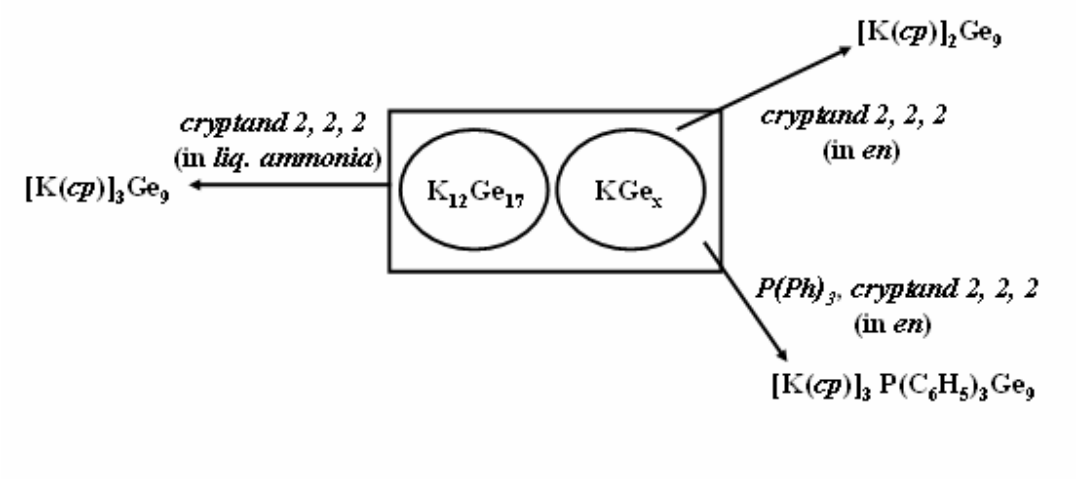

Figure 13: Reactions of KGe_x (x: 2, 1.5, 1.8) and $K_{12}Ge_{17}$.

CHAPTER 3

RESULTS & DISCUSSION

The sample preparation and sample handling for Raman spectroscopic measurements are described in Appendix B (B.1.3).

Raman Spectroscopy Investigations

3.1 Monomeric Ge_9^{n-} (n= 4, 3, 2) clusters:

The Raman spectrum of the precursor K_4Ge_9 shows [Fig. 14] one very strong and two medium intense bands at 221, 164 and 147 cm^{-1}, respectively. The band at 221 cm^{-1} represents the characteristic breathing mode, whose position is practically independent from the nature of the counter ions.

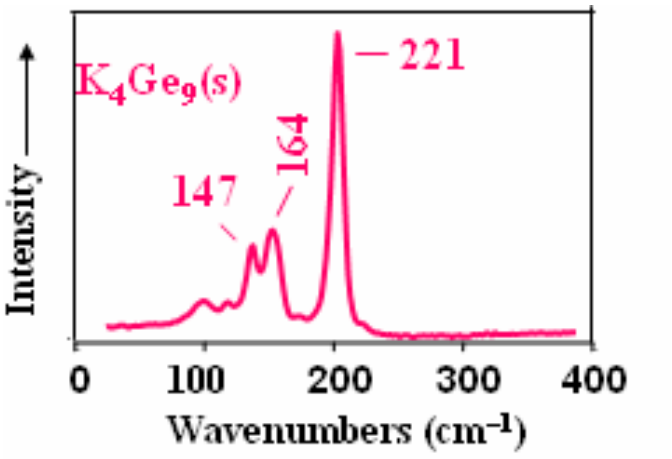

Figure 14: Raman spectrum of K_4Ge_9.

The compound, [K (*cp*)]$_2$Ge$_9$ [39], synthesized from the different precursors of $KGe_{1.5}$ and KGe_2 * is composed of diamagnetic Ge_9^{2-} clusters. The orange to red hexagonal-shaped single crystals were selected under microscope and sealed in a 2 mm capillary (glove box). The Raman spectra of the single crystals from two different samples are shown in figure 15 and 16.

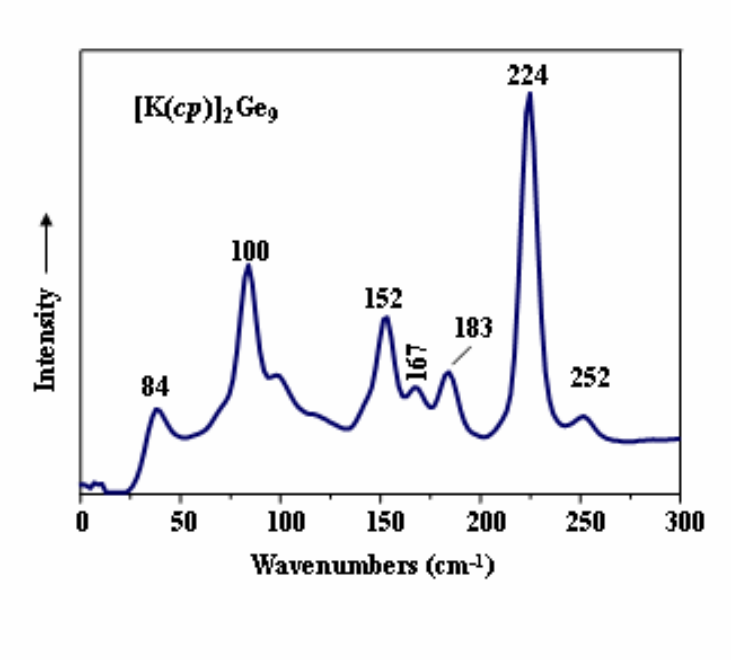

Figure 15: Raman spectrum of [K (*cp*)]$_2$Ge$_9$.

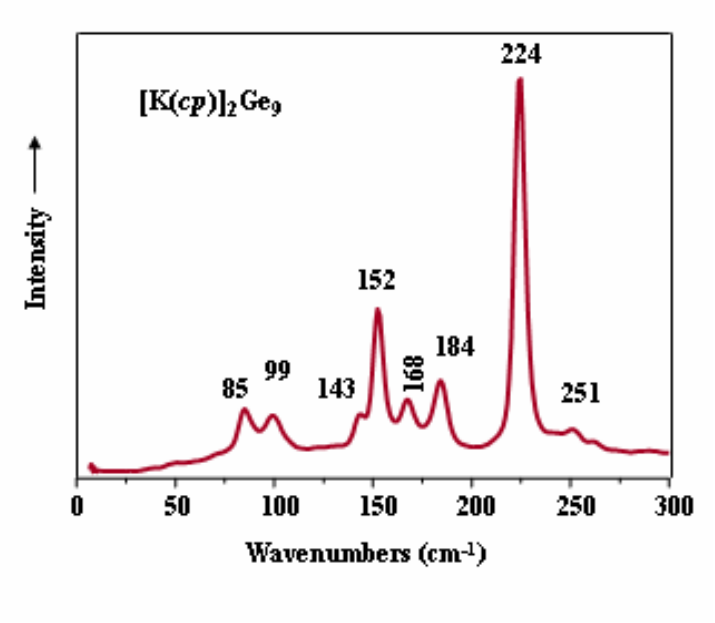

Figure 16: Raman spectrum of [K (*cp*)]$_2$Ge$_9$*.

Similarly, $[K(cp)]_3 P(C_6H_5)_3Ge_9$ was investigated by Raman spectroscopy. The germanium clusters in this compound were reported to be Ge_9^{3-} [40] , however its Raman spectrum (shown in figure 17), exhibits the vibrational patterns of the diamagnetic germanium cluster, Ge_9^{2-}.

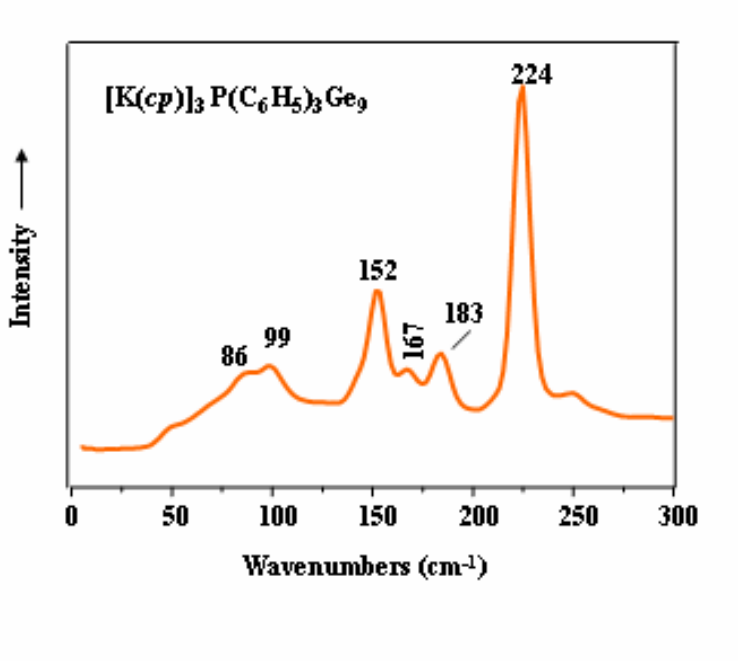

Figure 17: Raman spectrum of $[K\ (cp)]_3 P(C_6H_5)_3Ge_9$.

Prismatic orange-red crystals of the structurally well characterized compound $[K(cp)]_3Ge_9 \cdot en$ were reported to contain the paramagnetic $[Ge_9]^{3-}$ moieties. Its Raman spectrum is shown in figure 18 and was used for further identification.

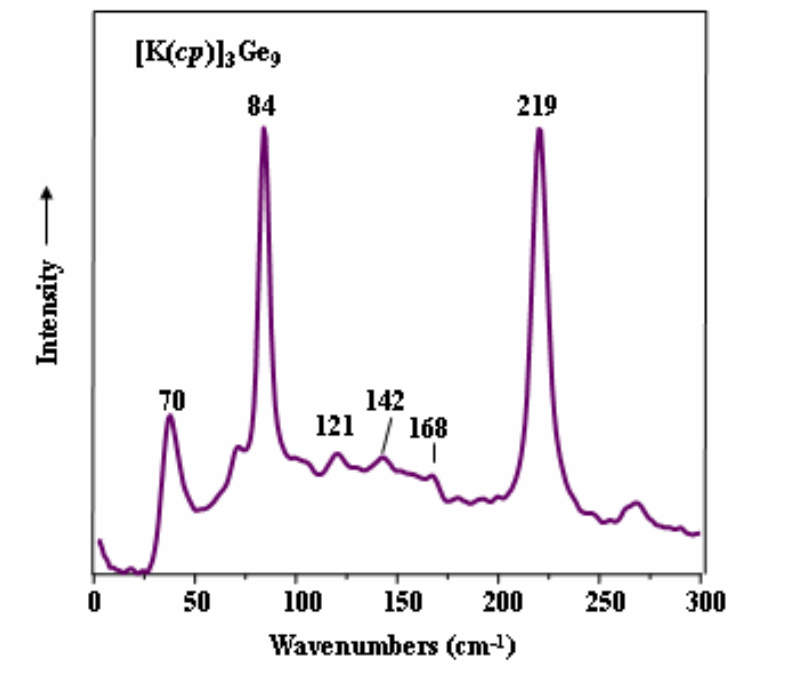

Figure 18: Raman spectrum of [K (*cp*)]$_3$Ge$_9$.

Oligomer species; $[Ge_9\text{-}Ge_9]^{6-}$, $[Ge_9{=}Ge_9{=}Ge_9]^{6-}$ and polymer species; $_\infty[\text{-}(Ge_9)\text{-}]^{2-}$:

The Raman spectra of the dimeric compounds; $[M_6\,(Ge_9–Ge_9)](DMF)_{12}$ (M = K, Rb) [45] exhibit two kind of characteristic bands at 267 cm^{-1} (υ_{inter}) /221 cm^{-1} (υ_{intra}) for $[Rb_6\,(Ge_9–Ge_9)](DMF)_{12}$ and 270 cm^{-1} (υ_{inter})/ 221 cm^{-1} (υ_{intra}) for $[K_6(Ge_9–Ge_9)](DMF)_{12}$, respectively [Fig. 19].

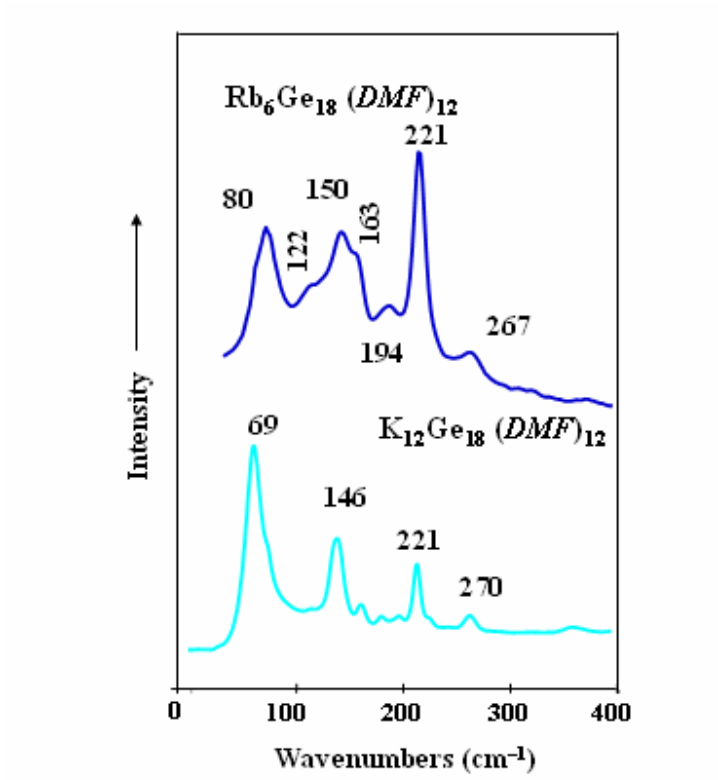

Figure 19: Raman spectra of $[M_6\,(Ge_9–Ge_9)]\,(DMF)_{12}$ (M = K, Rb).

100 mg of KGe_4 were placed in 2 ml *en*. The green solution was stirred until all KGe_4 dissolved and the Raman spectroscopic investigations were performed on solid KGe_4 and its *en* solution [Fig. 20].

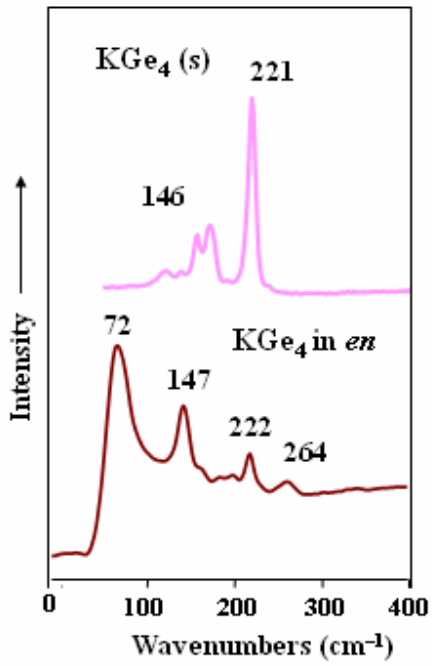

Figure 20: Raman spectrum of the *en* solution of KGe_4.

The characteristic bands of Ge_9^{4-} cluster and elemental germanium were observed in the Raman spectrum of solid KGe_4. In the case of *ethylenediamine* solution two significant bands, at 264 cm^{-1} for inter and 222 cm^{-1} for the symmetric intracluster vibrations of the dimeric species were recorded.

The bands for the dimer species of the black crystals of Cs_6Ge_{18} $(en)_x(s)$ were identified at 260 cm^{-1} and 221 cm^{-1} [Fig. 21].

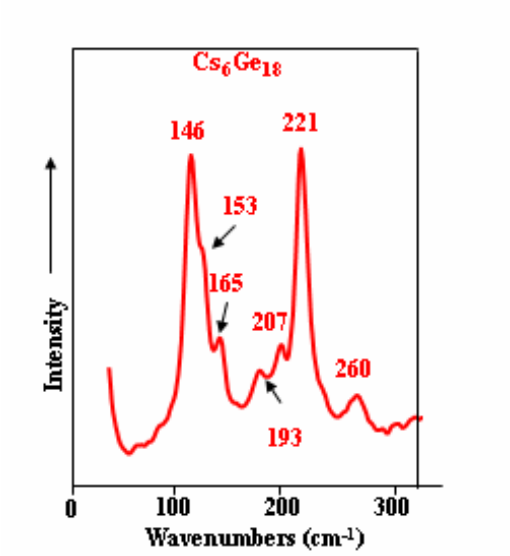

Figure 21: Raman spectrum of Cs_6Ge_{18} $(en)_x$.

The characteristic vibrations of trimer species for [Rb (cp)]$_6$[Ge_9=Ge_9=Ge_9]·3*en* [47] were also spectroscopically determined [Fig. 22].

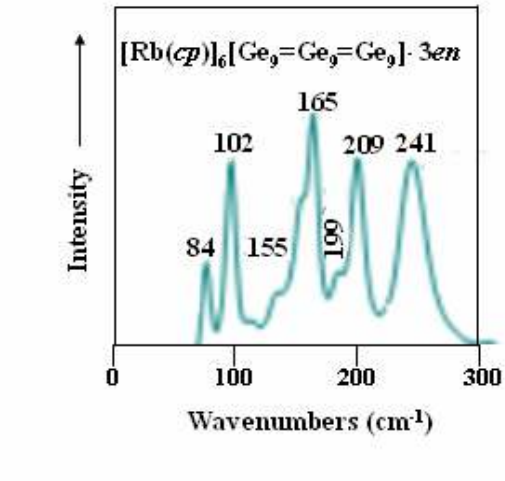

Figure 22: Raman spectrum of [Rb (cp)]$_6$[Ge_9=Ge_9=Ge_9]·3*en*.

The Raman spectrum of the compound [Rb (*cp*)]$_6$[Ge$_9$=Ge$_9$=Ge$_9$]·3*en* [47] presents two characteristic bands at 242 cm^{-1} and 200 cm^{-1}. These vibrational modes were used as identification sonde for Raman spectroscopical investigations of the compounds [*DoDe*]$_6$[Ge$_9$=Ge$_9$=Ge$_9$] and [M (*18-cr-6*)]$_6$[Ge$_9$=Ge$_9$=Ge$_9$] (M: K, Na) [Fig. 23, 24].

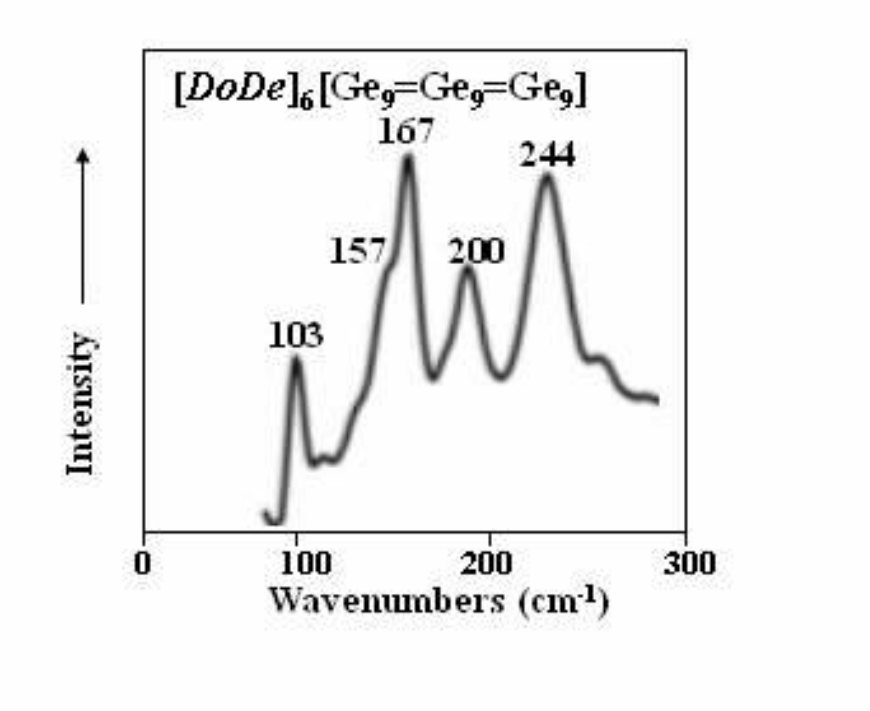

Figure 23: Raman spectrum of [*DoDe*]$_6$[Ge$_9$=Ge$_9$=Ge$_9$].

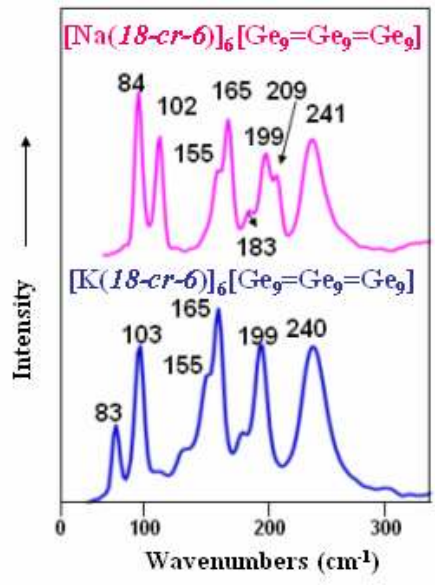

Figure 24: The Raman spectra of [M (*18-cr-6*)]$_6$[Ge$_9$=Ge$_9$=Ge$_9$] (M: K, Na).

The Raman spectroscopy investigation of the polymeric compound; [K (*18-crown-6*)]$_2$ [$_\infty$(Ge$_9$)] [51] is reported below [Fig. 25]

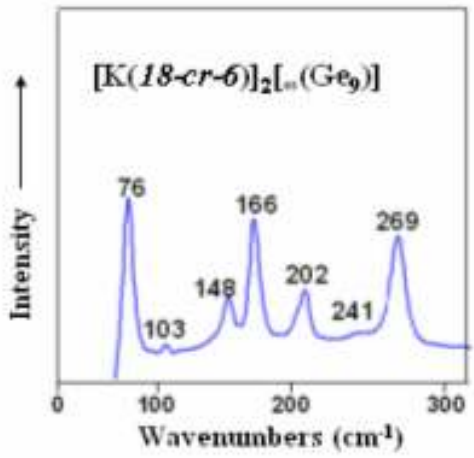

Figure 25: Raman spectrum of [K (*18-crown-6*)]$_2$[$_\infty$(Ge$_9$)].

The characteristic bond vibrations of $_{\infty}[\text{-}(Ge_9)\text{-}]^{2-}$ in $[K(\textit{18-crown-6})]_2[_{\infty}(Ge_9)]$ were measured at 269cm^{-1} (υ_{inter}), and, 202 cm^{-1} (υ_{intra}).

The polymeric unit in $[\textit{DoDe}]_2[_{\infty}(Ge_9)]$ was identified by the inter and intracluster vibrations bans at 277 cm^{-1} and 202 cm^{-1}.

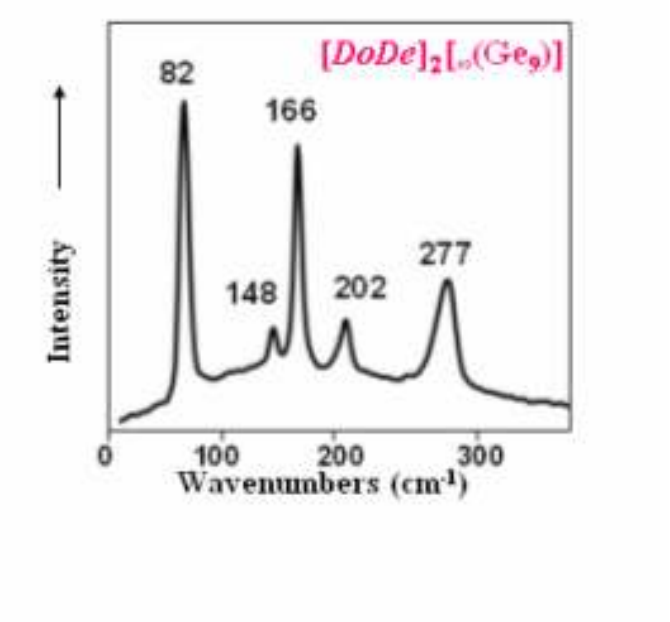

Figure 26: Raman spectrum of $[\textit{DoDe}]_2[_{\infty}(Ge_9)]$.

3.2 Quantum Chemical Calculations *

The wavenumbers, vibrational modes, symmetry types of $[Ge_9]^{4-}$, $[Ge_9]^{3-}$, $[Ge_9]^{2-}$, $[Ge_9\text{-}Ge_9]^{6-}$ and $[Ge_9{=}Ge_9{=}Ge_9]^{6-}$ clusters exhibiting C_{4v}, C_1, D_{3h} , C_{2h}, and, C_{2v} symmetry groups, were calculated using the DFT/ RB3LYP method with a 3-21 G basis set.

Ge_9^{n-} (n=4, 3, 2) Clusters:

The distinctive sharp band of the Ge_9^{4-} cluster experimentally determined at 221 cm^{-1} was calculated at 220 cm^{-1} as breathing modes of the intracluster bonds vibrations [Fig. 27, 28].

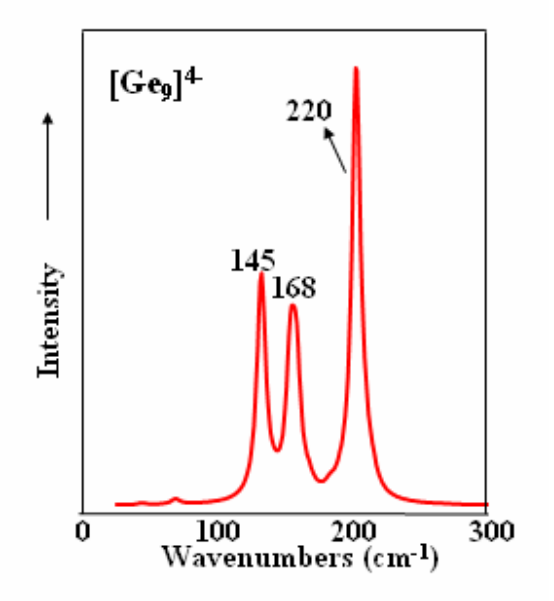

Figure 27: Theoretical Raman spectrum of Ge_9^{4-} cluster.

*All quantum chemical calculations were performed by Olcay Bölükbaşi.(Bölükbaşi; O., PhD thesis, in progress)

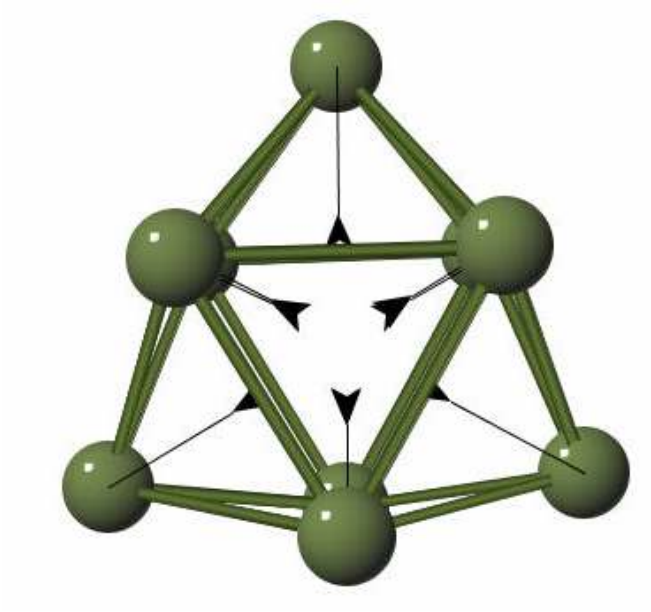

Figure 28: Schematic breathing mode of Ge_9^{4-} cluster.

The characteristic vibrations of the paramagnetic germanium cluster were experimentally observed as one strong band at 219 cm^{-1} and three broad bands at 168 cm^{-1}, 142 cm^{-1} and 121 cm^{-1}. These bands were calculated at 225 cm^{-1}, and, 172 cm^{-1}, 152 cm^{-1}, 132 cm^{-1}, respectively.

Raman spectrum of the diamagnetic $[Ge_9]^{2-}$ cluster exhibits one strong band at 224 cm^{-1} and three sharp bands at 183 cm^{-1}, 168 cm^{-1} and 152 cm^{-1}, respectively. Additionally, one broad band was observed at 252 cm^{-1}. These bands were calculated at 216 cm^{-1} and 188 cm^{-1}, 170 cm^{-1}, 154 cm^{-1}. Additional weak band recorded at 252 cm^{-1} was calculated at 232 cm^{-1}.

Dimer Species:

The characteristic vibration modes obtained from the quantum chemical calculations are shown in the theoretical Raman spectrum of the species [Fig. 29]

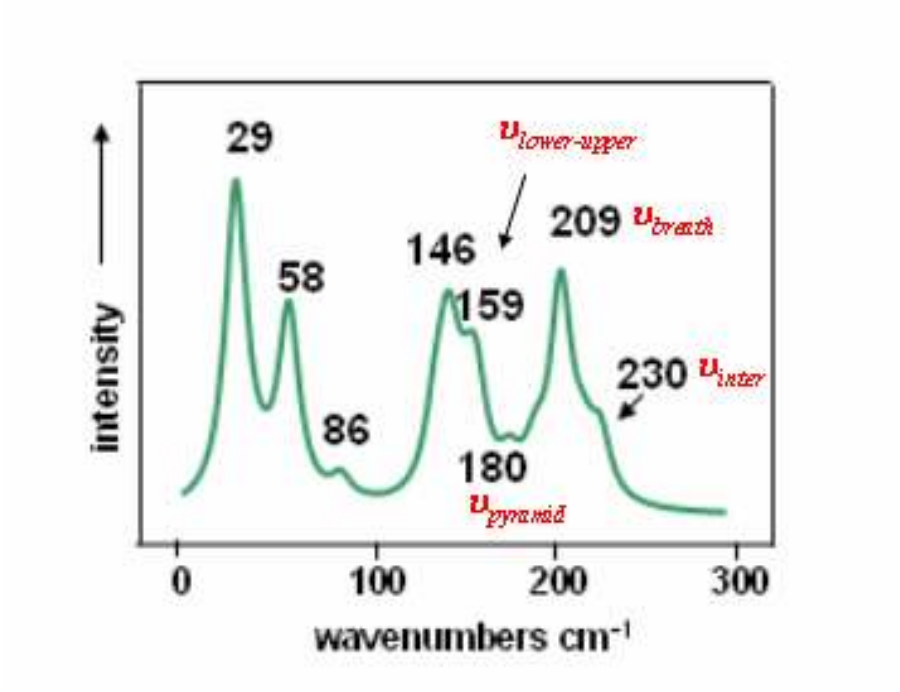

Figure 29: Theoretical Raman spectrum of dimer species. ($\nu_{Lower\text{-}upper}$= bond stretching between upper and lower tetragonal, $\nu_{pyramid}$= upper pyramid bond stretching, ν_{breath}= breathing motion, ν_{inter}=intercluster bond stretching)

The intercluster bond vibrations of the species were calculated at 230 cm^{-1} [Fig. 30] and similarly, the symmetric intracluster bond vibrations were determined at 209 cm^{-1} as breathing modes [Fig. 31].

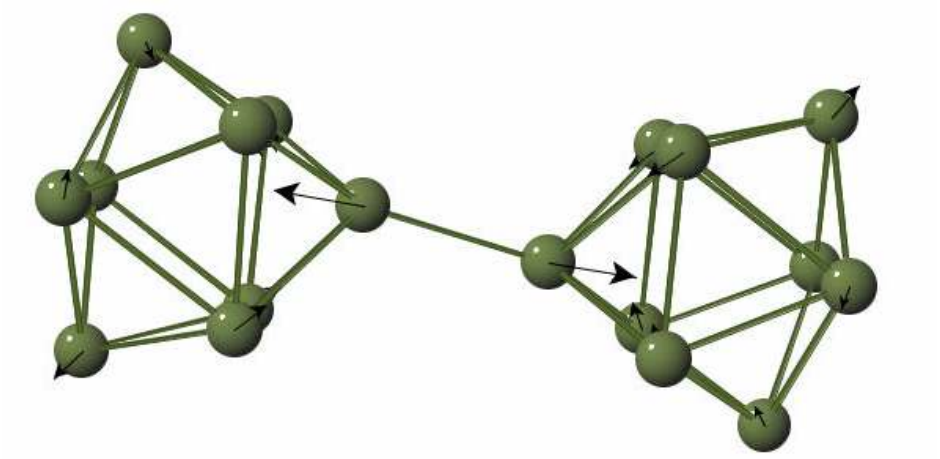

Figure 30: Scheme of intercluster bond vibration ($\upsilon_{stretching}$) of dimer species.

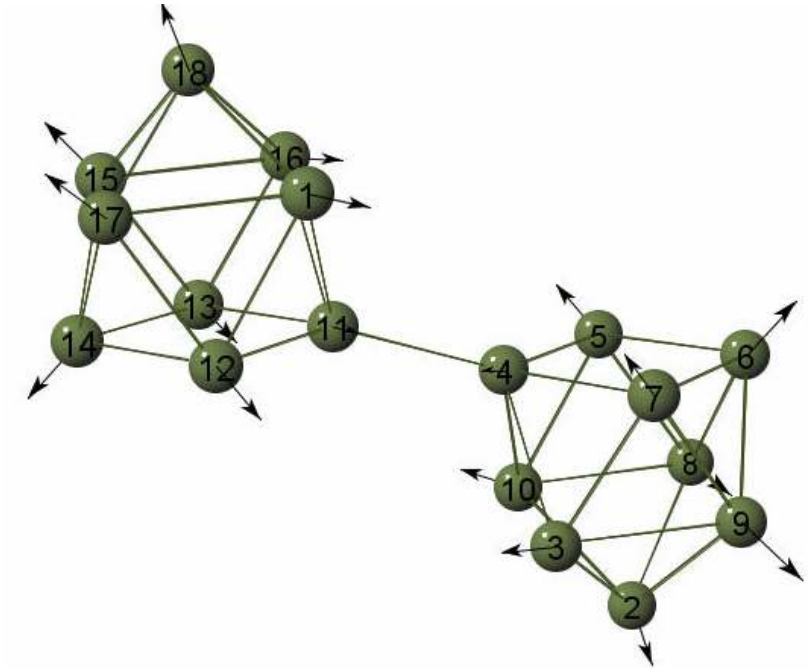

Figure 31: Scheme of intracluster bond vibrations (υ_{breath}) of dimer species

Trimer Species; $[Ge_9=Ge_9=Ge_9]^{6-}$

Theoretical Raman spectrum of the trimer species obtained by quantum chemical calculations exhibits following characteristic vibrational modes [Fig. 32].

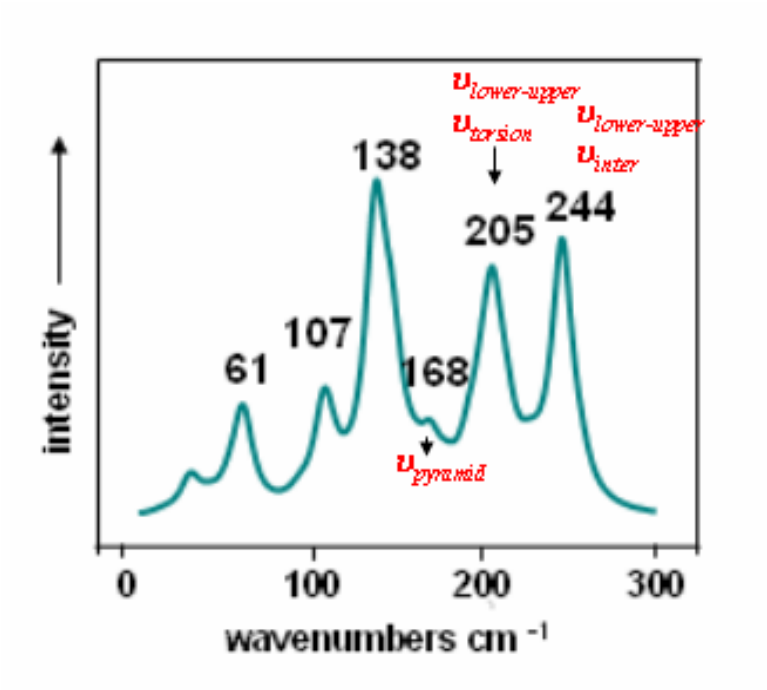

Figure 32: Theoretical Raman spectrum of trimer species. ($\nu_{lower\text{-}upper}$= bond stretching between upper and lower tetragonal, $\nu_{pyramid}$=upper pyramid bond stretching, ν_{inter}=intercluster bond stretching)

Intercluster and intracluster bond vibrations were calculated at 244 cm^{-1}, 205 cm^{-1}, respectively. Figure 33 shows the modes for intercluster bond vibrations of the trimer.

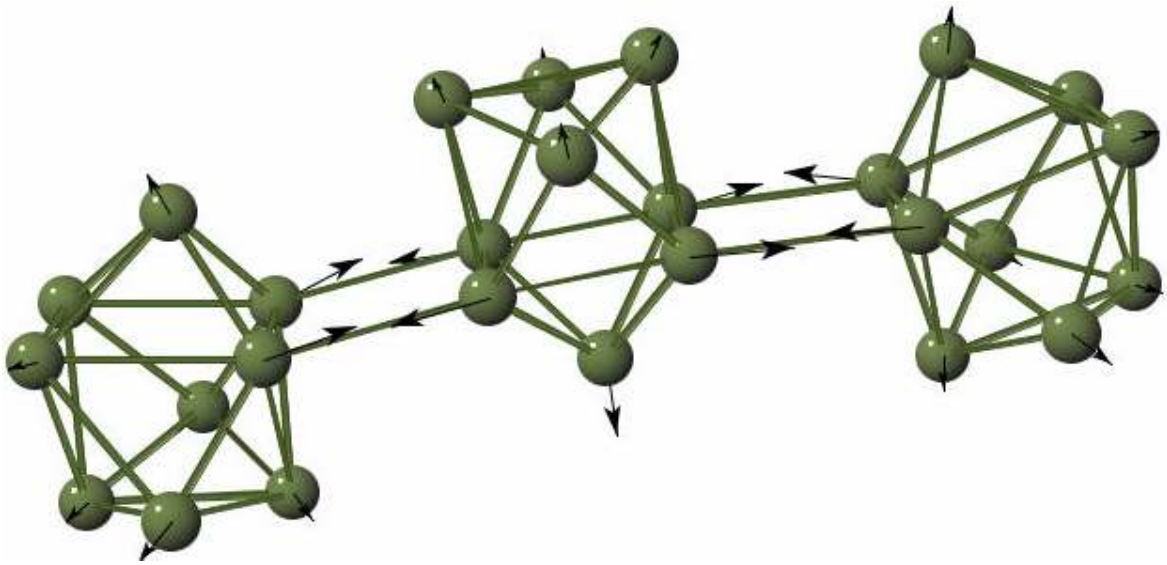

Figure 33: Scheme of intercluster vibrations modes of trimer species.

3.3 Attempts for Oxidation of K_4Ge_9

As mentioned before, the cluster species investigated in this study are extremely reactive and can be used as building blocks, e.g. for the synthesis of clathrates. Clathrates are a very interesting class of compounds due to their unique structures, super conductive, electro optic and thermoelectric properties. The most well-known chlathrate types are I (e.g. K_8Ge_{46}) and II ($Na_{24}Si_{136}$), both built up by the large 20- / 24- and 20- / 28-atoms cages, respectively, formed by the element 14 atoms whose voids are filled by the Na and K. Very recently, the synthesis of the empty clathrate, $[]_{24}Ge_{136}$, was published, obtained from the reaction of Na_4Ge_9 with dodecyltrimethyl-ammonium chloride and aluminium trichloride in low melting ionic liquids [22]. Similar results were reported also for the oxidation reactions of K_4Ge_4 with *NH_4Cl*, gaseous *HCl* and water vapor yielding K_8Ge_{46} as main product.

In the light of this findings, several new oxidative coupling reactions of $[K(18\text{-}cr\text{-}6)]_2[_\infty(Ge_9)]$ and the precursor K_4Ge_9 have been performed using elemental Ge, air, oxygen, water, *$E15(Ph)_3$* (E15 = P, As, Sb, Bi; Ph = phenyl), *DMF*, dodecyltrimetylammonium bromide *[DoDe]Br*, aqueous *HCl* solution and *NH_4Cl* in *liquid ammonia* as oxidizing agents. The reactions products were followed by Raman spectroscopy and powder XRD.

The compound, $[K(18\text{-}cr\text{-}6)]_2[_\infty(Ge_9)]$ [51], was decomposed under air during DTA/TG measurement (5^o/ min., up to 600^oC) and the final product was characterized by powder X-ray diffraction measurements [Fig. 34, 35].

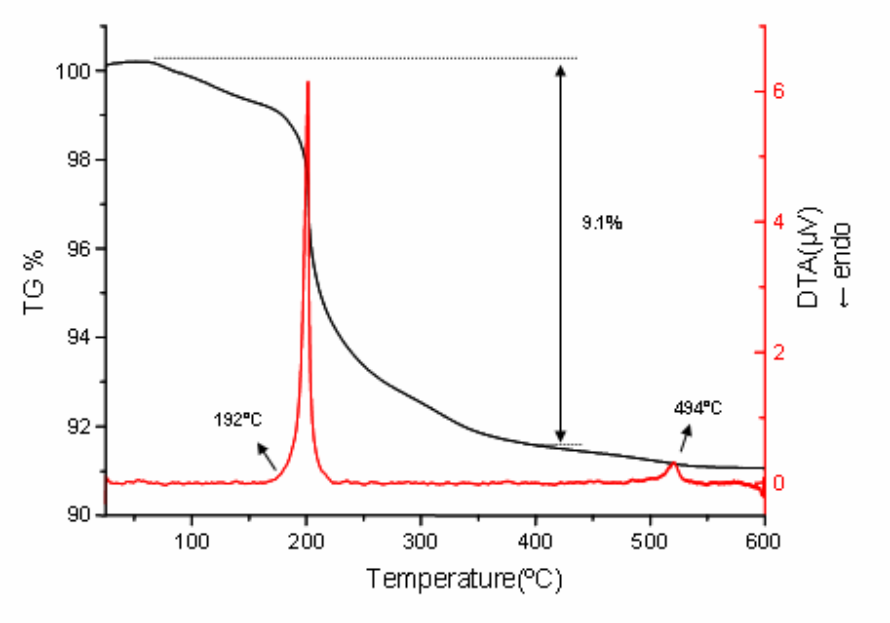

Figure 34: DTA/TG diagram of [K (*18-cr-6*)]$_2$ [$_\infty$(Ge$_9$)].

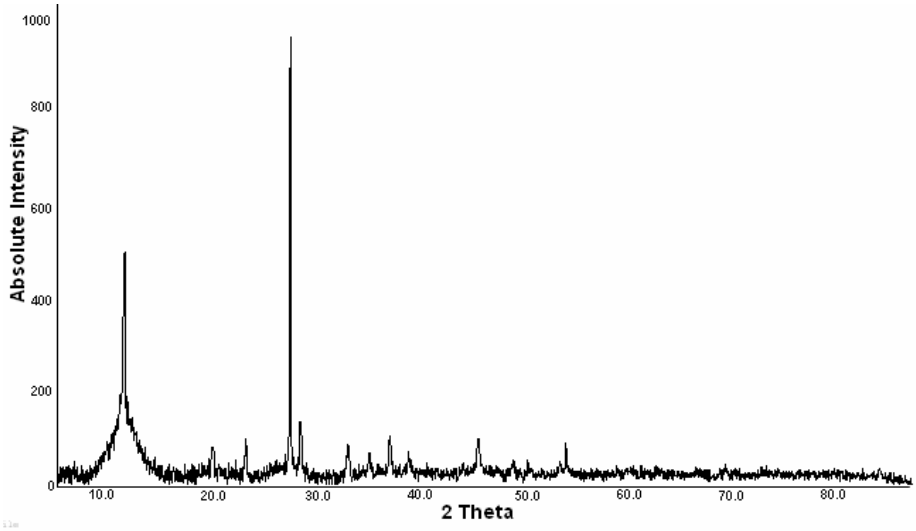

Figure 35: Powder X-ray patterns of decomposed [K (*18-cr-6*)]$_2$ [$_\infty$(Ge$_9$)].

The DTA/TG measurement of the compound showed an exothermic effect at 191.5 ^{o}C, accompanied by a weight loss of 6% which is completed at 493.9 ^{o}C. The X-ray diffraction pattern of the decomposed compound was identified as and $K_3HGe_7O_{16} \cdot 4\ H_2O$ [Fig. 36], indicating that the starting $[K(\textit{18-cr-6})]_2[_{\infty}(Ge_9)]$ was converted to the well-known potassium germanates and not to the desired clathrate. The phase conversion started at 191.5 ^{o}C and was completed at 493.9 ^{o}C according to DTA/TG diagram. During the phase conversion process, a total of 9.1% weight loss was determined which is mainly caused by the evaporation of 18-*crown*-6 molecules.

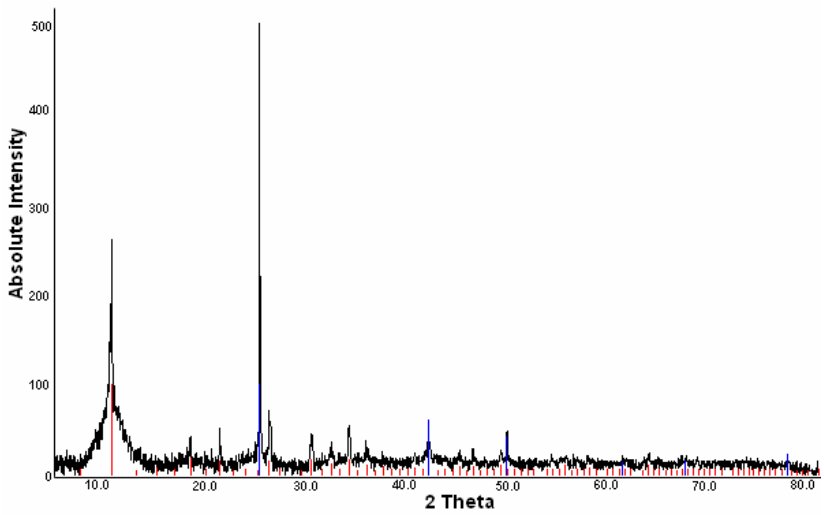

Figure 36: Powder x-ray diffraction pattern of decomposed $[K(\textit{18-crown-6})]_2[-(Ge_9)-]$ (black), germanium (blue), and, $K_3HGe_7O_{16} \cdot 4(H_2O)$ (red).

Reaction of the compound in HCl/H_2O mixture was investigated. Powder X-ray diffraction pattern of the product can be seen in figure 37.

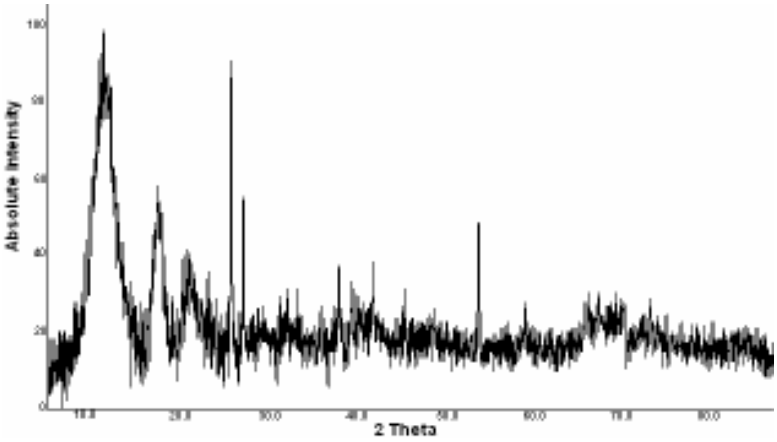

Figure 37: Powder X-ray pattern of the black precipitate obtained at the end of the reaction between the polymeric compound and HCl/H_2O solution.

At the end of the reaction, the green powder of the polymeric compound turned to dark brown. The powder X-ray diffraction of the precipitate exhibits the same patterns as for the decomposed polymeric compound, $[K(\textit{18-cr-6})]_2[_\infty(Ge_9)]$ [Fig. 38].

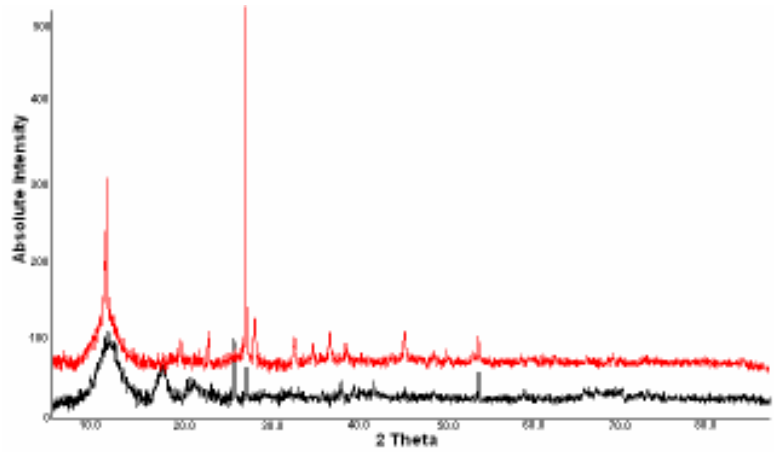

Figure 38: Powder X-ray patterns of the decomposed polymeric compound (red), and, the dark brown powder obtained at the end of the reaction (black).

K_4Ge_9, whose powder XRD pattern is shown in figure 39, was used as a starting material for the following experiments.

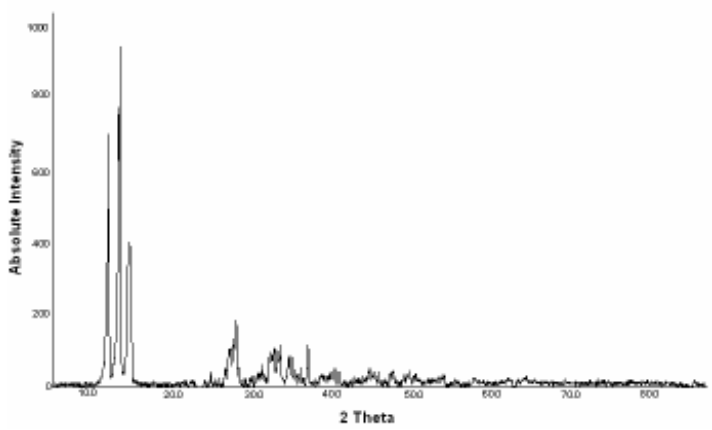

Figure 39: Powder X-ray pattern of K_4Ge_9.

K_4Ge_9 was exposed to air for 2 days and characterized by powder X-ray diffraction. It was also decomposed under air during DTA/TG measurements (5^o/min., up to 600^oC) [Fig. 40, 41]. In the first case, the powder X-ray diffraction pattern of the final product indicated the presence of $K_3HGe_7O_{16} \cdot 4(H_2O)$ phase.

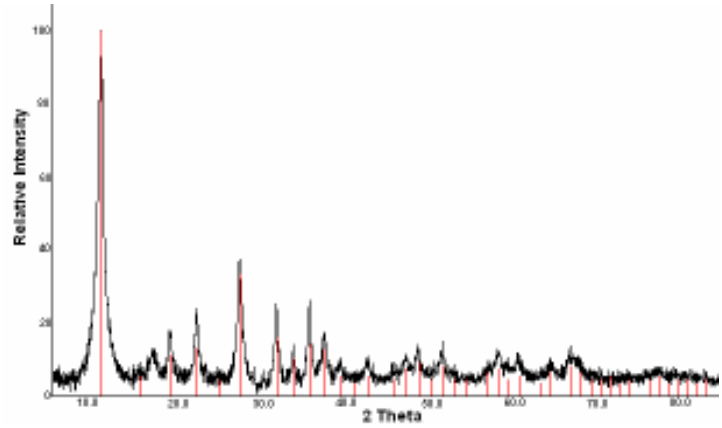

Figure 40: Powder x-ray diffraction patterns of air exposed K_4Ge_9 (black) and $K_3HGe_7O_{16} \cdot 4(H_2O)$ (red).

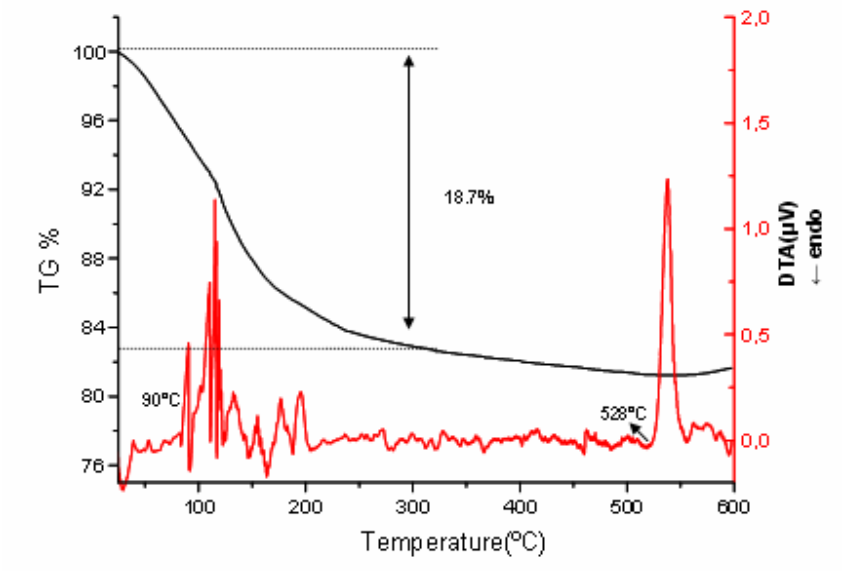

Figure 41: DTA/TG diagram of decomposed K_4Ge_9.

Weight loss started at 90.8 °C and is completed at 528.4 °C. A total of 18.7 % weight loss was registered, resulting mainly from to the loss of water during the thermal analysis. Powder X-ray diffraction pattern of the sample after decomposition shows an additional unknown (?) phase, when compared to that of air exposed sample of the K_4Ge_9 precursor [Fig. 42].

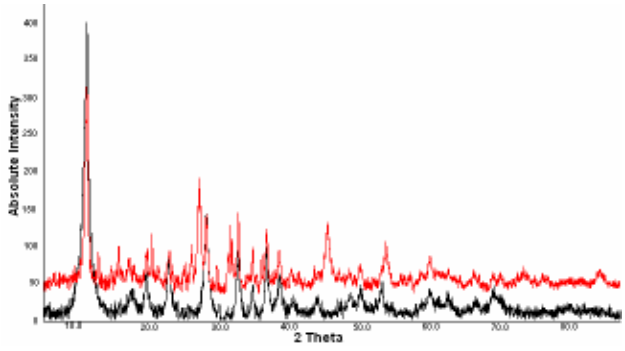

Figure 42: Powder X-ray diffraction patterns of air exposed K_4Ge_9 before decomposition (black), and, air exposed K_4Ge_9 after decomposition (red).

Additionally, two samples containing 15 mg K_4Ge_9 precursor each were decomposed under nitrogen and oxygen. Sudden changes in the temperature during the measurements led to difficulties in the interpretation of the thermal analyses diagrams of the samples.
When the samples reached 120 ^oC, an oxidation reaction took place and the temperature suddenly increased to 400 ^oC and the samples decomposed. The powder X-ray diffraction patterns of the specimen show that the phases are almost converted to germanium during the thermal analysis [Fig. 43].

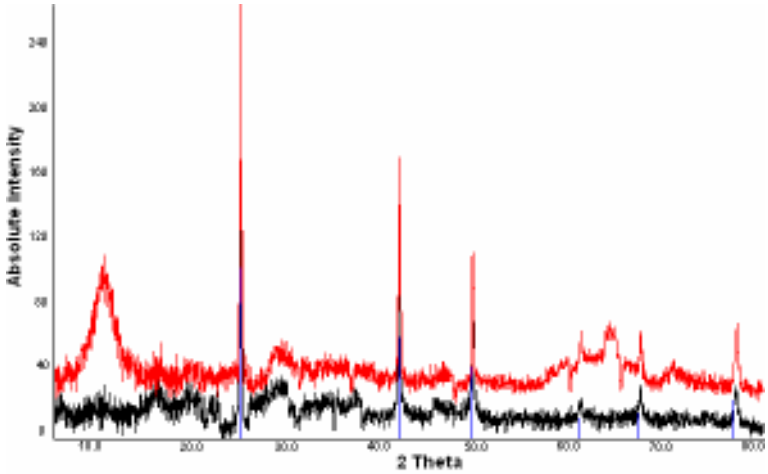

Figure 43: Powder X-ray patterns of decomposed K_4Ge_9 under nitrogen (black), under oxygen (red) and germanium (blue).

In addition to these experiments, the interaction of K_4Ge_9 phases with H_2O was investigated. A black precipitation was obtained at the end of the reaction and the powder X-ray diffraction pattern shows the $K_3HGe_7 \cdot 4(H_2O)$ phase [Fig. 44].

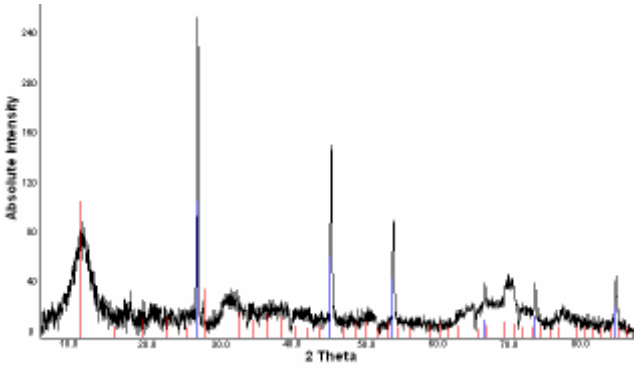

Figure 44: Powder X-ray diffraction patterns of black precipitation obtained at the end of the reaction (black), $K_3HGe_7 \cdot 4(H_2O)$ (red), and, germanium (blue).

Clathrate of K_8Ge_{46} obtained by the oxidation of K_4Ge_9 with NH_4Cl was characterized by powder X-ray diffraction. At the end of the reaction, a black crystalline powder was obtained. The clathrate phase, K_8Ge_{46} and germanium were identified [Fig. 45].

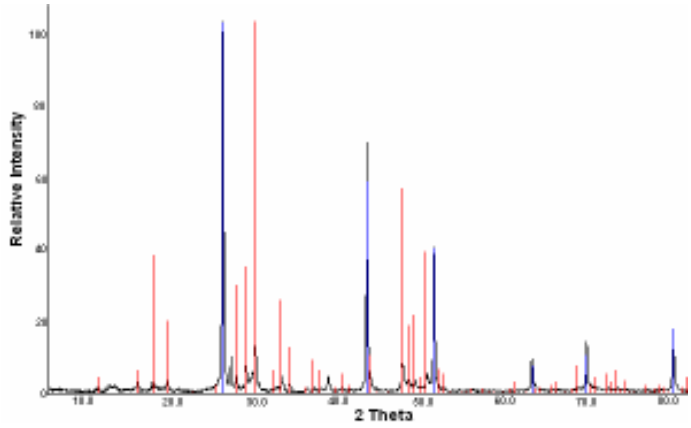

Figure 45: Powder diffraction patterns of the black crystalline powder obtained at the end of the reaction (black), germanium (blue), and, K_8Ge_{46} (red).

3.4 Conclusion

The monomer, oligomer and polymer species of the deltahedral germanium anion such as, $[Ge_9]^{4-}$ [13, 15], $[Ge_9]^{3-}$ [40, 41], $[Ge_9]^{2-}$ [39], the dimer $[Ge_9\text{-}Ge_9]^{6-}$ [44, 45], trimer $[Ge_9{=}Ge_9{=}Ge_9]^{6-}$ [47, 48], and, polymer $_\infty[\text{-}(Ge_9)\text{-}]^{2-}$ [51] bring a new perspective to controlled step-growth oligomerization. Clarifying the reaction mechanism and the electron distribution of the clusters is very important as they could be designed to be used as building blocks for the synthesis of 3-D materials and clathrates. In this study, vibrational spectroscopic investigations were employed to confirm and establish the structure of known and novel compounds, respectively. The experimental results were back upped by quantum chemical calculations.

The "units" relevant in vibrational spectroscopy for the distinction between the monomer and the oligomer (Ge_9) species are the intercluster ($–Ge_9–Ge_9–$) exobonds which are considerably shorter than those within the cluster. Thus, oligomer species are expected to give rise to two groups of bands, representing the inter and intra cluster vibrations, respectively, with $\upsilon(Ge_9–Ge_9)_{inter} > \upsilon(Ge_9 \approx 220\ cm^{-1})_{intra}$. While monomer species exhibit only one group of bands representing the symmetric 'intracluster' breathing mode vibrations at 220cm^{-1} (Ge_9^{4-}), 219 cm^{-1} (Ge_9^{3-}) and 224 cm^{-1} (Ge_9^{2-}).

All inter and intracluster vibrations for monomeric, oligomeric and polymeric units are experimentally found between 200 cm^{-1} and 300 cm^{-1}. The characteristic inter and intra cluster vibrations of the species are summarized in table 2.

	$\upsilon_{(inter)}$ cm^{-1}	$\upsilon_{(intra)}$ cm^{-1}
$[Ge_9]^{4-}$	-	221
$[Ge_9]^{3-}$	-	219
$[Ge_9]^{2-}$	-	224
$[Ge_9\text{-}Ge_9]^{6-}$	268	220
$[Ge_9{=}Ge_9{=}Ge_9]^{6-}$	241	209
$_\infty[\text{-}(Ge_9)\text{-}]^{2-}$	269	200

Table 2: Intracluster vibrations of $[Ge_9]^{n-}$ (n = 4, 3, 2) and inter / intracluster vibrations of the dimer, trimer, and polymer species.

Raman spectra of the diamagnetic germanium clusters, $[Ge_9]^{2-}$ exhibit one strong line at 224 cm^{-1} and further three sharp bands at 183 cm^{-1}, 168 cm^{-1} and 152 cm^{-1}, respectively. Additionally, one weak broad band was observed at 252 cm^{-1}. These bands were theoretically calculated at 216 cm^{-1} and 188 cm^{-1}, 170 cm^{-1}, 154 cm^{-1}. For the paramagnetic germanium clusters $[Ge_9]^{3-}$ one strong band at 219 cm^{-1} and three broad bands at 168 cm^{-1}, 142 cm^{-1} and 121 cm^{-1} were registered in the Raman spectra. The quantum-chemical calculated spectrum of the diamagnetic germanium cluster $[Ge_9]^{2-}$ reveals a characteristic vibrational pattern composed of five bands at 225 cm^{-1}, 172 cm^{-1}, 152 cm^{-1} and 132 cm^{-1}, respectively, which is very similar to that measured for the

compound, $[K(cp)]_3P(C_6H_5)_3Ge_9$ [40]. These findings suggest that the structural units in this phase are also $[Ge_9]^{2-}$.

For the dimer species, the significant bands for the intercluster vibrations were observed at 267-270 cm^{-1} and that for the intracluster vibration at 221cm^{-1}. These vibrations were calculated at 230 cm^{-1}, 209 cm^{-1}, respectively. The Raman spectrum of KGe_4(s) indicates that the precursor contains K_4Ge_9 and elemental germanium.

An interesting detail is that the Raman spectrum obtained from the green *en* solution of KGe_4, indicating the presence of the dimeric species, characterized by the band at 264 cm^{-1}. An additional proof for the existence of the dimeric units is that the intensity of the band at 222 cm^{-1} for Ge_9^{4-} is decreased by the effect of coupling. This can be explained by the oxidation of the deltahedral Ge clusters by elemental Ge present in KGe_4, to dimeric units. Finally, the addition of *CsI* to the dark green solution precipitates as main product $Cs_6Ge_{18}\cdot(en)_x$.

The characteristic dimeric unit bands at 260 cm^{-1} for intercluster and 221 cm^{-1} for intracluster vibrations in the Raman spectrum of the compound are in agreement with that of the well- know dimer species, $[M_6(Ge_9–Ge_9)](DMF)_{12}$ (M = K, Rb).

The characteristic bands for the symmetric intercluster and intracluster vibrations in the trimeric species $[Rb(cp)]_6[Ge_9=Ge_9=Ge_9]\cdot 3en$ were observed at 241 cm^{-1} and 209 cm^{-1}. According to quantum chemical calculations the bands are at 241cm^{-1} and 251cm^{-1}. The intercluster vibrations of the trimer species in the compound, $[DoDe]_6[Ge_9=Ge_9=Ge_9]$ can be observed at 244 cm^{-1} and the band at 200 cm^{-1} indicates the intracluster vibration of the trimeric unit.

The intercluster bond vibrations of the compounds; $[Na(18\text{-}cr\text{-}6)]_6[Ge_9=Ge_9=Ge_9]$ and $[K(18\text{-}cr\text{-}6)]_6[Ge_9=Ge_9=Ge_9]$ were registered at 241cm^{-1} and 240 cm^{-1}, respectively. The intracluster bonds vibrations are detected at 199 cm^{-1} for both compounds.

The characteristic inter and intra cluster vibrations for the polymeric unit $_{\infty}[-(Ge_9)-]^{2-}$ in $[K(18\text{-}cr\text{-}6)]_2[_{\infty}(Ge_9)]$ are observed at 269 cm^{-1} and 202 cm^{-1}. The presence of the polymeric species in $[DoDe]_2[_{\infty}(Ge_9)]$ is proved by the bands at 277 cm^{-1} for intercluster and 202 cm^{-1} for intracluster vibrations, respectively.

One important point is that increasing the number of intercluster bonds induces an increase in the intensity of the intercluster vibrations bands; this situation can be clearly seen in the Raman spectra of compounds of dimeric and polymeric species [Fig. 46].

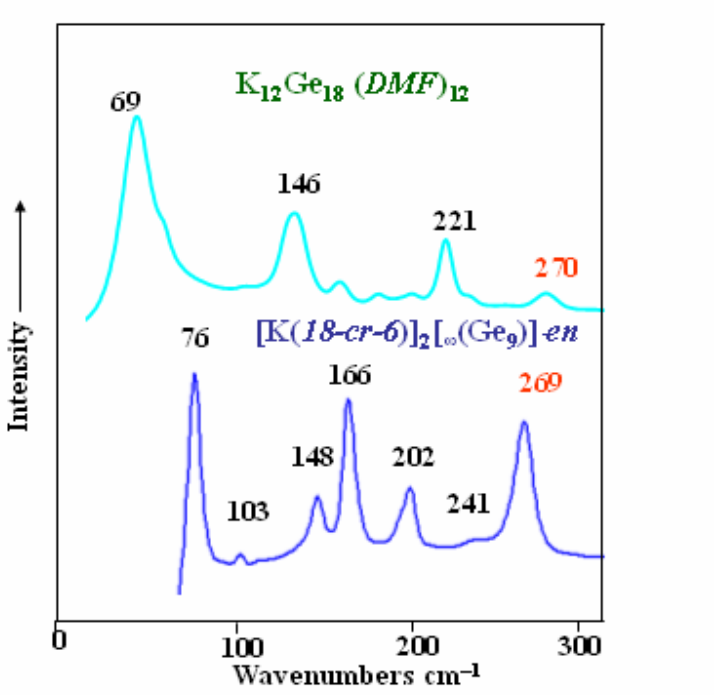

Figure 46: Raman spectra of K_6Ge_{18} $(DMF)_{12}$ and $[K(18\text{-}cr\text{-}6)]_2$ $[_{\infty}(Ge_9)]$.

Another important issue is the difference between the experimental and theoretical spectra for all studies species. Their common feature is that the vawenumbers in the calculated spectra are systematically lower than those measured. This can be explained by the fact that

quantum-chemical calculations are performed on an isolated cluster in the gas phase while experimental studies were done in solutions or solid phase in which the cluster anions are embedded in a cationic matrix. That means that the effective negative charge on the isolated moieties is more emphasized when the counterions are absent. This is important, since the increase of the effective negative charge is known to weaken the bond strength and lower the force constants. In this sense, the observed downshift of the wavenumbers with respect to the experimental values may be attributed to the relatively high effective negative charge obtained from the calculations.

Monomeric clusters $[Ge_9]^{n-}$ (n = 4, 3, 2) and their condensed dimeric, trimeric, and polymeric derivatives were Raman spectroscopically investigated and characterized with respect to their inter and intracluster vibrations. As expected, the band intensities alter due to the ratio of the intra and intercluster bonds, allowing a more detailed analysis of the spectra. Using the above mentioned characteristic frequencies as identification probes, several new phases, such as $Cs_6Ge_{18} \cdot (en)_x$, $[Na(cp)]_3Ge_9$, $[DoDe]_6[Ge_9{=}Ge_9{=}Ge_9]$, $[DoDe]_2[_\infty(Ge_9)]$, were identified and structurally characterized for the first time.

The high reactivity of the $[Ge_9]^{4-}$ and the condensed species towards oxidation can be employed for preparative purposes, e.g. as building blocks for the synthesis of new materials. Several oxidation reactions were performed in which K_4Ge_9 was used as bprecursor. Worth mentioning is the synthesis of the clathrate-I phase K_8Ge_{46} [18] obtained after the reaction of K_4Ge_9 with *NH_4Cl* in *liquid ammonia*. To avoid the formation of the undesired potassium germanates all oxidation reactions with K_4Ge_9 precursor must be performed in absence of air (i.e. O_2 and moisture). The samples of K_4Ge_9 exposed for at least 2h to air yielded in all cases $K_3HGe_7O_{16} \cdot 4H_2O$ as final product.

SYNTHESIS and CHARACTERIZATION of the NOVEL COMPOUND [Na (*cp*)]$_3$Ge$_9$

4.1 Experimental Part:

Synthesis of [Na (*cp*)]$_3$Ge$_9$ in different solvated media: *ethylenediamine* (1), *liquid ammonia* (2), and their mixtures (3).

All manipulations were carried out in a glove- box with moisture and oxygen levels below 1 ppm. The precursor of $Na_{12}Ge_{17}$ was prepared from stoichiometric mixtures of the element Na (0.200 g) and Ge (0.894 g) in an alumina crucible that was placed in a sealed stainless ampoule. The sample was heated up to 1000 ^{0}C (5h) and annealed at 740 ^{0}C (48h) and cooled down to room temperature (32h) [16].

(1) 0.150 g of $Na_{12}Ge_{17}$ were dissolved in 2 ml *en* and stirred overnight. The dark red solution was filtered and transferred onto 0.128 g of *cryptand 2, 2, 2*. After that, the mixture was stirred until all *cp* dissolved and layered with 2 ml *toluene*. 2 weeks later, orange-red needle like prismatic crystals of the compound, [Na(*cp*)]$_3$Ge$_9$ (1) deposited from the solution.

(2) 0.75 g of $Na_{12}Ge_{17}$ and 0.102 g of *cp* were placed on the frit and in the bulb of the soxhlet apparatus, respectively. The apparatus was connected to a vacuum line and ammonia was condensed in the reaction tube using liquid nitrogen as coolant. After sealing under vacuum, the soxhlet was allowed to warm up to room temperature. Extraction with *liquid ammonia* started immediately after the water cooling system was turned on. At the end of three days, orange-red prismatic crystals of the compound, [Na(*cp*)]$_3$Ge$_9$ (2), deposited on the wall of the reaction tube. The *liquid ammonia* solution was then cautiously decanted into the bulb, frozen (liq. N_2) and the reaction tube containing the product was sealed off.

(3) $Na_{12}Ge_{17}$ (0.150 g) was placed on the filter of a soxhlet. 0.128 g of *cp* was dissolved in 2 ml *en* and transferred to the bulb of the soxhlet. After completion of the process of condensation of *liquid ammonia* mentioned above, the extraction started. 3 days later, orange-red prismatic crystals of the compound, [Na(*cp*)]$_3$Ge$_9$ (3), were obtained in the reaction tube.

4.2 Single Crystal X-ray Diffraction Measurements:

The X-ray diffraction data of the crystal of the title compound was obtained from an Oxford-Diffraction Xcalibur 3 Diffractometer, MoK_α radiation. The structure was solved by direct method, using SHELXS-97.

The crystal data, the conditions for data collection, crystal refinement, atomic coordinates (x 10^4), its equivalent isotropic displacement parameters (Å^{2}x 10^3), bond lengths [Å], angles [°], anisotropic displacement parameters (Å^{2}x 10^3), hydrogen coordinates (x 10^4) and isotropic displacement parameters (Å^{2}x 10^3) of [Na(*cp*)]$_3$[Ge$_9$] are reported in tables presented in appendix A.

The crystal structure of the orange red prismatic crystals of [Na(*cp*)]$_3$Ge$_9$ was determined by single crystal X-ray diffraction. The crystal system of the compound is monoclinic (Space group: $P2_1/n$, a=22.7596(7) Å, b=14.2822(2) Å, c=24.0187(7) Å, β=108.518(3)° and Z=4) and the crystal structure is a variant of Al_3Ti-type structure [Fig. 47]

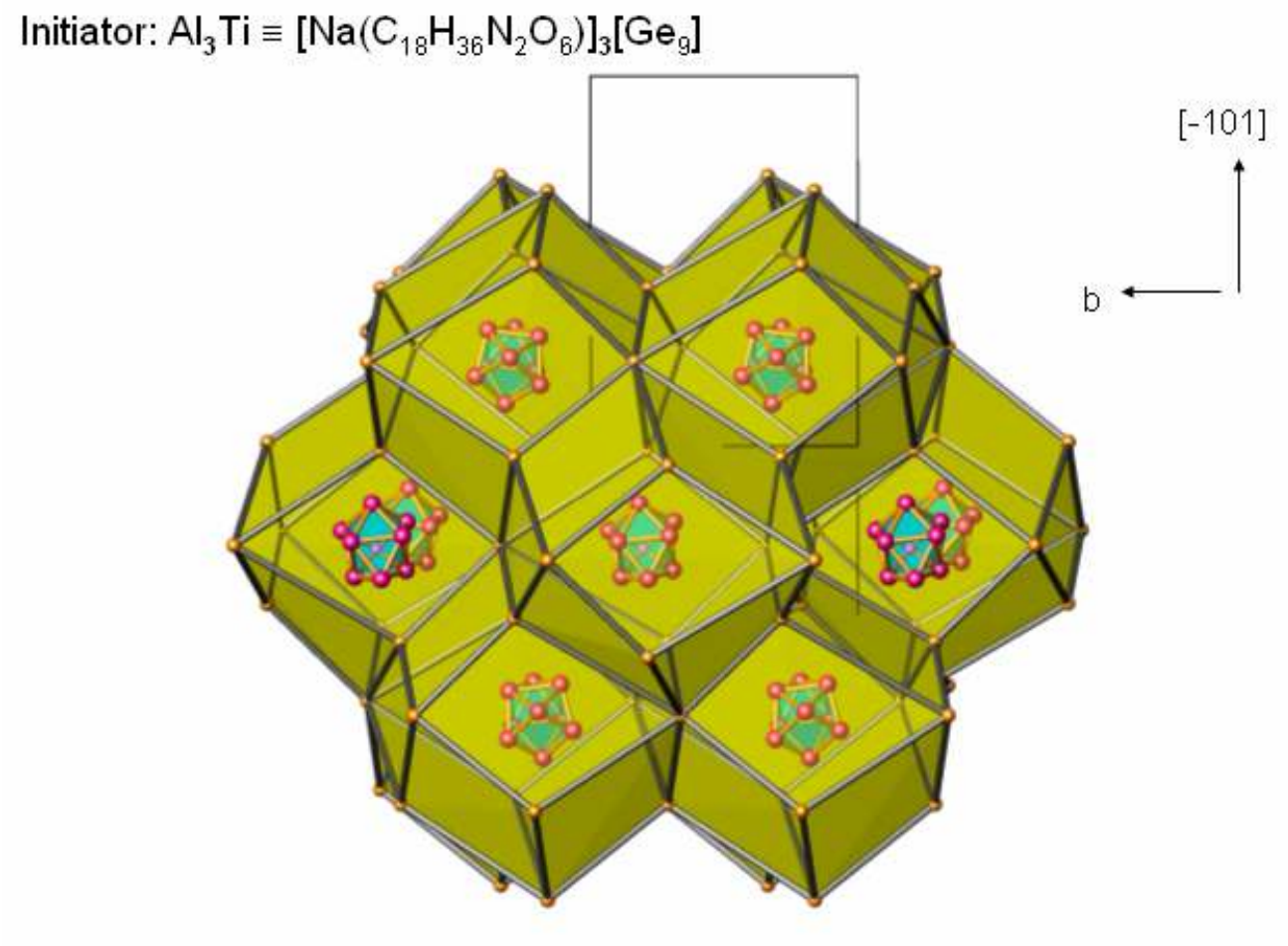

Figure 47: The crystal structure of $[Na(cp)]_3Ge_9$.

In the crystal structure, the [Na(*cp*)] moieties are arranged to disordered (3, 6, 3)-polyhedra that are further condensed via common faces to a space-filling 3D framework. Each polyhedron is centered by a $[Ge_9]^{3-}$.

Bond lengths of the $[Ge_9]^{3-}$ cluster anion can be seen in figure 48.

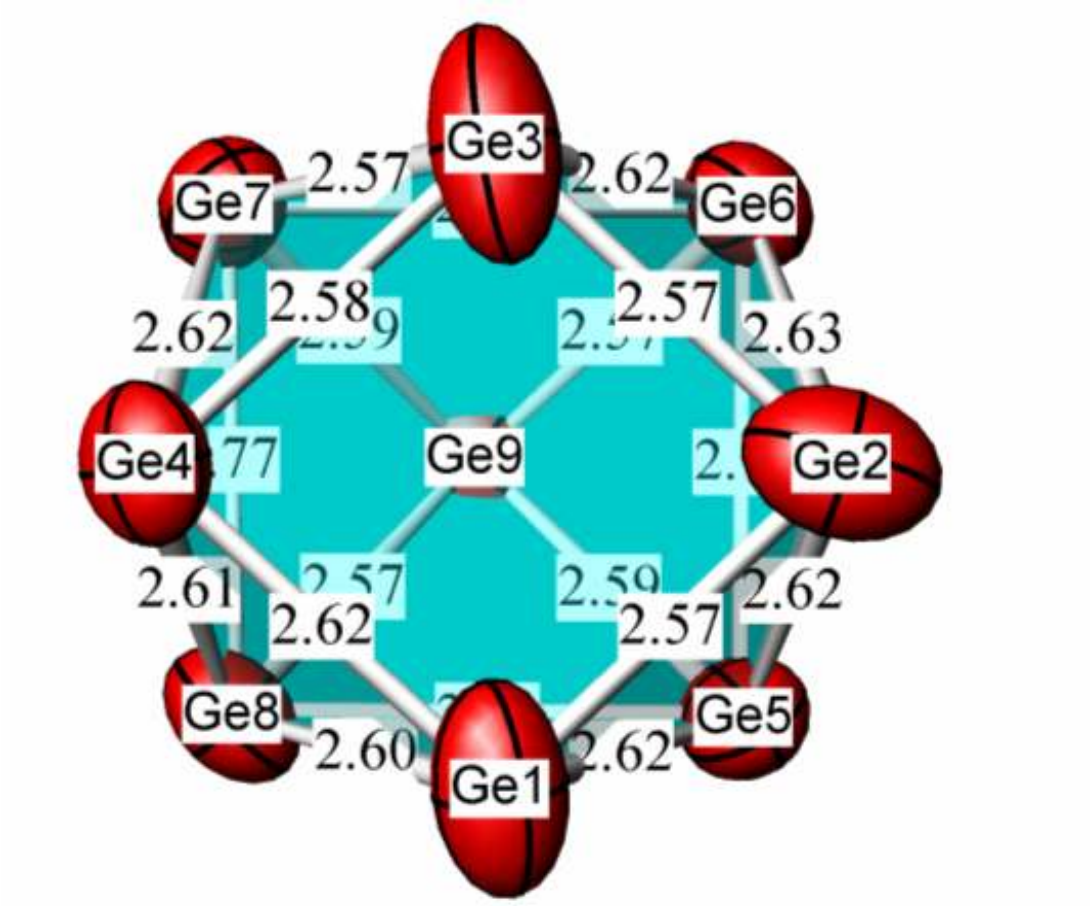

Figure 48: Bond lengths of the $[Ge_9]^{3-}$ cluster.

4.2 Raman Spectroscopy Measurements:

The orange-red prismatic crystals of the compound obtained in the three different solvents were separately collected in sealed capillaries and Raman spectroscopically investigated. The spectra of the samples (1, 2, and, 3) are shown below [Fig. 49, 50, 51].

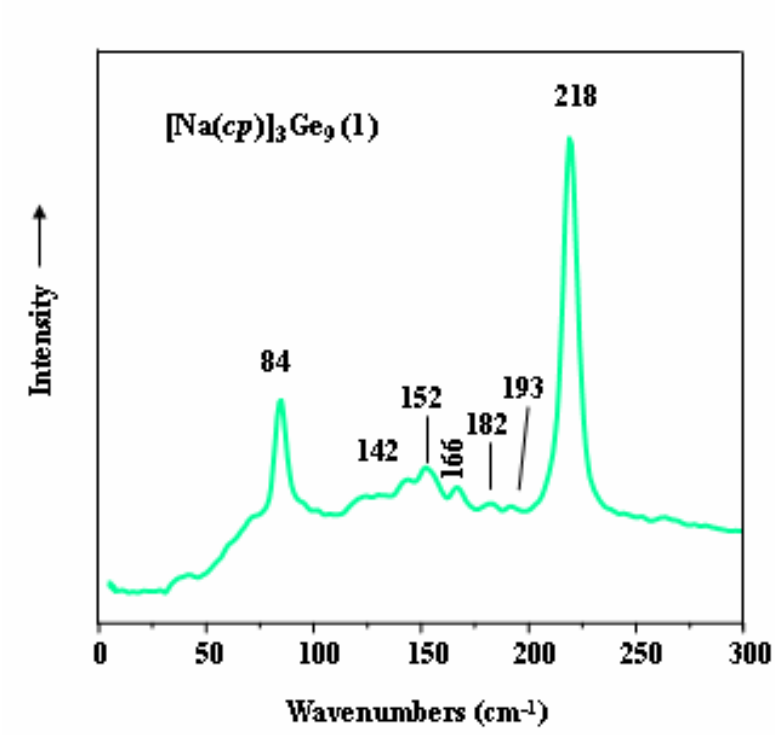

Figure 49: Raman spectrum of [Na(*cp*)]$_3$Ge$_9$ (1).

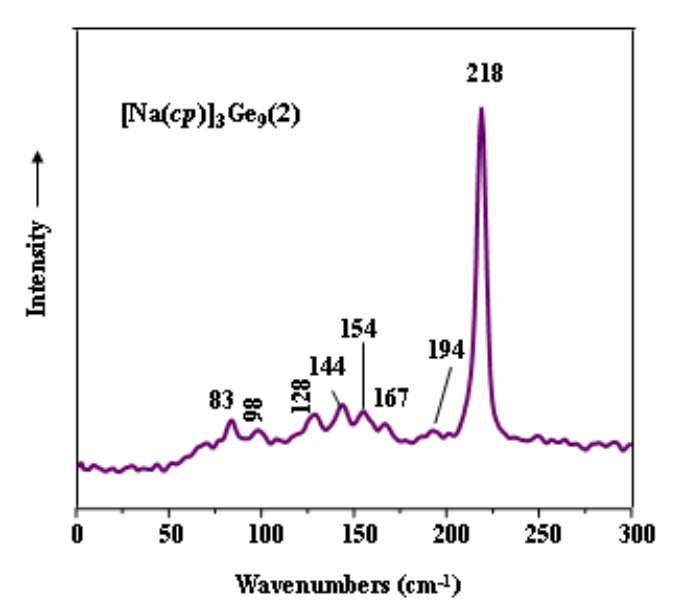

Figure 50: Raman spectrum of [Na (*cp*)]$_3$Ge$_9$ (2).

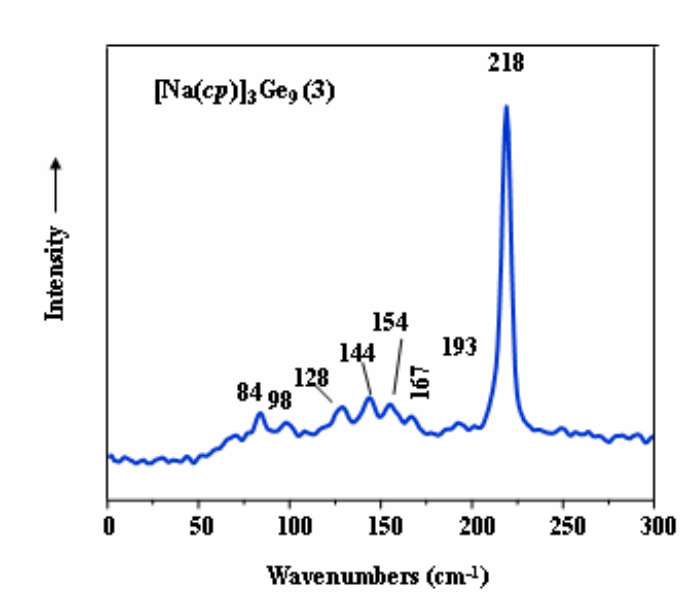

Figure 51: Raman spectrum of [Na (*cp*)]$_3$Ge$_9$ (3).

The characteristic vibrations of the paramagnetic germanium cluster in the compound; [Na (*cp*)]$_3$Ge$_9$ (**3**) were detected as one strong band at 218 cm^{-1} and five further bands at 193 cm^{-1} , 167 cm^{-1}, 154 cm^{-1}, 144 cm^{-1} and 128 cm^{-1}. The observed wavenumbers for **1** and **2** are practically the same.

4.4 ESR (Electron Spin Resonance) or EPR (Electron Paramagnetic Resonance) Measurements:

For the verification of the paramagnetic properties of the $[Ge_9]^{3-}$ moieties X-band (9.5 GHz) continuous wave EPR measurements were performed, in which two different EPR centres for sample **1** ([Na (*cp*)]$_3$Ge$_9$ synthesized in *liquid ammonia*) and only one center for sample **2** ([Na(*cp*)]$_3$Ge$_9$ synthesized in the mixture of *liquid ammonia* and *ethylenediamine*) were identified. g- factors were observed at the values of g_1= 2.002 for the first centre of the sample 1 and g_2= 2.024 for the second centre of the sample 1. For the second sample, the g-factors are $g_{x, y}$=2.001 and g_z=2.041 [Tab. 3].

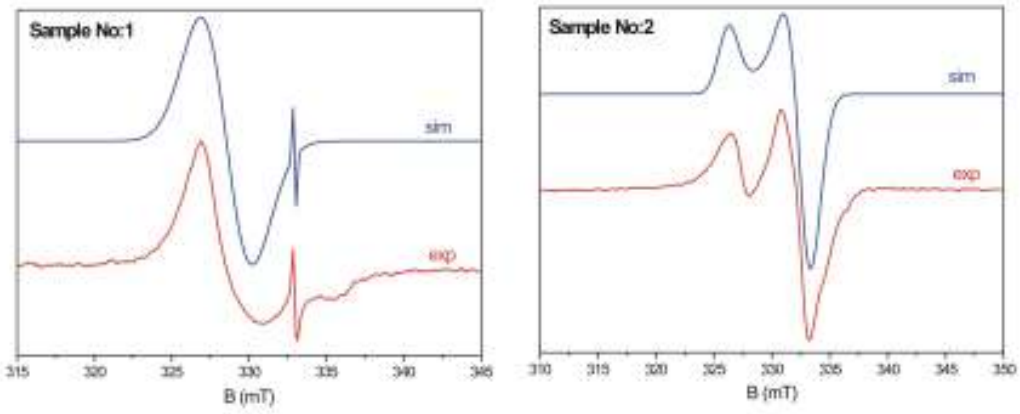

Measured at X band @ 10K

Simulation parameters

Sample No: 1	**g-factor**	**Linewidth (mT)**
Center 1	$g1_{x,y,z}$=2.002	0.2
Center 2	$g2_{x,y,z}$=2.024	3.5
Sample No: 2		
	$g_{x,y}$=2.001 g_z =2.041	1.1

Table 3: EPR parameters of the compound; $[Na(cp)]_3Ge_9$.

4.5 Conclusion:

The characteristic structural units in the new compound, $[Na(cp)]_3Ge_9$, are the paramagnetic cluster anions $[Ge_9]^{3-}$. The compound, synthesized in *ethylenediamine* (**1**), *liquid ammonia* (**2**), and, their mixture of *ethylenediamine* and *liquid ammonia* (**3**) solvated media was investigated by single crystal X-ray diffraction and Raman spectroscopy. Single crystal X-ray diffraction measurements give the same structure of the compound in all solvated media. This proves that the compound crystallizes solvent free.

Crystal structure of $[Na(cp)]_3Ge_9$, is a variant of Al_3Ti type structure. The compound crystallizes in monoclinic crystal system (Space group: $P2_1/n$) with the parameters; a = 22.7596(7) Å, b = 14.2822(2) Å, c = 24.0187(7) Å, β = 108.518(3)° and Z = 4. In the structure, the [Na(*cp*)] moieties are arranged to disordered (3, 6, 3)-polyhedra that are further condensed via common faces to a space-filling 3D framework. Each polyhedra is centered by one $[Ge_9]^{3-}$.

Raman spectra of the compounds, synthesized in three different solvated media, reveals the characteristic breathing mode of the $[Ge_9]^{3-}$ cluster at 218 cm^{-1}. Samples synthesized in solvated media *liquid ammonia* (sample 1) and liquid ammonia- *ethylenediamine* mixture (sample 2), were investigated by EPR to prove the paramagnetic behavior of the compound. We identified two different EPR active centers for sample 1 and one centre for sample 2. The g-factor of sample 1 was determined from both experiment and simulation as

isotropic g-factor, g_1= 2.002 for the first centre. The value is very close to the free electron g factor (g_e= 2.0023), so that one may conclude that this centre is a kind of radical in the sample. The second EPR centre in sample 1 had axial g-factor which indicates anisotropy. Sample 2 had also anisotropy. The ongoing EPR measurements in Q band will provide more detailed data about the samples.

APPENDIX A
SINGLE CRYSTAL X-RAY DATA of the COMPOUND; [Na(*cp*)]$_3$Ge$_9$

Table A.1: Crystal data and structure refinement for [Na(*cp*)]$_3$[Ge$_9$].

Identification code	nacpge9
Empirical formula	C_{54} H_{108} Ge_9 N_6 Na_3 O_{18}
Formula weight	1851.74 g/mol
Temperature	150(2) K
Wavelength	0.71073 Å
Crystal system	*Monoclinic*
Space group	$P2_1/n$
Unit cell dimensions	a = 22.7596(7) Å
	b = 14.2822(2) Å β = 108.518(3)°
	c = 24.0187(7) Å
Volume	7403.2(3) Å³
Z	4
Density (calculated)	1.661 g/cm³
Absorption coefficient	3.683 mm^{-1}
F(000)	3756
Crystal size	0.10 x 0.05 x 0.02 mm³
Theta range for data collection	2.73 to 23.35°
Index ranges	-25<=h<=24, 0<=k<=15, 0<=l<=26
Reflections collected	113764
Independent reflections	10727 [R_{int} = 0.051]
Completeness to theta = 23.35°	99.7 %
Absorption correction	Semi-empirical from equivalents
Max. and min. transmission	0.9964 and 0.6809
Refinement method	Full-matrix least-squares on F^2

Table A.1: Continued of crystal data and structure refinement for $[Na(cp)]_3[Ge_9]$.

Data / restraints / parameters	10727 / 0 / 840
Goodness-of-fit on F^2	0.987
Final R indices [$I>2\sigma(I)$]	$R_1 = 0.034$, $wR_2 = 0.079$
R indices (all data)	$R_1 = 0.057$, $wR_2 = 0.087$
Largest diff. peak and hole	1.717 and -1.653 e $Å^{-3}$

Table A.2: Atomic coordinates (x 10^4) and equivalent isotropic displacement parameters (Å^{2}x10^3) for [Na(*cp*)]$_3$[Ge$_9$]. U(eq) is defined as one third of the trace of the orthogonalized U^{ij} tensor.

	x	y	z	U(eq)
Ge(1)	7953(1)	1890(1)	1067(1)	52(1)
Ge(2)	7133(1)	3193(1)	841(1)	51(1)
Ge(3)	8037(1)	4319(1)	931(1)	57(1)
Ge(4)	8881(1)	3040(1)	1178(1)	37(1)
Ge(5)	7190(1)	2067(1)	-2(1)	33(1)
Ge(6)	7238(1)	3999(1)	-108(1)	34(1)
Ge(7)	8556(1)	3893(1)	160(1)	33(1)
Ge(8)	8477(1)	1967(1)	253(1)	33(1)
Ge(9)	7775(1)	2883(1)	-633(1)	37(1)
Na(1)	4022(1)	2131(1)	9000(1)	32(1)
Na(2)	1643(1)	2113(1)	1170(1)	32(1)
Na(3)	9835(1)	8390(1)	2134(1)	32(1)
O(1)	4992(1)	2519(2)	8786(1)	47(1)
O(2)	4286(2)	991(2)	8225(2)	54(1)
O(3)	4476(1)	1006(2)	9891(1)	42(1)
O(4)	3255(1)	1115(2)	9249(1)	46(1)
O(5)	3669(2)	3370(3)	9524(2)	58(1)
O(6)	3401(2)	3489(2)	8325(1)	44(1)
O(7)	2324(2)	1950(2)	529(1)	48(1)
O(8)	2287(1)	3531(2)	1160(1)	40(1)
O(9)	899(2)	857(2)	804(1)	40(1)
O(10)	619(1)	2630(2)	305(1)	36(1)

O(11)	2452(2)	1648(2)	2144(1)	50(1)
O(12)	1294(1)	2295(2)	2107(1)	41(1)
O(13)	9817(2)	7093(2)	2818(1)	46(1)
O(14)	9049(1)	8644(2)	2660(1)	43(1)
O(15)	10703(1)	8104(2)	1710(1)	42(1)
O(16)	10907(1)	8526(3)	2869(2)	52(1)
O(17)	8821(1)	8205(2)	1334(1)	31(1)
O(18)	9680(1)	9659(2)	1438(1)	35(1)
N(1)	4940(2)	2860(3)	9920(2)	44(1)
N(2)	2994(2)	1555(3)	8004(2)	45(1)
N(3)	2150(2)	386(3)	1187(2)	64(2)
N(4)	1076(2)	3921(2)	1288(2)	38(1)
N(5)	9720(2)	6696(2)	1593(2)	38(1)
N(6)	9986(2)	10056(3)	2689(2)	42(1)
C(1)	5319(3)	3415(4)	9653(3)	64(2)
C(2)	5519(2)	2883(4)	9218(3)	61(2)
C(3)	5167(3)	1937(4)	8392(3)	67(2)
C(4)	4594(3)	1589(4)	7938(3)	67(2)
C(5)	3775(3)	518(4)	7826(3)	68(2)
C(6)	3217(3)	1120(4)	7559(2)	60(2)
C(7)	5300(2)	2087(3)	10267(2)	45(1)
C(8)	4908(2)	1355(4)	10417(2)	50(1)
C(9)	4047(2)	366(4)	9996(2)	48(1)
C(10)	3536(2)	218(3)	9430(2)	49(1)
C(11)	2646(2)	1088(4)	8836(2)	58(2)
C(12)	2644(2)	883(4)	8233(2)	65(2)
C(13)	4657(3)	3461(5)	10251(2)	73(2)
C(14A)	4145(7)	4001(12)	9955(6)	71(5)
C(14B)	3978(6)	3340(14)	10106(5)	49(5)
C(15)	3453(4)	4204(5)	9197(3)	94(2)

C(16)	3075(3)	4012(4)	8640(2)	59(2)
C(17)	3020(3)	3220(4)	7747(2)	55(2)
C(18)	2620(2)	2389(4)	7756(2)	57(2)
C(19)	2291(3)	295(4)	633(2)	69(2)
C(20)	2649(3)	1101(5)	519(2)	76(2)
C(21)	2644(3)	2785(5)	468(2)	67(2)
C(22)	2299(3)	3599(4)	577(2)	57(2)
C(23)	2138(2)	4396(3)	1406(2)	51(1)
C(24)	1473(2)	4653(3)	1183(2)	44(1)
C(25)	1671(4)	-281(4)	1224(2)	78(2)
C(26)	1057(3)	-101(3)	779(2)	57(2)
C(27)	324(2)	1056(3)	376(2)	40(1)
C(28)	164(2)	2055(3)	424(2)	41(1)
C(29)	440(2)	3605(3)	270(2)	41(1)
C(30)	455(2)	4004(3)	851(2)	39(1)
C(31A)	2866(10)	506(16)	1655(9)	34(5)
C(32A)	2752(7)	712(11)	2249(8)	33(5)
C(31B)	2640(7)	184(11)	1716(6)	42(3)
C(32B)	2917(5)	1068(10)	1997(6)	44(4)
C(33)	2234(3)	1536(4)	2618(2)	60(2)
C(34)	1821(2)	2332(4)	2628(2)	55(2)
C(35)	862(2)	3017(3)	2078(2)	43(1)
C(36)	1038(2)	3950(3)	1890(2)	43(1)
C(37)	9639(2)	5986(3)	2001(2)	48(1)
C(38)	9993(2)	6221(4)	2635(3)	58(2)
C(39)	9249(2)	7073(4)	2948(2)	47(1)
C(40)	9135(2)	8029(4)	3137(2)	49(1)
C(41)	8985(2)	9605(3)	2804(2)	50(1)
C(42)	9606(2)	10077(4)	3083(2)	51(1)
C(43)	10283(2)	6540(3)	1438(2)	47(1)

C(44)	10525(2)	7428(3)	1250(2)	45(1)
C(45)	11277(2)	7901(4)	2138(3)	61(2)
C(46)	11389(2)	8617(4)	2614(2)	61(2)
C(47)	10929(2)	9231(5)	3292(2)	67(2)
C(48)	10651(3)	10149(4)	3021(2)	61(2)
C(49)	9179(2)	6720(3)	1062(2)	41(1)
C(50)	8653(2)	7271(3)	1163(2)	40(1)
C(51)	8817(2)	8796(3)	857(2)	41(1)
C(52)	9043(2)	9737(3)	1100(2)	45(1)
C(53)	9947(2)	10525(3)	1687(2)	46(1)
C(54)	9786(3)	10777(3)	2230(2)	48(1)

Table A.3: Bond lengths [Å] and angles [°] for $[Na\ (cp)]_3[Ge_9]$.

O(5)-C(14A)	1.532(15)	N(2)-C(12)	1.462(6)
O(6)-C(16)	1.428(5)	N(2)-C(18)	1.475(6)
O(6)-C(17)	1.435(6)	N(3)-C(31B)	1.429(13)
O(7)-C(20)	1.425(6)	N(3)-C(19)	1.468(7)
O(7)-C(21)	1.431(6)	N(3)-C(25)	1.472(8)
O(8)-C(22)	1.412(5)	N(3)-C(31A)	1.67(2)
O(8)-C(23)	1.454(5)	N(4)-C(24)	1.455(5)
O(9)-C(27)	1.413(5)	N(4)-C(36)	1.475(5)
O(9)-C(26)	1.420(5)	N(4)-C(30)	1.475(6)
O(10)-C(28)	1.420(5)	N(5)-C(43)	1.461(6)
O(10)-C(29)	1.446(5)	N(5)-C(37)	1.461(6)
O(11)-C(33)	1.387(6)	N(5)-C(49)	1.465(6)
O(11)-C(32B)	1.474(10)	N(6)-C(54)	1.471(6)
O(11)-C(32A)	1.485(13)	N(6)-C(42)	1.471(6)
O(12)-C(35)	1.411(5)	N(6)-C(48)	1.476(6)
O(12)-C(34)	1.432(5)	C(1)-C(2)	1.477(8)
O(13)-C(38)	1.420(6)	C(1)-H(1A)	0.9900
O(13)-C(39)	1.425(6)	C(1)-H(1B)	0.9900
O(14)-C(40)	1.407(5)	C(2)-H(2A)	0.9900
O(14)-C(41)	1.434(6)	C(2)-H(2B)	0.9900
O(15)-C(45)	1.412(6)	C(3)-C(4)	1.494(8)
O(15)-C(44)	1.425(5)	C(3)-H(3A)	0.9900
O(16)-C(46)	1.420(6)	C(3)-H(3B)	0.9900
O(16)-C(47)	1.421(7)	C(4)-H(4A)	0.9900
O(17)-C(50)	1.413(5)	C(4)-H(4B)	0.9900
O(17)-C(51)	1.420(5)	C(5)-C(6)	1.499(7)
O(18)-C(53)	1.424(5)	C(5)-H(5A)	0.9900

O(18)-C(52)	1.425(5)	C(5)-H(5B)	0.9900
N(1)-C(13)	1.453(6)	C(6)-H(6A)	0.9900
N(1)-C(1)	1.461(7)	C(6)-H(6B)	0.9900
N(1)-C(7)	1.467(6)	C(7)-C(8)	1.491(7)
N(2)-C(6)	1.458(6)	C(7)-H(7A)	0.9900
C(7)-H(7B)	0.9900	C(18)-H(18A)	0.9900
C(8)-H(8A)	0.9900	C(18)-H(18B)	0.9900
C(8)-H(8B)	0.9900	C(19)-C(20)	1.486(8)
C(9)-C(10)	1.497(7)	C(19)-H(19A)	0.9900
C(9)-H(9A)	0.9900	C(19)-H(19B)	0.9900
C(9)-H(9B)	0.9900	C(20)-H(20A)	0.9900
C(10)-H(10A)	0.9900	C(20)-H(20B)	0.9900
C(10)-H(10B)	0.9900	C(21)-C(22)	1.473(8)
C(11)-C(12)	1.477(7)	C(21)-H(21A)	0.9900
C(11)-H(11A)	0.9900	C(21)-H(21B)	0.9900
C(11)-H(11B)	0.9900	C(22)-H(22A)	0.9900
C(12)-H(12A)	0.9900	C(22)-H(22B)	0.9900
C(12)-H(12B)	0.9900	C(23)-C(24)	1.482(6)
C(13)-C(14A)	1.389(12)	C(23)-H(23A)	0.9900
C(13)-C(14B)	1.481(14)	C(23)-H(23B)	0.9900
C(13)-H(13A)	0.9900	C(24)-H(24A)	0.9900
C(13)-H(13B)	0.9900	C(24)-H(24B)	0.9900
C(14A)-C(15)	2.016(14)	C(25)-C(26)	1.488(8)
C(14A)-H(14A)	0.9900	C(25)-H(25A)	0.9900
C(14A)-H(14B)	0.9900	C(25)-H(25B)	0.9900
C(14B)-H(14C)	0.9900	C(26)-H(26A)	0.9900
C(14B)-H(14D)	0.9900	C(26)-H(26B)	0.9900
C(15)-C(16)	1.367(8)	C(27)-C(28)	1.486(6)
C(15)-H(15A)	0.9900	C(27)-H(27A)	0.9900
C(15)-H(15B)	0.9900	C(27)-H(27B)	0.9900

C(16)-H(16A)	0.9900	C(28)-H(28A)	0.9900
C(16)-H(16B)	0.9900	C(28)-H(28B)	0.9900
C(17)-C(18)	1.500(7)	C(29)-C(30)	1.497(6)
C(17)-H(17A)	0.9900	C(29)-H(29A)	0.9900
C(17)-H(17B)	0.9900	C(29)-H(29B)	0.9900
C(30)-H(30A)	0.9900	C(40)-H(40A)	0.9900
C(30)-H(30B)	0.9900	C(40)-H(40B)	0.9900
C(31A)-C(32A)	1.56(4)	C(41)-C(42)	1.515(7)
C(31A)-H(31A)	0.9900	C(41)-H(41A)	0.9900
C(31A)-H(31B)	0.9900	C(41)-H(41B)	0.9900
C(32A)-H(32A)	0.9900	C(42)-H(42A)	0.9900
C(32A)-H(32B)	0.9900	C(42)-H(42B)	0.9900
C(31B)-C(32B)	1.48(2)	C(43)-C(44)	1.508(6)
C(31B)-H(31C)	0.9900	C(43)-H(43A)	0.9900
C(31B)-H(31D)	0.9900	C(43)-H(43B)	0.9900
C(32B)-H(32C)	0.9900	C(44)-H(44A)	0.9900
C(32B)-H(32D)	0.9900	C(44)-H(44B)	0.9900
C(33)-C(34)	1.481(7)	C(45)-C(46)	1.495(8)
C(33)-H(33A)	0.9900	C(45)-H(45A)	0.9900
C(33)-H(33B)	0.9900	C(45)-H(45B)	0.9900
C(34)-H(34A)	0.9900	C(46)-H(46A)	0.9900
C(34)-H(34B)	0.9900	C(46)-H(46B)	0.9900
C(35)-C(36)	1.502(6)	C(47)-C(48)	1.511(8)
C(35)-H(35A)	0.9900	C(47)-H(47A)	0.9900
C(35)-H(35B)	0.9900	C(47)-H(47B)	0.9900
C(36)-H(36A)	0.9900	C(48)-H(48A)	0.9900
C(36)-H(36B)	0.9900	C(48)-H(48B)	0.9900
C(37)-C(38)	1.518(7)	C(49)-C(50)	1.516(6)
C(37)-H(37A)	0.9900	C(49)-H(49A)	0.9900
C(37)-H(37B)	0.9900	C(49)-H(49B)	0.9900

C(38)-H(38A)	0.9900	C(50)-H(50A)	0.9900
C(38)-H(38B)	0.9900	C(50)-H(50B)	0.9900
C(39)-C(40)	1.486(7)	C(51)-C(52)	1.490(6)
C(39)-H(39A)	0.9900	C(51)-H(51A)	0.9900
C(39)-H(39B)	0.9900	C(51)-H(51B)	0.9900
C(52)-H(52A)	0.9900	Ge(8)-Ge(4)-Ge(1)	59.460(19)
C(52)-H(52B)	0.9900	Ge(7)-Ge(4)-Ge(1)	102.55(2)
C(53)-C(54)	1.506(6)	Ge(9)-Ge(5)-Ge(1)	108.26(2)
C(53)-H(53A)	0.9900	Ge(9)-Ge(5)-Ge(2)	109.64(2)
C(53)-H(53B)	0.9900	Ge(1)-Ge(5)-Ge(2)	58.77(2)
C(54)-H(54A)	0.9900	Ge(9)-Ge(5)-Ge(6)	57.080(17)
C(54)-H(54B)	0.9900	Ge(1)-Ge(5)-Ge(6)	98.79(2)
		Ge(2)-Ge(5)-Ge(6)	58.240(18)
Ge(2)-Ge(1)-Ge(8)	106.64(2)	Ge(9)-Ge(5)-Ge(8)	56.917(17)
Ge(2)-Ge(1)-Ge(5)	60.72(2)	Ge(1)-Ge(5)-Ge(8)	57.189(17)
Ge(8)-Ge(1)-Ge(5)	64.969(19)	Ge(2)-Ge(5)-Ge(8)	99.65(2)
Ge(2)-Ge(1)-Ge(4)	94.32(3)	Ge(6)-Ge(5)-Ge(8)	90.097(19)
Ge(8)-Ge(1)-Ge(4)	60.129(19)	Ge(9)-Ge(6)-Ge(3)	106.34(2)
Ge(5)-Ge(1)-Ge(4)	107.55(2)	Ge(9)-Ge(6)-Ge(2)	109.98(2)
Ge(3)-Ge(2)-Ge(1)	85.81(3)	Ge(3)-Ge(6)-Ge(2)	58.52(2)
Ge(3)-Ge(2)-Ge(5)	102.43(2)	Ge(9)-Ge(6)-Ge(5)	57.801(17)
Ge(1)-Ge(2)-Ge(5)	60.52(2)	Ge(3)-Ge(6)-Ge(5)	96.99(2)
Ge(3)-Ge(2)-Ge(6)	60.53(2)	Ge(2)-Ge(6)-Ge(5)	57.897(18)
Ge(1)-Ge(2)-Ge(6)	103.93(2)	Ge(9)-Ge(6)-Ge(7)	56.663(17)
Ge(5)-Ge(2)-Ge(6)	63.863(19)	Ge(3)-Ge(6)-Ge(7)	55.571(17)
Ge(2)-Ge(3)-Ge(7)	109.33(3)	Ge(2)-Ge(6)-Ge(7)	99.15(2)
Ge(2)-Ge(3)-Ge(4)	95.41(3)	Ge(5)-Ge(6)-Ge(7)	89.769(18)
Ge(7)-Ge(3)-Ge(4)	61.191(19)	Ge(3)-Ge(7)-Ge(9)	107.26(2)
Ge(2)-Ge(3)-Ge(6)	60.95(2)	Ge(3)-Ge(7)-Ge(4)	59.67(2)
Ge(7)-Ge(3)-Ge(6)	67.08(2)	Ge(9)-Ge(7)-Ge(4)	110.55(2)

Ge(4)-Ge(3)-Ge(6)	109.65(3)	Ge(3)-Ge(7)-Ge(8)	96.93(2)
Ge(3)-Ge(4)-Ge(8)	100.64(2)	Ge(9)-Ge(7)-Ge(8)	57.262(17)
Ge(3)-Ge(4)-Ge(7)	59.141(19)	Ge(4)-Ge(7)-Ge(8)	57.938(17)
Ge(8)-Ge(4)-Ge(7)	63.943(18)	Ge(3)-Ge(7)-Ge(6)	57.354(18)
Ge(3)-Ge(4)-Ge(1)	84.45(2)	Ge(9)-Ge(7)-Ge(6)	55.908(17)
Ge(4)-Ge(7)-Ge(6)	101.50(2)	O(4)-Na(1)-O(2)	98.16(12)
Ge(8)-Ge(7)-Ge(6)	88.862(19)	O(3)-Na(1)-O(2)	94.47(11)
Ge(9)-Ge(8)-Ge(1)	109.33(2)	O(6)-Na(1)-O(2)	102.41(11)
Ge(9)-Ge(8)-Ge(4)	111.28(2)	O(5)-Na(1)-N(1)	66.33(12)
Ge(1)-Ge(8)-Ge(4)	60.41(2)	O(1)-Na(1)-N(1)	65.11(12)
Ge(9)-Ge(8)-Ge(7)	57.877(17)	O(4)-Na(1)-N(1)	116.39(13)
Ge(1)-Ge(8)-Ge(7)	99.19(2)	O(3)-Na(1)-N(1)	64.39(12)
Ge(4)-Ge(8)-Ge(7)	58.119(17)	O(6)-Na(1)-N(1)	110.01(12)
Ge(9)-Ge(8)-Ge(5)	57.455(18)	O(2)-Na(1)-N(1)	120.85(13)
Ge(1)-Ge(8)-Ge(5)	57.842(18)	O(5)-Na(1)-N(2)	108.70(13)
Ge(4)-Ge(8)-Ge(5)	102.54(2)	O(1)-Na(1)-N(2)	115.60(12)
Ge(7)-Ge(8)-Ge(5)	91.271(18)	O(4)-Na(1)-N(2)	65.57(12)
Ge(6)-Ge(9)-Ge(8)	100.19(2)	O(3)-Na(1)-N(2)	120.63(12)
Ge(6)-Ge(9)-Ge(5)	65.119(19)	O(6)-Na(1)-N(2)	64.15(12)
Ge(8)-Ge(9)-Ge(5)	65.628(19)	O(2)-Na(1)-N(2)	63.41(12)
Ge(6)-Ge(9)-Ge(7)	67.429(19)	N(1)-Na(1)-N(2)	173.96(13)
Ge(8)-Ge(9)-Ge(7)	64.861(19)	O(9)-Na(2)-O(8)	159.29(12)
Ge(5)-Ge(9)-Ge(7)	100.41(2)	O(9)-Na(2)-O(7)	101.74(12)
O(5)-Na(1)-O(1)	113.77(14)	O(8)-Na(2)-O(7)	65.99(11)
O(5)-Na(1)-O(4)	85.91(13)	O(9)-Na(2)-O(11)	110.77(12)
O(1)-Na(1)-O(4)	156.74(13)	O(8)-Na(2)-O(11)	88.04(12)
O(5)-Na(1)-O(3)	97.60(12)	O(7)-Na(2)-O(11)	97.52(12)
O(1)-Na(1)-O(3)	99.24(11)	O(9)-Na(2)-O(12)	91.04(11)
O(4)-Na(1)-O(3)	64.44(11)	O(8)-Na(2)-O(12)	105.38(11)
O(5)-Na(1)-O(6)	65.45(11)	O(7)-Na(2)-O(12)	160.95(12)

O(1)-Na(1)-O(6)	92.72(11)	O(11)-Na(2)-O(12)	64.45(11)
O(4)-Na(1)-O(6)	107.31(11)	O(9)-Na(2)-O(10)	65.77(10)
O(3)-Na(1)-O(6)	162.30(11)	O(8)-Na(2)-O(10)	97.87(10)
O(5)-Na(1)-O(2)	167.86(13)	O(7)-Na(2)-O(10)	95.94(11)
O(1)-Na(1)-O(2)	65.26(12)	O(11)-Na(2)-O(10)	166.54(12)
O(12)-Na(2)-O(10)	102.22(10)	O(13)-Na(3)-N(6)	111.01(13)
O(9)-Na(2)-N(3)	65.12(14)	O(17)-Na(3)-N(6)	114.51(12)
O(8)-Na(2)-N(3)	119.13(16)	O(14)-Na(3)-N(6)	68.02(11)
O(7)-Na(2)-N(3)	65.43(14)	O(16)-Na(3)-N(6)	69.10(13)
O(11)-Na(2)-N(3)	64.70(11)	O(15)-Na(3)-N(6)	110.39(12)
O(12)-Na(2)-N(3)	108.67(13)	O(18)-Na(3)-N(5)	111.43(12)
O(10)-Na(2)-N(3)	121.36(12)	O(13)-Na(3)-N(5)	68.48(12)
O(9)-Na(2)-N(4)	114.01(12)	O(17)-Na(3)-N(5)	67.28(11)
O(8)-Na(2)-N(4)	64.31(11)	O(14)-Na(3)-N(5)	113.05(12)
O(7)-Na(2)-N(4)	120.92(12)	O(16)-Na(3)-N(5)	109.08(13)
O(11)-Na(2)-N(4)	110.47(11)	O(15)-Na(3)-N(5)	68.39(11)
O(12)-Na(2)-N(4)	64.48(10)	N(6)-Na(3)-N(5)	178.18(14)
O(10)-Na(2)-N(4)	62.24(10)	C(3)-O(1)-C(2)	110.9(4)
N(3)-Na(2)-N(4)	173.14(13)	C(3)-O(1)-Na(1)	117.9(3)
O(18)-Na(3)-O(13)	171.15(13)	C(2)-O(1)-Na(1)	122.2(3)
O(18)-Na(3)-O(17)	69.59(10)	C(4)-O(2)-C(5)	112.7(4)
O(13)-Na(3)-O(17)	102.98(11)	C(4)-O(2)-Na(1)	103.1(3)
O(18)-Na(3)-O(14)	105.60(12)	C(5)-O(2)-Na(1)	116.2(3)
O(13)-Na(3)-O(14)	67.28(12)	C(9)-O(3)-C(8)	112.9(4)
O(17)-Na(3)-O(14)	76.86(10)	C(9)-O(3)-Na(1)	115.3(3)
O(18)-Na(3)-O(16)	108.77(12)	C(8)-O(3)-Na(1)	119.6(3)
O(13)-Na(3)-O(16)	79.09(11)	C(11)-O(4)-C(10)	115.3(4)
O(17)-Na(3)-O(16)	174.32(13)	C(11)-O(4)-Na(1)	116.7(3)
O(14)-Na(3)-O(16)	108.78(12)	C(10)-O(4)-Na(1)	108.4(3)
O(18)-Na(3)-O(15)	78.59(11)	C(14B)-O(5)-C(15)	124.9(9)

O(13)-Na(3)-O(15)	108.93(12)	C(14B)-O(5)-C(14A)	45.2(6)
O(17)-Na(3)-O(15)	108.68(11)	C(15)-O(5)-C(14A)	85.9(7)
O(14)-Na(3)-O(15)	174.12(12)	C(14B)-O(5)-Na(1)	111.1(7)
O(16)-Na(3)-O(15)	65.66(12)	C(15)-O(5)-Na(1)	115.6(3)
O(18)-Na(3)-N(6)	69.37(12)	C(14A)-O(5)-Na(1)	119.7(5)
C(16)-O(6)-C(17)	113.5(4)	C(45)-O(15)-C(44)	113.3(4)
C(16)-O(6)-Na(1)	109.1(3)	C(45)-O(15)-Na(3)	113.6(3)
C(17)-O(6)-Na(1)	116.0(3)	C(44)-O(15)-Na(3)	110.8(2)
C(20)-O(7)-C(21)	115.0(4)	C(46)-O(16)-C(47)	112.8(4)
C(20)-O(7)-Na(2)	120.9(3)	C(46)-O(16)-Na(3)	114.4(3)
C(21)-O(7)-Na(2)	114.8(3)	C(47)-O(16)-Na(3)	111.2(3)
C(22)-O(8)-C(23)	115.1(4)	C(50)-O(17)-C(51)	113.3(3)
C(22)-O(8)-Na(2)	105.2(3)	C(50)-O(17)-Na(3)	114.9(2)
C(23)-O(8)-Na(2)	118.0(3)	C(51)-O(17)-Na(3)	109.0(2)
C(27)-O(9)-C(26)	110.6(4)	C(53)-O(18)-C(52)	113.1(3)
C(27)-O(9)-Na(2)	119.5(2)	C(53)-O(18)-Na(3)	114.3(3)
C(26)-O(9)-Na(2)	124.8(3)	C(52)-O(18)-Na(3)	110.6(2)
C(28)-O(10)-C(29)	111.0(3)	C(13)-N(1)-C(1)	110.2(5)
C(28)-O(10)-Na(2)	101.2(3)	C(13)-N(1)-C(7)	113.5(4)
C(29)-O(10)-Na(2)	117.9(2)	C(1)-N(1)-C(7)	110.9(4)
C(33)-O(11)-C(32B)	127.1(8)	C(13)-N(1)-Na(1)	108.1(3)
C(33)-O(11)-C(32A)	91.3(10)	C(1)-N(1)-Na(1)	105.0(3)
C(32B)-O(11)-C(32A)	37.6(5)	C(7)-N(1)-Na(1)	108.7(3)
C(33)-O(11)-Na(2)	116.0(3)	C(6)-N(2)-C(12)	110.7(4)
C(32B)-O(11)-Na(2)	106.8(5)	C(6)-N(2)-C(18)	109.8(4)
C(32A)-O(11)-Na(2)	123.1(6)	C(12)-N(2)-C(18)	111.6(4)
C(35)-O(12)-C(34)	113.1(4)	C(6)-N(2)-Na(1)	110.5(3)
C(35)-O(12)-Na(2)	115.2(2)	C(12)-N(2)-Na(1)	105.7(3)
C(34)-O(12)-Na(2)	110.8(3)	C(18)-N(2)-Na(1)	108.4(3)
C(38)-O(13)-C(39)	114.6(4)	C(31B)-N(3)-C(19)	117.1(7)

C(38)-O(13)-Na(3)	112.6(3)	C(31B)-N(3)-C(25)	101.4(8)
C(39)-O(13)-Na(3)	111.5(3)	C(19)-N(3)-C(25)	112.1(5)
C(40)-O(14)-C(41)	113.5(4)	C(31B)-N(3)-C(31A)	26.2(6)
C(40)-O(14)-Na(3)	112.3(3)	C(19)-N(3)-C(31A)	100.0(9)
C(41)-O(14)-Na(3)	113.6(3)	C(25)-N(3)-C(31A)	127.5(9)
C(31B)-N(3)-Na(2)	113.8(6)	C(1)-C(2)-H(2A)	109.8
C(19)-N(3)-Na(2)	106.3(3)	O(1)-C(2)-H(2B)	109.8
C(25)-N(3)-Na(2)	105.6(3)	C(1)-C(2)-H(2B)	109.8
C(31A)-N(3)-Na(2)	103.6(8)	H(2A)-C(2)-H(2B)	108.3
C(24)-N(4)-C(36)	112.5(4)	O(1)-C(3)-C(4)	108.6(4)
C(24)-N(4)-C(30)	109.1(4)	O(1)-C(3)-H(3A)	110.0
C(36)-N(4)-C(30)	110.7(4)	C(4)-C(3)-H(3A)	110.0
C(24)-N(4)-Na(2)	107.4(3)	O(1)-C(3)-H(3B)	110.0
C(36)-N(4)-Na(2)	106.4(3)	C(4)-C(3)-H(3B)	110.0
C(30)-N(4)-Na(2)	110.6(2)	H(3A)-C(3)-H(3B)	108.4
C(43)-N(5)-C(37)	111.8(4)	O(2)-C(4)-C(3)	107.4(5)
C(43)-N(5)-C(49)	110.2(4)	O(2)-C(4)-H(4A)	110.2
C(37)-N(5)-C(49)	110.5(4)	C(3)-C(4)-H(4A)	110.2
C(43)-N(5)-Na(3)	107.4(3)	O(2)-C(4)-H(4B)	110.2
C(37)-N(5)-Na(3)	108.0(3)	C(3)-C(4)-H(4B)	110.2
C(49)-N(5)-Na(3)	108.8(3)	H(4A)-C(4)-H(4B)	108.5
C(54)-N(6)-C(42)	111.2(4)	O(2)-C(5)-C(6)	114.6(4)
C(54)-N(6)-C(48)	111.3(4)	O(2)-C(5)-H(5A)	108.6
C(42)-N(6)-C(48)	111.3(4)	C(6)-C(5)-H(5A)	108.6
C(54)-N(6)-Na(3)	106.7(3)	O(2)-C(5)-H(5B)	108.6
C(42)-N(6)-Na(3)	109.0(3)	C(6)-C(5)-H(5B)	108.6
C(48)-N(6)-Na(3)	107.1(3)	H(5A)-C(5)-H(5B)	107.6
N(1)-C(1)-C(2)	112.9(4)	N(2)-C(6)-C(5)	112.1(4)
N(1)-C(1)-H(1A)	109.0	N(2)-C(6)-H(6A)	109.2
C(2)-C(1)-H(1A)	109.0	C(5)-C(6)-H(6A)	109.2

N(1)-C(1)-H(1B)	109.0	N(2)-C(6)-H(6B)	109.2
C(2)-C(1)-H(1B)	109.0	C(5)-C(6)-H(6B)	109.2
H(1A)-C(1)-H(1B)	107.8	H(6A)-C(6)-H(6B)	107.9
O(1)-C(2)-C(1)	109.2(4)	N(1)-C(7)-C(8)	113.3(4)
O(1)-C(2)-H(2A)	109.8	N(1)-C(7)-H(7A)	108.9
C(8)-C(7)-H(7A)	108.9	C(11)-C(12)-H(12A)	108.8
N(1)-C(7)-H(7B)	108.9	N(2)-C(12)-H(12B)	108.8
C(8)-C(7)-H(7B)	108.9	C(11)-C(12)-H(12B)	108.8
H(7A)-C(7)-H(7B)	107.7	H(12A)-C(12)-H(12B)	107.7
O(3)-C(8)-C(7)	109.3(4)	C(14A)-C(13)-N(1)	119.5(7)
O(3)-C(8)-H(8A)	109.8	C(14A)-C(13)-C(14B)	45.8(7)
C(7)-C(8)-H(8A)	109.8	N(1)-C(13)-C(14B)	114.3(7)
O(3)-C(8)-H(8B)	109.8	C(14A)-C(13)-H(13A)	107.4
C(7)-C(8)-H(8B)	109.8	N(1)-C(13)-H(13A)	107.4
H(8A)-C(8)-H(8B)	108.3	C(14B)-C(13)-H(13A)	66.2
O(3)-C(9)-C(10)	108.1(4)	C(14A)-C(13)-H(13B)	107.4
O(3)-C(9)-H(9A)	110.1	N(1)-C(13)-H(13B)	107.4
C(10)-C(9)-H(9A)	110.1	C(14B)-C(13)-H(13B)	137.8
O(3)-C(9)-H(9B)	110.1	H(13A)-C(13)-H(13B)	107.0
C(10)-C(9)-H(9B)	110.1	C(13)-C(14A)-O(5)	108.6(10)
H(9A)-C(9)-H(9B)	108.4	C(13)-C(14A)-C(15)	146.1(8)
O(4)-C(10)-C(9)	107.0(4)	O(5)-C(14A)-C(15)	44.8(4)
O(4)-C(10)-H(10A)	110.3	C(13)-C(14A)-H(14A)	110.0
C(9)-C(10)-H(10A)	110.3	O(5)-C(14A)-H(14A)	110.0
O(4)-C(10)-H(10B)	110.3	C(15)-C(14A)-H(14A)	72.3
C(9)-C(10)-H(10B)	110.3	C(13)-C(14A)-H(14B)	110.0
H(10A)-C(10)-H(10B)	108.6	O(5)-C(14A)-H(14B)	110.0
O(4)-C(11)-C(12)	112.8(4)	C(15)-C(14A)-H(14B)	100.6
O(4)-C(11)-H(11A)	109.0	H(14A)-C(14A)-H(14B)	108.4
C(12)-C(11)-H(11A)	109.0	O(5)-C(14B)-C(13)	113.6(10)

O(4)-C(11)-H(11B)	109.0	O(5)-C(14B)-H(14C)	108.8
C(12)-C(11)-H(11B)	109.0	C(13)-C(14B)-H(14C)	108.8
H(11A)-C(11)-H(11B)	107.8	O(5)-C(14B)-H(14D)	108.8
N(2)-C(12)-C(11)	114.0(4)	C(13)-C(14B)-H(14D)	108.8
N(2)-C(12)-H(12A)	108.8	H(14C)-C(14B)-H(14D)	107.7
C(16)-C(15)-O(5)	111.8(5)	C(20)-C(19)-H(19A)	109.0
C(16)-C(15)-C(14A)	157.4(6)	N(3)-C(19)-H(19B)	109.0
O(5)-C(15)-C(14A)	49.3(6)	C(20)-C(19)-H(19B)	109.0
C(16)-C(15)-H(15A)	109.3	H(19A)-C(19)-H(19B)	107.8
O(5)-C(15)-H(15A)	109.3	O(7)-C(20)-C(19)	109.7(4)
C(14A)-C(15)-H(15A)	90.7	O(7)-C(20)-H(20A)	109.7
C(16)-C(15)-H(15B)	109.3	C(19)-C(20)-H(20A)	109.7
O(5)-C(15)-H(15B)	109.3	O(7)-C(20)-H(20B)	109.7
C(14A)-C(15)-H(15B)	72.7	C(19)-C(20)-H(20B)	109.7
H(15A)-C(15)-H(15B)	107.9	H(20A)-C(20)-H(20B)	108.2
C(15)-C(16)-O(6)	110.6(5)	O(7)-C(21)-C(22)	108.7(4)
C(15)-C(16)-H(16A)	109.5	O(7)-C(21)-H(21A)	110.0
O(6)-C(16)-H(16A)	109.5	C(22)-C(21)-H(21A)	110.0
C(15)-C(16)-H(16B)	109.5	O(7)-C(21)-H(21B)	110.0
O(6)-C(16)-H(16B)	109.5	C(22)-C(21)-H(21B)	110.0
H(16A)-C(16)-H(16B)	108.1	H(21A)-C(21)-H(21B)	108.3
O(6)-C(17)-C(18)	112.4(4)	O(8)-C(22)-C(21)	107.6(4)
O(6)-C(17)-H(17A)	109.1	O(8)-C(22)-H(22A)	110.2
C(18)-C(17)-H(17A)	109.1	C(21)-C(22)-H(22A)	110.2
O(6)-C(17)-H(17B)	109.1	O(8)-C(22)-H(22B)	110.2
C(18)-C(17)-H(17B)	109.1	C(21)-C(22)-H(22B)	110.2
H(17A)-C(17)-H(17B)	107.9	H(22A)-C(22)-H(22B)	108.5
N(2)-C(18)-C(17)	111.7(4)	O(8)-C(23)-C(24)	114.0(4)
N(2)-C(18)-H(18A)	109.3	O(8)-C(23)-H(23A)	108.8
C(17)-C(18)-H(18A)	109.3	C(24)-C(23)-H(23A)	108.8

N(2)-C(18)-H(18B)	109.3	O(8)-C(23)-H(23B)	108.8
C(17)-C(18)-H(18B)	109.3	C(24)-C(23)-H(23B)	108.8
H(18A)-C(18)-H(18B)	107.9	H(23A)-C(23)-H(23B)	107.7
N(3)-C(19)-C(20)	112.9(5)	N(4)-C(24)-C(23)	112.2(4)
N(3)-C(19)-H(19A)	109.0	N(4)-C(24)-H(24A)	109.2
C(23)-C(24)-H(24A)	109.2	C(30)-C(29)-H(29A)	109.0
N(4)-C(24)-H(24B)	109.2	O(10)-C(29)-H(29B)	109.0
C(23)-C(24)-H(24B)	109.2	C(30)-C(29)-H(29B)	109.0
H(24A)-C(24)-H(24B)	107.9	H(29A)-C(29)-H(29B)	107.8
N(3)-C(25)-C(26)	112.9(4)	N(4)-C(30)-C(29)	111.5(4)
N(3)-C(25)-H(25A)	109.0	N(4)-C(30)-H(30A)	109.3
C(26)-C(25)-H(25A)	109.0	C(29)-C(30)-H(30A)	109.3
N(3)-C(25)-H(25B)	109.0	N(4)-C(30)-H(30B)	109.3
C(26)-C(25)-H(25B)	109.0	C(29)-C(30)-H(30B)	109.3
H(25A)-C(25)-H(25B)	107.8	H(30A)-C(30)-H(30B)	108.0
O(9)-C(26)-C(25)	109.2(4)	C(32A)-C(31A)-N(3)	103.0(16)
O(9)-C(26)-H(26A)	109.8	C(32A)-C(31A)-H(31A)	111.2
C(25)-C(26)-H(26A)	109.8	N(3)-C(31A)-H(31A)	111.2
O(9)-C(26)-H(26B)	109.8	C(32A)-C(31A)-H(31B)	111.2
C(25)-C(26)-H(26B)	109.8	N(3)-C(31A)-H(31B)	111.2
H(26A)-C(26)-H(26B)	108.3	H(31A)-C(31A)-H(31B)	109.1
O(9)-C(27)-C(28)	109.3(4)	O(11)-C(32A)-C(31A)	102.5(16)
O(9)-C(27)-H(27A)	109.8	O(11)-C(32A)-H(32A)	111.3
C(28)-C(27)-H(27A)	109.8	C(31A)-C(32A)-H(32A)	111.3
O(9)-C(27)-H(27B)	109.8	O(11)-C(32A)-H(32B)	111.3
C(28)-C(27)-H(27B)	109.8	C(31A)-C(32A)-H(32B)	111.3
H(27A)-C(27)-H(27B)	108.3	H(32A)-C(32A)-H(32B)	109.2
O(10)-C(28)-C(27)	109.1(4)	N(3)-C(31B)-C(32B)	109.5(12)
O(10)-C(28)-H(28A)	109.9	N(3)-C(31B)-H(31C)	109.8
C(27)-C(28)-H(28A)	109.9	C(32B)-C(31B)-H(31C)	109.8

O(10)-C(28)-H(28B)	109.9	N(3)-C(31B)-H(31D)	109.8
C(27)-C(28)-H(28B)	109.9	C(32B)-C(31B)-H(31D)	109.8
H(28A)-C(28)-H(28B)	108.3	H(31C)-C(31B)-H(31D)	108.2
O(10)-C(29)-C(30)	113.0(4)	O(11)-C(32B)-C(31B)	110.7(12)
O(10)-C(29)-H(29A)	109.0	O(11)-C(32B)-H(32C)	109.5
C(31B)-C(32B)-H(32C)	109.5	C(38)-C(37)-H(37A)	109.1
O(11)-C(32B)-H(32D)	109.5	N(5)-C(37)-H(37B)	109.1
C(31B)-C(32B)-H(32D)	109.5	C(38)-C(37)-H(37B)	109.1
H(32C)-C(32B)-H(32D)	108.1	H(37A)-C(37)-H(37B)	107.9
O(11)-C(33)-C(34)	108.6(4)	O(13)-C(38)-C(37)	113.1(4)
O(11)-C(33)-H(33A)	110.0	O(13)-C(38)-H(38A)	109.0
C(34)-C(33)-H(33A)	110.0	C(37)-C(38)-H(38A)	109.0
O(11)-C(33)-H(33B)	110.0	O(13)-C(38)-H(38B)	109.0
C(34)-C(33)-H(33B)	110.0	C(37)-C(38)-H(38B)	109.0
H(33A)-C(33)-H(33B)	108.4	H(38A)-C(38)-H(38B)	107.8
O(12)-C(34)-C(33)	108.5(4)	O(13)-C(39)-C(40)	107.8(4)
O(12)-C(34)-H(34A)	110.0	O(13)-C(39)-H(39A)	110.1
C(33)-C(34)-H(34A)	110.0	C(40)-C(39)-H(39A)	110.1
O(12)-C(34)-H(34B)	110.0	O(13)-C(39)-H(39B)	110.1
C(33)-C(34)-H(34B)	110.0	C(40)-C(39)-H(39B)	110.1
H(34A)-C(34)-H(34B)	108.4	H(39A)-C(39)-H(39B)	108.5
O(12)-C(35)-C(36)	114.5(4)	O(14)-C(40)-C(39)	108.5(4)
O(12)-C(35)-H(35A)	108.6	O(14)-C(40)-H(40A)	110.0
C(36)-C(35)-H(35A)	108.6	C(39)-C(40)-H(40A)	110.0
O(12)-C(35)-H(35B)	108.6	O(14)-C(40)-H(40B)	110.0
C(36)-C(35)-H(35B)	108.6	C(39)-C(40)-H(40B)	110.0
H(35A)-C(35)-H(35B)	107.6	H(40A)-C(40)-H(40B)	108.4
N(4)-C(36)-C(35)	112.0(4)	O(14)-C(41)-C(42)	112.4(4)
N(4)-C(36)-H(36A)	109.2	O(14)-C(41)-H(41A)	109.1
C(35)-C(36)-H(36A)	109.2	C(42)-C(41)-H(41A)	109.1

N(4)-C(36)-H(36B)	109.2	O(14)-C(41)-H(41B)	109.1
C(35)-C(36)-H(36B)	109.2	C(42)-C(41)-H(41B)	109.1
H(36A)-C(36)-H(36B)	107.9	H(41A)-C(41)-H(41B)	107.9
N(5)-C(37)-C(38)	112.3(4)	N(6)-C(42)-C(41)	111.3(4)
N(5)-C(37)-H(37A)	109.1	N(6)-C(42)-H(42A)	109.4
C(41)-C(42)-H(42A)	109.4	C(48)-C(47)-H(47A)	109.0
N(6)-C(42)-H(42B)	109.4	O(16)-C(47)-H(47B)	109.0
C(41)-C(42)-H(42B)	109.4	C(48)-C(47)-H(47B)	109.0
H(42A)-C(42)-H(42B)	108.0	H(47A)-C(47)-H(47B)	107.8
N(5)-C(43)-C(44)	112.4(4)	N(6)-C(48)-C(47)	111.9(4)
N(5)-C(43)-H(43A)	109.1	N(6)-C(48)-H(48A)	109.2
C(44)-C(43)-H(43A)	109.1	C(47)-C(48)-H(48A)	109.2
N(5)-C(43)-H(43B)	109.1	N(6)-C(48)-H(48B)	109.2
C(44)-C(43)-H(43B)	109.1	C(47)-C(48)-H(48B)	109.2
H(43A)-C(43)-H(43B)	107.9	H(48A)-C(48)-H(48B)	107.9
O(15)-C(44)-C(43)	112.2(4)	N(5)-C(49)-C(50)	111.2(4)
O(15)-C(44)-H(44A)	109.2	N(5)-C(49)-H(49A)	109.4
C(43)-C(44)-H(44A)	109.2	C(50)-C(49)-H(49A)	109.4
O(15)-C(44)-H(44B)	109.2	N(5)-C(49)-H(49B)	109.4
C(43)-C(44)-H(44B)	109.2	C(50)-C(49)-H(49B)	109.4
H(44A)-C(44)-H(44B)	107.9	H(49A)-C(49)-H(49B)	108.0
O(15)-C(45)-C(46)	108.1(4)	O(17)-C(50)-C(49)	112.4(4)
O(15)-C(45)-H(45A)	110.1	O(17)-C(50)-H(50A)	109.1
C(46)-C(45)-H(45A)	110.1	C(49)-C(50)-H(50A)	109.1
O(15)-C(45)-H(45B)	110.1	O(17)-C(50)-H(50B)	109.1
C(46)-C(45)-H(45B)	110.1	C(49)-C(50)-H(50B)	109.1
H(45A)-C(45)-H(45B)	108.4	H(50A)-C(50)-H(50B)	107.9
O(16)-C(46)-C(45)	107.5(4)	O(17)-C(51)-C(52)	107.8(4)
O(16)-C(46)-H(46A)	110.2	O(17)-C(51)-H(51A)	110.1
C(45)-C(46)-H(46A)	110.2	C(52)-C(51)-H(51A)	110.1

O(16)-C(46)-H(46B)	110.2	O(17)-C(51)-H(51B)	110.1
C(45)-C(46)-H(46B)	110.2	C(52)-C(51)-H(51B)	110.1
H(46A)-C(46)-H(46B)	108.5	H(51A)-C(51)-H(51B)	108.5
O(16)-C(47)-C(48)	113.0(4)	O(18)-C(52)-C(51)	108.3(4)
O(16)-C(47)-H(47A)	109.0	O(18)-C(52)-H(52A)	110.0
C(51)-C(52)-H(52A)	110.0		
O(18)-C(52)-H(52B)	110.0		
C(51)-C(52)-H(52B)	110.0		
H(52A)-C(52)-H(52B)	108.4		
O(18)-C(53)-C(54)	112.5(4)		
O(18)-C(53)-H(53A)	109.1		
C(54)-C(53)-H(53A)	109.1		
O(18)-C(53)-H(53B)	109.1		
C(54)-C(53)-H(53B)	109.1		
H(53A)-C(53)-H(53B)	107.8		
N(6)-C(54)-C(53)	112.3(4)		
N(6)-C(54)-H(54A)	109.2		
C(53)-C(54)-H(54A)	109.2		
N(6)-C(54)-H(54B)	109.2		
C(53)-C(54)-H(54B)	109.2		
H(54A)-C(54)-H(54B)	107.9		

Table A.4: Anisotropic displacement parameters ($Å^2 x\ 10^3$) for $[Na\ (cp)]_3[Ge_9]$. The anisotropic displacement factor exponent takes the form: $-2\pi^2[\ h^2 a^{*2} U^{11} + ... + 2\ h\ k\ a^*\ b^*\ U^{12}\ ]$

	U^{11}	U^{22}	U^{33}	U^{23}	U^{13}	U^{12}
Ge(1)	37(1)	85(1)	35(1)	9(1)	13(1)	10(1)
Ge(2)	72(1)	42(1)	39(1)	1(1)	20(1)	8(1)
Ge(3)	34(1)	98(1)	39(1)	-10(1)	10(1)	12(1)
Ge(4)	31(1)	49(1)	28(1)	1(1)	5(1)	4(1)
Ge(5)	31(1)	28(1)	38(1)	-3(1)	7(1)	-3(1)
Ge(6)	30(1)	29(1)	39(1)	4(1)	6(1)	5(1)
Ge(7)	31(1)	34(1)	34(1)	5(1)	12(1)	-2(1)
Ge(8)	35(1)	32(1)	33(1)	1(1)	12(1)	10(1)
Ge(9)	44(1)	42(1)	24(1)	1(1)	9(1)	4(1)
Na(1)	30(1)	33(1)	33(1)	-1(1)	12(1)	1(1)
Na(2)	40(1)	29(1)	28(1)	0(1)	11(1)	1(1)
Na(3)	32(1)	34(1)	28(1)	4(1)	5(1)	-2(1)
O(1)	34(2)	63(2)	45(2)	11(2)	16(2)	9(2)
O(2)	62(2)	59(2)	48(2)	5(2)	28(2)	13(2)
O(3)	39(2)	56(2)	33(2)	8(2)	12(2)	0(2)
O(4)	38(2)	49(2)	52(2)	12(2)	16(2)	-2(2)
O(5)	60(2)	63(2)	42(2)	-7(2)	5(2)	31(2)
O(6)	49(2)	43(2)	44(2)	4(2)	20(2)	18(2)
O(7)	38(2)	66(2)	39(2)	-18(2)	13(2)	-2(2)
O(8)	37(2)	43(2)	36(2)	3(2)	6(2)	-9(2)
O(9)	63(2)	24(2)	38(2)	-4(1)	20(2)	-1(2)
O(10)	40(2)	28(2)	45(2)	-4(1)	22(2)	-1(2)

O(11)	51(2)	51(2)	35(2)	-17(2)	-4(2)	13(2)
O(12)	39(2)	50(2)	31(2)	7(2)	6(2)	-3(2)
O(13)	40(2)	52(2)	42(2)	14(2)	7(2)	-8(2)
O(14)	52(2)	51(2)	26(2)	-5(2)	14(2)	-11(2)
O(15)	30(2)	36(2)	60(2)	2(2)	15(2)	3(2)
O(16)	32(2)	67(2)	50(2)	13(2)	4(2)	-10(2)
O(17)	33(2)	37(2)	22(2)	0(1)	6(1)	2(1)
O(18)	38(2)	30(2)	35(2)	5(1)	10(2)	4(1)
N(1)	40(2)	50(3)	32(2)	-9(2)	-4(2)	8(2)
N(2)	41(2)	55(3)	35(2)	-2(2)	7(2)	-4(2)
N(3)	89(4)	65(3)	21(2)	-9(2)	-4(2)	47(3)
N(4)	49(3)	30(2)	38(2)	-3(2)	19(2)	-10(2)
N(5)	40(2)	26(2)	51(3)	0(2)	20(2)	-3(2)
N(6)	50(3)	44(2)	36(2)	-14(2)	19(2)	-15(2)
C(1)	45(4)	58(4)	67(4)	7(3)	-14(3)	-19(3)
C(2)	30(3)	81(4)	66(4)	29(3)	6(3)	-5(3)
C(3)	62(4)	83(4)	76(4)	12(4)	50(4)	19(3)
C(4)	99(5)	67(4)	55(4)	3(3)	53(4)	15(4)
C(5)	96(5)	54(4)	61(4)	-13(3)	36(4)	11(4)
C(6)	77(4)	59(4)	35(3)	-9(3)	5(3)	-2(3)
C(7)	35(3)	63(3)	32(3)	-4(3)	3(2)	6(3)
C(8)	44(3)	73(4)	32(3)	7(3)	11(2)	14(3)
C(9)	46(3)	55(3)	47(3)	14(3)	20(3)	8(3)
C(10)	48(3)	41(3)	64(4)	6(3)	27(3)	-3(3)
C(11)	30(3)	75(4)	70(4)	11(3)	15(3)	-5(3)
C(12)	38(3)	78(4)	63(4)	-7(3)	-4(3)	-21(3)
C(13)	71(5)	80(4)	50(4)	-31(3)	-3(3)	19(4)
C(14A)	96(10)	50(10)	60(8)	-10(7)	14(7)	24(8)
C(14B)	55(8)	66(12)	24(7)	1(6)	11(6)	12(7)
C(15)	129(6)	84(5)	73(5)	-23(4)	39(5)	31(5)

C(16)	65(4)	65(4)	50(4)	9(3)	25(3)	40(3)
C(17)	62(4)	63(4)	36(3)	7(3)	12(3)	24(3)
C(18)	41(3)	79(4)	42(3)	2(3)	-3(3)	9(3)
C(19)	87(5)	72(4)	36(3)	-16(3)	3(3)	50(4)
C(20)	46(4)	137(6)	39(3)	-33(4)	5(3)	34(4)
C(21)	45(3)	130(6)	33(3)	-21(3)	23(3)	-23(4)
C(22)	64(4)	71(4)	33(3)	7(3)	10(3)	-29(3)
C(23)	54(4)	36(3)	54(3)	-2(3)	6(3)	-11(3)
C(24)	46(3)	39(3)	47(3)	1(2)	15(2)	-6(2)
C(25)	152(7)	32(3)	38(4)	4(3)	13(4)	29(4)
C(26)	104(5)	25(3)	40(3)	-1(2)	18(3)	4(3)
C(27)	50(3)	38(3)	40(3)	-9(2)	25(3)	-12(2)
C(28)	38(3)	40(3)	51(3)	-9(2)	23(2)	-7(2)
C(29)	52(3)	31(3)	37(3)	-2(2)	11(2)	6(2)
C(30)	44(3)	27(3)	40(3)	-3(2)	6(2)	4(2)
C(31A)	29(11)	42(12)	23(9)	7(8)	-1(8)	9(8)
C(32A)	34(8)	36(9)	23(9)	8(7)	1(6)	6(6)
C(31B)	42(8)	43(8)	43(7)	-2(6)	15(5)	11(6)
C(32B)	36(5)	58(8)	30(6)	-3(6)	0(4)	9(5)
C(33)	51(4)	50(3)	58(4)	25(3)	-10(3)	-10(3)
C(34)	48(3)	92(4)	20(3)	4(3)	5(2)	1(3)
C(35)	39(3)	65(4)	28(3)	4(2)	14(2)	-1(3)
C(36)	49(3)	50(3)	32(3)	-6(2)	13(2)	-8(3)
C(37)	49(3)	30(3)	71(4)	10(3)	27(3)	-1(2)
C(38)	42(3)	49(4)	80(4)	31(3)	14(3)	7(3)
C(39)	47(3)	61(4)	30(3)	10(2)	9(2)	-17(3)
C(40)	52(3)	65(4)	30(3)	-4(3)	14(2)	-20(3)
C(41)	57(3)	54(3)	48(3)	-13(3)	28(3)	-12(3)
C(42)	63(4)	52(3)	44(3)	-17(3)	28(3)	-13(3)
C(43)	46(3)	32(3)	72(4)	-8(3)	32(3)	0(2)

C(44)	42(3)	37(3)	63(4)	-1(3)	27(3)	4(2)
C(45)	24(3)	54(4)	100(5)	7(3)	14(3)	1(3)
C(46)	29(3)	81(4)	66(4)	9(3)	6(3)	-5(3)
C(47)	42(3)	119(6)	32(3)	6(4)	0(3)	-21(3)
C(48)	67(4)	73(4)	44(3)	-25(3)	17(3)	-30(3)
C(49)	46(3)	38(3)	45(3)	-17(2)	24(3)	-12(2)
C(50)	38(3)	48(3)	35(3)	-5(2)	14(2)	-11(2)
C(51)	40(3)	52(3)	28(3)	10(2)	5(2)	7(2)
C(52)	49(3)	46(3)	39(3)	18(2)	16(2)	16(3)
C(53)	59(3)	32(3)	53(3)	6(2)	26(3)	-3(2)
C(54)	65(4)	29(3)	57(4)	-5(2)	29(3)	-9(2)

Table A. 5: Hydrogen coordinates (x 10^4) and isotropic displacement parameters (Å^{2}x 10^3) for [Na (*cp*)]$_3$[Ge$_9$].

	x	y	z	U(eq)
H(1A)	5690	3643	9966	77
H(1B)	5078	3969	9459	77
H(2A)	5751	3298	9033	74
H(2B)	5796	2364	9415	74
H(3A)	5414	1402	8606	81
H(3B)	5424	2293	8202	81
H(4A)	4323	2122	7755	80
H(4B)	4703	1243	7628	80
H(5A)	3655	-9	8034	81
H(5B)	3910	251	7506	81
H(6A)	3322	1615	7319	72
H(6B)	2882	733	7296	72
H(7A)	5590	2343	10636	54
H(7B)	5550	1794	10044	54
H(8A)	5173	837	10633	60
H(8B)	4684	1625	10671	60
H(9A)	3877	621	10297	57
H(9B)	4255	-236	10141	57
H(10A)	3703	-40	9129	59
H(10B)	3226	-228	9487	59
H(11A)	2442	1700	8839	70
H(11B)	2401	603	8958	70

H(12A)	2819	250	8226	77
H(12B)	2209	873	7969	77
H(13A)	4535	3060	10532	87
H(13B)	4982	3893	10486	87
H(14A)	4272	4513	9740	85
H(14B)	3962	4282	10238	85
H(14C)	3896	2730	10263	58
H(14D)	3816	3838	10304	58
H(15A)	3223	4586	9402	113
H(15B)	3813	4575	9175	113
H(16A)	2924	4606	8431	70
H(16B)	2711	3650	8660	70
H(17A)	3290	3069	7507	66
H(17B)	2753	3754	7560	66
H(18A)	2348	2540	7993	69
H(18B)	2353	2251	7351	69
H(19A)	1897	239	306	83
H(19B)	2530	-287	645	83
H(20A)	3062	1123	822	91
H(20B)	2709	1025	131	91
H(21A)	2676	2821	66	80
H(21B)	3069	2781	752	80
H(22A)	2506	4188	525	68
H(22B)	1872	3600	299	68
H(23A)	2385	4911	1317	61
H(23B)	2263	4332	1838	61
H(24A)	1408	5237	1378	53
H(24B)	1355	4776	756	53
H(25A)	1628	-244	1621	93
H(25B)	1806	-924	1170	93

H(26A)	1073	-254	382	69
H(26B)	738	-502	860	69
H(27A)	-2	648	437	48
H(27B)	350	931	-21	48
H(28A)	-249	2192	140	49
H(28B)	149	2184	824	49
H(29A)	15	3670	-10	49
H(29B)	722	3971	114	49
H(30A)	334	4673	801	46
H(30B)	151	3670	995	46
H(31A)	3110	-75	1678	41
H(31B)	3086	1031	1539	41
H(32A)	2475	238	2334	40
H(32B)	3146	731	2577	40
H(31C)	2959	-203	1627	51
H(31D)	2475	-174	1987	51
H(32C)	3263	928	2359	52
H(32D)	3088	1418	1727	52
H(33A)	2586	1519	2988	71
H(33B)	2004	939	2581	71
H(34A)	1684	2292	2979	66
H(34B)	2044	2931	2643	66
H(35A)	811	3088	2470	52
H(35B)	457	2828	1800	52
H(36A)	727	4423	1909	52
H(36B)	1444	4144	2165	52
H(37A)	9784	5374	1901	58
H(37B)	9193	5928	1956	58
H(38A)	9923	5720	2891	70
H(38B)	10442	6237	2685	70

H(39A)	9275	6617	3265	56
H(39B)	8905	6884	2596	56
H(40A)	8762	8028	3264	59
H(40B)	9493	8235	3471	59
H(41A)	8741	9638	3079	60
H(41B)	8755	9948	2443	60
H(42A)	9538	10735	3176	61
H(42B)	9829	9755	3455	61
H(43A)	10196	6077	1115	56
H(43B)	10607	6273	1782	56
H(44A)	10887	7276	1122	55
H(44B)	10200	7699	910	55
H(45A)	11614	7922	1960	73
H(45B)	11267	7267	2300	73
H(46A)	11797	8511	2914	73
H(46B)	11385	9254	2450	73
H(47A)	11366	9337	3533	81
H(47B)	10703	9008	3558	81
H(48A)	10705	10622	3334	74
H(48B)	10875	10374	2754	74
H(49A)	9039	6072	944	49
H(49B)	9296	7011	738	49
H(50A)	8295	7272	797	48
H(50B)	8522	6958	1472	48
H(51A)	8391	8845	577	49
H(51B)	9090	8536	646	49
H(52A)	8992	10191	776	53
H(52B)	8800	9963	1350	53
H(53A)	9800	11028	1392	56
H(53B)	10403	10485	1788	56

H(54A)	9985	11380	2387	58
H(54B)	9331	10861	2124	58

APPENDIX B
CHARACTERIZATION TECHNIQUES

B.1 Raman Spectroscopy

The theory of Raman spectroscopy is based on an inelastic photon scattering. The first indication of the light scattering by long wave elastic sound waves was detected by Brillouin in 1922. It is called Brilliouin scattering and used for examination of solids. The following development was done by Smekal on a system that consists of two quantized energy levels in 1923. This theory builds the basic of the spontaneous Raman scattering studied out by Raman, Landsberg and Mandelstam in 1928.

It is proverbial that when a molecule is exposed to a light beam, this causes the transitions between the energy levels. Essentially, an incident photon of energy $\hbar\upsilon_i$ collides with a molecule of energy Ei in the initial energy level, end of the collision, $\hbar\upsilon_s$, energy of scattered photon and E_f, energy of the molecule remain unchanged, and the collision is called elastic (Rayleigh scattering). If energy transfer occurs between the molecule and the photon during the collision, it is called inelastic (Raman scattering). It means that the energy difference $\Delta E=E_f - E_i= \hbar (\upsilon_f - \upsilon_i)$, observed is rotational, vibrational, or electronic energy of the molecule. In the case of Raman scattering, the frequencies of incident and scattered photon are different. If the frequency of incident photon is higher than that of scattered photon, it gives rise to Stokes radiation, if the incident photon's frequency is less than the frequency of scattered photon; it is referred as anti- Stokes radiation [Fig.B.1]. Stokes radiation is generally more intense than anti- stokes radiation, because the photon loses the energy which appears in an excited vibrational or rotational energy of the molecule [53].

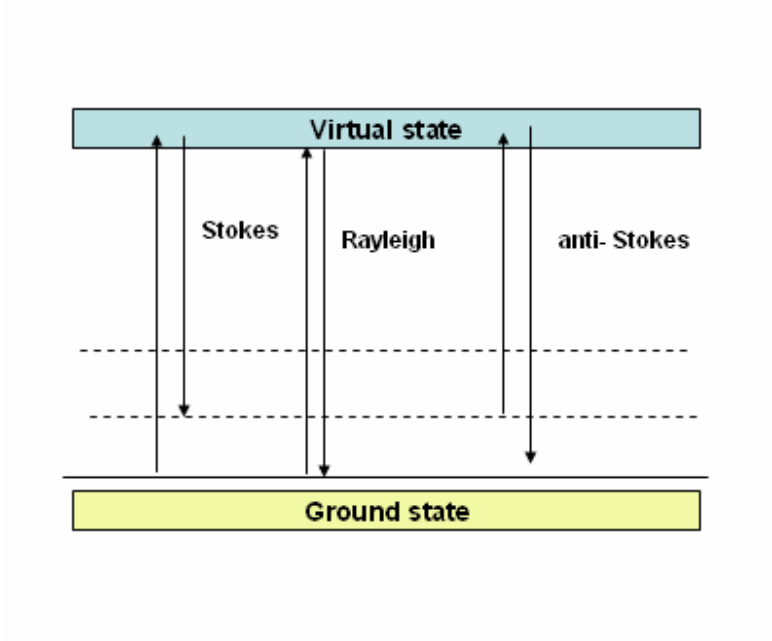

Figure B.1: Scheme of Raman energy levels.

Radiation scattered by molecules contains photons with the same frequency as the incident radiation, but may also contain photons with charged or shifted frequency. This effect is very weak approximately one photon out of a million (0.0001%). The photon will scatter from that sample at a wavelength slightly shifted from the original wavelength. The shifting frequency is referred as Raman effect.

B.1.1 Selection Rules

Selection rules are considered for assignment molecular vibrations that are Raman or infrared active. Especially, two basic rules are intrinsically important for the classification

of Raman and infrared active vibrations. The first one is called Mutual exclusion and the second one is based on the changes dipole moment or polarizability of a molecule.

According to mutual exclusion rule, the centre of symmetry in a molecule plays an important role in predicting Raman or infrared activity. If a molecule has centre of symmetry, then its vibration is Raman active and infrared inactive [54].

The other important criteria for the classification of vibrations according to Raman and infrared activities is that if normal vibrations alter the dipole moment of a molecule, the vibrations of the molecule are infrared active. Besides, if the polarizability of a molecule is changed during the normal vibrations, the vibrations are Raman active.

B.1.2 Types of Raman Spectroscopy

Several types of Raman spectroscopy have been developed to improve the sensitivity, spatial resolution and to get specific information. In the following, some of these types are explained briefly.

Spontaneous Raman spectroscopy:

Spontaneous Raman spectroscopy is widely used for the temperature dependent spectroscopic measurement of a molecule. The quality of the resolution of Raman spectra is high in this type Raman spectroscopy, on the other hand the laser used in this type must have high light intensity because the spontaneous signals are weak and this is the direct reason to use of rotating sample holder to prevent decomposition of the molecule during the measurement.

Resonance Raman spectroscopy:

Resonance Raman spectroscopy is a suitable technique for the characterization of large biomolecules. The incident laser energy or excitation frequency coincides with an electronic transition of the molecule or crystal, so the intensities of vibrational modes are increased and the Raman spectrum is easily interpreted.

Surface- Enhanced Raman Scattering:

In surface-enhanced Raman scattering (SERS), the sample that will be investigated is adsorbed at a metal surface such as silver, gold and copper. Fleishmann and coworkers observed that the Raman effect is enhanced when it is adsorbed on a metal surface in 1974 and the theory was explained by Van Duyne in 1977. The theory is based on the easiest excitation in metal surface by laser beam, so the nearby molecules of metal surface are done Raman active by the resulting electric field.

Coherent Anti-Stokes Raman Scattering:

This class of spectroscopy is commonly used in chemistry, physics and related fields. Coherent anti-Stokes Raman spectroscopy refers to Raman spectroscopy and lasing process. The difference of CASRS according to Raman spectroscopy is the lasing process that enhances the signals. The process was first found by Marker and Terhune. A sample exposes to Stokes frequency laser beam, the result of the interaction, a coherent anti-Stokes frequency beam is generated.

Coherent Stokes Raman Spectroscopy:

This technique is the inverse of the CASRS, in this process an anti – stokes frequency simulation beam is used for generation of a Stokes frequency beam. In spite of the

inclusive of the lasing process, it is disadvantageous according to starting of anti-stokes processes in a less populated excited state [55].

B.1.3 Instrumentation

Before the innovation of laser, mercury arc lamps were commonly used as an exciting source for Raman measurements, but the measurements took many hours because of the disability of the lamps. Now, lasers are preferred as a source for Raman spectrometer due to the advanced specialties such as; high beam quality, high stability, extended lifetime, extreme powerful. However, there are many different types of lasers that have different operation wavelengths and application areas. Krypton, xenon ion, helium-cadmium, helium-mercury, helium- selenium, Nd:YAG are frequently used laser types for scientific research.

Fundamentally, a Raman spectrometer consists of one laser beam, a sample holder, a collecting lens, a monochromator (a grating and a detector). The sample which is put in narrow glass or quartz tube is subjected to the laser beam. The light scattered from the sample is collected by a lens and transferred to monochromator. After the amplification, the spectrum presents in a computer.

In this research, RFS 100 Raman spectrometer is used for the all measurements. The laser is **Nd: YAG** (**neodymium-doped yttrium aluminium garnet**; **Nd:$Y_3Al_5O_{12}$**) that emits light at 1064 nm [56]. Besides, Ge (germanium) detector designed for 800- 1800 nm is used in the spectrometer and cooled with liquid nitrogen. All Raman spectroscopy measurements were performed with laser power: 200, scan: 1500 and, resolution:2 parameters. Additionally, 2 mm glass capillaries are used as a sample holder and the preparation is done in glove-box and the sample cell is sealed.

B.1.4 Advantages of Raman Technique

- It is possible to use glass or quartz as a sample cell because the incident and scattered radiation are at ultra-violet or visible frequencies.
- The small amount of samples can be measured in a short time due to the easily focused feature of the laser beam.
- Aqueous solutions can be identified correctly, because water has weak Raman scattering.
- Besides liquids and solid, samples in the gas phase can be characterized by Raman spectroscopy. In this case, laser beam is reflected several times back and forth to get good signals.

B.1.5 Disadvantages of Raman Technique

- The intense laser beam causes decomposition on the colored samples by heating for the reason that the colored sample may exhibit absorption band around the same frequency as incident laser. The rotation of the sample during the measurements is one of the solution ways for this problem.
- Sometimes, defects or impurities in the sample cause the fluorescence. When an exited molecule fails to ground state, the radiation is emitting and this is called fluorescence. The radiation inhibits the observation of weak Raman signal, but the problem is almost solved by using near- IR lasers (exp: Nd:YAG) because the Raman scattering is weak at the lower operating wavelength of this kind of lasers.

B.1.6 Application Area

Vibrations of the chemical bonds in a molecule are exclusive for every molecule, for this reason Raman spectrum of a molecule perceives the fingerprint of the molecule. This point of view, Raman spectroscopy is widely used many areas such as analysis of aerosol particles, molecular orientational relaxation, evaluation of the diameter of carbon nanotubes, determination of unsaturation in food oils and fats and so on.
Especially, changes in chemical bonds can be easily detected by Raman spectroscopy after the addition of a substrate in a molecule. However, if the crystal structure of a matter is known, it is easy to get information about the crystal orientation. Some fibers such as aramid, carbon and polypropylene have specific vibrational modes, when the changes with the applied of stress [55].

In addition to this, Raman spectroscopy facilitates the identification of the interaction metals with proteins due to the easy measurements of solution samples. Therefore Raman spectroscopy is an irrefutable characterization technique for biomedical applications.
As a result, because of supreme specialties of the Raman spectroscopy, it is commonly used as a spectroscopic characterization technique.

B.2 Glove Box

Glove box is a sealed container that is oxygen free atmosphere, filled with argon or nitrogen gas [Fig. B.2]. One or all sides of the boxes are transparent to allow the see manipulations. The transparent part has two gloves to achieve the manipulations in it. There are two types glove boxes are commonly used. One of them is to work actinide substances; the other is to work oxygen sensitive materials.

In this research, MBraun Unilab glove-box in which the oxygen and water levels are below 1 ppm, is used to prepare the precursors and to store the pure solvents. The argon gas is pumped from the argon tube and purified by removing solvent, water and oxygen from the gas. Heated copper metal, hydrogen-nitrogen mixture and molecular sieves are used in different steps for purification of gas before the arriving of the gas into the glove box.

Figure B.2: Inert atmosphere glove-box [57].

B.3 X- Ray Diffraction:

B.3.1 History:

X-rays were discovered by Wilhelm Conrad Röntgen in 1985. It has been firstly used in battlefield, in Italian- Ethiopian campaign because, it is possible to detect foreign bodies such as bullets, coins, etc. Besides, X-rays can be used to photograph the bones in the bodies [58].

In 1912, Max von Laue developed X-ray crystallography due to his diffraction experiment from a single crystal. In light, X-ray crystallography is widely used to identify structure of crystalline and amorphous compound in today.

B.3.2 Features of X-rays:

Acceleration or deceleration of electric charge in where electric (E) and magnetic (M) field exist, produces electromagnetic radiation. Electromagnetic radiations are classified according to their frequencies such as, radio waves, microwaves, terahertz radiation, infrared radiation, visible light, ultraviolet radiation, X-rays and gamma rays. The x-rays have wavelengths from ≈ 0.1 to ≈ 100 Å [Fig. 6]. Besides, the wavelenghts of x-rays in crystallography are the range that is the same order of magnitude as the shortest interatomic distances observed in both organic and inorganic materials, between ≈ 0.5 Å and ≈ 2.5 Å. When a sample is exposed to x-rays, there are three possible processes that may occur due to phenomenon of diffraction. The first one is coherent scattering. It means that inherent beam and scattering beam from the sample have the same wavelength. In this case, photon's energy in coherent scattering beam remains same that in the incident beam. The second one, incoherent (or Compton) scattering is that partial lose of photon energy in collisions with core electrons causes increasing the wavelength of the scattering beam [59].

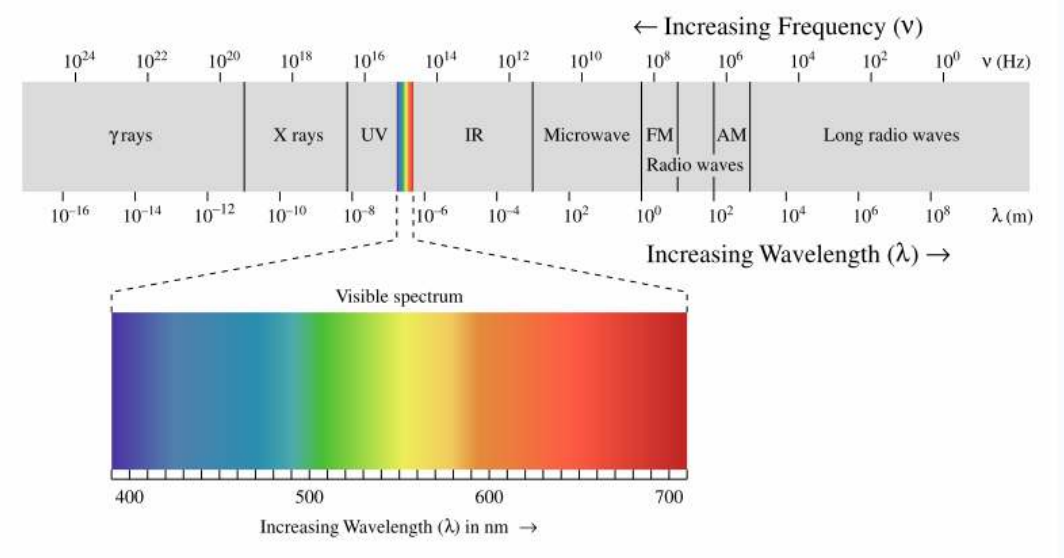

Figure B.3: Image of electromagnetic spectrum.

The last one is absorption of the x-rays, in this process, scattering leads to dispersion of some photons in random directions. Besides, in some cases, ejecting of electrons causes losing energy in some photon because of the photoelectric effect.

Basically, kinematical and dynamical theories of diffraction are two approximations that are used to get rid of the complications of the interaction of x-rays with a crystal. In the case of kinematical diffraction, it is assumed that interaction between the diffracted beam and the crystal is negligibly small. It means that when the beam is scattered, it is not possible to scatter it one more time.

On the other hand, the theory of dynamical diffraction is based on the considered scattering of the diffracted beam and other interactions of waves in the crystal.

B.3.3 Production of X-rays:

There are two different methods to produce X-ray radiation. In the first method, x-ray tube that has an anode made from tungsten, platinum, or another heavy metal of high melting

point and a cathode, is used. Application of high voltage gives rise to acceleration of electron stream from the cathode to the anode; as a result x-ray is produced [60].
The second method is based on synchrotron radiation. It means that high energy electrons are collected in a storage ring. The movement of the electrons causes the acceleration of them towards the center of the ring, thus emitting electromagnetic radiation. The strength of the magnetic field and electron's energy determine the maximum intensity that occurs as radio waves, visible light, or X-rays.
Finally, using of x-ray tube or synchrotron radiation to produce x-ray doesn't affect the diffraction phenomena.

B.3.4 Theory:

The interference pattern of X-rays scattering is explained by Bragg's law. According to Bragg's law, when x-rays are scattered from a crystal, angle of scattering and the pathlenght difference (equal to integer number of wavelengths) are determined peaks of scattered intensity and it is calculated by Bragg's equation (b.1).

$$n\lambda = 2d_{hkl}\sin\theta \quad \text{(b.1)}$$

where;

n: order of diffraction

λ: wavelength of the X-rays
d : the spacing of the layers

hkl: Miller indices (specifying plane orientation)
θ: the incident angle of the photons

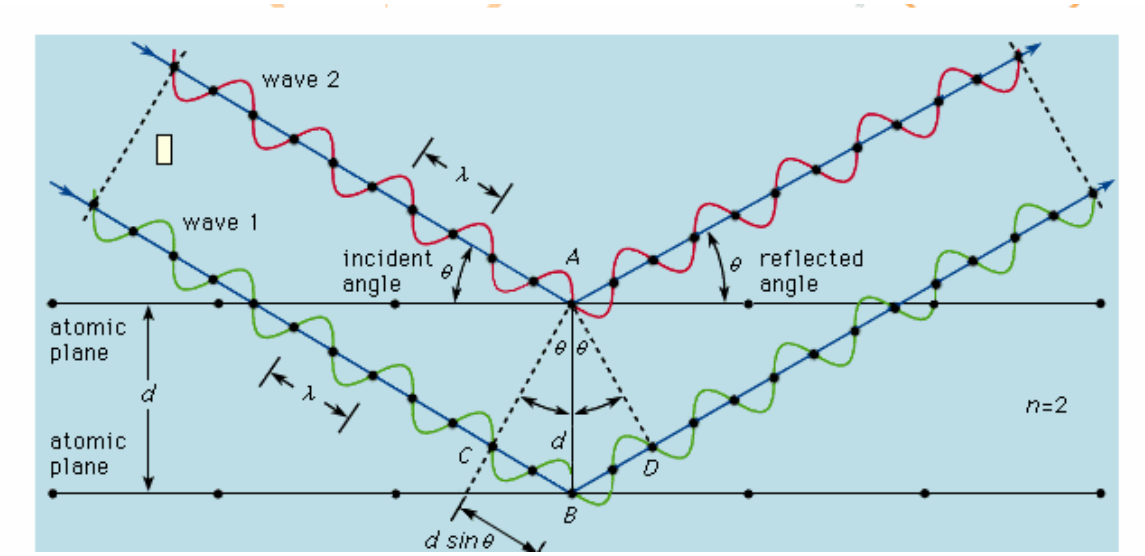

Figure B.4: Diffraction of X-rays on lattice planes due to Bragg equation.

Due to the equation b.1, in the case of single crystal diffraction, exhibiting a diffraction pattern with discrete diffraction beams in a defined direction relative to the orientation of the crystal and the incident beam [61]. It is important to express that the crystal is rotated in the X-ray beam in order to generate the complete diffraction pattern. Otherwise, some crystals from the same sample are exposed to X-rays, so each of them shows its characteristic pattern and then it will be superimpose.

On the other hand, in the case of powder diffraction, the sample has many tiny crystals so at the end of measurement, it is obtained complete circle for particular reflection. Additionally, if electronic detectors are used for measurement, it is possible to measure the intensity as a function of angle and a Bragg angle and intensity are obtained for each reflection. From this point of view, the 3D diffraction pattern is converted to 1D pattern by using variables of powder diffraction [61].

B.3.5 Powder Diffraction Method:

Powder diffraction is used to identify the structure of powder or microcrystalline samples. The technique has many advantageous such as; easy sample preparation, rapidity of measurements, and the ability of analyze mixed phases. On the other hand, powder data lack the three-dimensionality of a diffraction image. It means that each powder diffraction pattern represents a one-dimensional snapshot of the three-dimensional reciprocal lattice of a crystal.

Powder diffraction data are collected by powder diffractometers, affording digitized experimental data in the form of diffracted intensity as a numerical function of Bragg angle.

On the other hand, commonly, powder diffractometers use self-focusing geometries, that improve the diffracted intensity and the resolution of instrument. The focusing powder diffractometers perform θ-2θ scanning mode. When the incident and diffracted beams are formed by the angle of θ on the sample surface, the diffracted beam is formed by 2θ with incident beam [Fig. B.5].

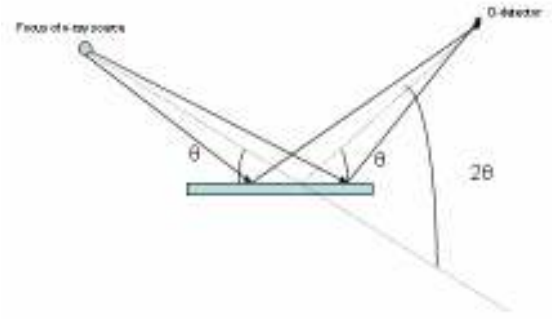

Figure B.5: The angles of the incident and the diffracted beam.

A powder diffraction pattern is basically considered by peak positions, peak intensities, peak shapes, and, background intensity distribution. In order, peak position determining unit- cell dimensions, peak intensities showing the positions of atoms in the unit cell, peak shape described using 2θ-dependent analytical functions, and, background intensity distribution producing from number of sources like fluorescent radiation emitted by the specimen, diffraction of a continuous spectrum of wavelengths, diffraction scattering from materials other than the specimen can be mentioned [62].

Consequently, when the x-ray beams interact with the crystalline powder of a sample, the beams are diffracted and diffracted beams are collected by a detector. After the conversion of diffraction data according to Bragg's law, the characteristic peaks of the sample are used for interpretation of the structure of the sample.

B.3.6 Sample preparation:

Sample preparation is very important for X-ray powder diffraction because the good powder diffraction pattern can be obtained from the same size particles. For this reason, the sample is grinded by using mortar and pestle or mechanical mills to reduce particle size. After that, the powder is placed in a capillary or a flat sample ring for measurement. If the sample is air sensitive, all operation is done in a glove-box and the grinded sample is sandwiched between two polyimide films. If the sample is air-stable, less air-tight Mylar film can be used for preparation.

All X-ray powder diffraction analysis was performed using HUBER image plate Guinier-camera (HUBER G670) equipped with a germanium monochromator and $CuK_{\alpha 1}$ radiation. The data were collected in the range of $3^0 \leq 2\theta \geq 100^0$ and a step size of 0.005 $^0 2\theta$.

B.3.7 Single Crystal Diffraction:

The method is used to characterize the 3D structure of complex and large inorganic and organometallic molecules. In this method, the X-ray beam is focused on a single crystal of the sample. Therefore, a single crystal that has identical unit cell must be selected for taking clear diffraction pattern. The electron numbers of the atoms are directly proportional to the intensities of X-rays diffracted by a crystal. However, X-rays are also absorbed by crystals in ratio to crystals dimension [61].
The size of crystal that will be measured should be a few tenths of millimeter. The quality of crystal to be measured is determined, recording of diffracted X-rays on photographic film. The figure B.6 shows the photographic film of a perfectly aligned single crystal.

Figure B.6: The photographic film by obtained recording of diffracted X-rays of well-aligned crystal [63].

Due to the obtained diffraction pattern, the space group can be assigned by comparison of intensities which are equivalent by symmetry and by noting that special subsets of reflections have zero intensity. During the measurement, data are collected and at the end, a list of reflections each with Miller indices and a measured intensity associated with

standard uncertainty (a measure of precision or reliability of the measurement) are indicated as a file. After that, the data are corrected and reduced due to changes in the incident X-ray beam intensity or in the scattering power of the crystal during the measurement [61]. Therefore, the data are used to interpret the structure according to atomic positions in the unit cell. The picture of an electron density distribution in the unit cell is expressed by the recombination of the objective to the diffracted beams and equation b.2 mathematically defines the process.

$$\rho(xyz) = \frac{1}{V}\sum_{h,k,l}\left|F(hkl)\right|\exp\left[i\varphi(hkl)\right]\exp\left[-2\pi i(hx+ky+lz)\right] \quad \text{(b.2)}$$

where;

F(hkl) : amplitude

φ : phase of wave

The important point is that the phases of reflection is unknown, despite the amplitude is measured and final exponential term is calculated. For this reason, Patterson, Direct methods are used to solve this. In the case of 'Direct methods'; the approximate reflection phases are determined from measured intensities. The method is mainly based on consideration of the most important reflections, the probe relation, and the probability relationships. Additionally, Fourier transforms are calculated using the observed amplitudes and trial phases to investigate molecular features [61]. At the end of the calculation, the accuracy of the obtained structure model is checked using 'residual or agreement index'. It is called R value which is expressed by equation b.3.

$$R = \frac{\sum_h \left|F_o(h)\right| - \left|F_c(h)\right|}{\sum_h \left|F_o(h)\right|} \quad \text{(b.3)}$$

where;

F_0: derived from the experiment

Fc: calculated from structure model

Finally, R value indicates the familiarity of the model to the real structure [63]. In addition to this, the equation 2.8 is converted to equation b.4 using F^2 instead of F values and weighting factor.

$$wR = \sqrt{\frac{\sum_0 w(F_0^2(h) - F_c^2(h))}{\sum_h w(F_0^2(h))^2}} \quad \text{(b.4)}$$

where;
w represents included weights, and 2 is written to remark that F^2 values are used to instead of F values [61].

Furthermore, the last value that is considered to support of quality of crystal structure refinement, is GooF (goodness of fit). GooF is expressed by equation b.5.

$$GooF = S = \sqrt{\frac{\sum_h w(F_0^2(h) - F_c^2(h))^2}{n - p}} \quad \text{(b.5)}$$

where;
n: number of reflections
p: total number of refined parameters

If the structure is correct, the GooF value is equal to 1.

B.3.8 Sample Preparation:

A well-shaped crystal which has a suitable size and well-formed edges and faces, can be held on a thin glass tube by using grease or on a glass fiber by using superglue or epoxy resin. After that, the crystal is placed on a detector and cooled by using liquid nitrogen to prevent radiation damage and to decrease thermal motion in the crystal.

In this research, the crystals were characterized with Oxford-Diffraction Xcalibur3 Diffractometer and MoK_α radiation. Therefore, the structure was solved and refined, using SHELXS-97 [64].

B.4 Electron Paramagnetic Resonance:

Electron paramagnetic resonance (EPR) or electron spin resonance (ESR) spectroscopy deals with the interaction of electromagnetic radiation with magnetic moments that arises from electrons. Significantly, the technique, developed by Zavoisky in 1944, is used to detect the species which have unpaired electrons [65].

EPR is similar with NMR (Nuclear magnetic resonance) spectroscopy due to their physical concepts, but in the case of EPR magnetic moments proceed by electrons rather than nuclei. However, EPR requires microwave-frequency radiation (GHz).

EPR spectroscopy is mainly used in the systems such as; free radicals in the solid, liquid or gaseous phase, transition ions including actinide ions, various point defects in solids, systems with more than one unpaired electron, and systems with conducting electrons.

B.4.1 Theory:

When an electron is placed in an external magnetic field of strength B_0, the electron aligns itself parallel or antiparallel to the magnetic field via its magnetic moment. From this interaction the electron absorbs energy due to its spin moment, ($m_s = \pm 1/2$, for a free electron).

$$E = h\nu = g\mu_B B \quad \text{(b.6)}$$

where;

g : gyromagnetic ratio (g factor)

μ_B : Bohr magneton

B : field strength of the external magnetic field

b.6 is the fundamental equation for EPR spectroscopy. Each magnetic species has a single unique g factor. Additionally, g factor is equal to $g_e = 2.0023$ for free electrons [66].

The energy, absorbed during the movement of a paramagnetic electron between two energy levels [Fig. B.7] is calculated and converted to an EPR spectrum.

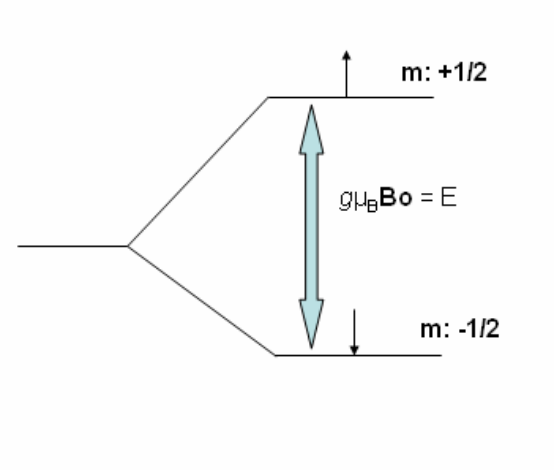

Figure B.7: Energy level scheme for a free electron, applied magnetic field B.

In general, the resonance appears at a magnetic field around 0.3 T, if frequency is equal to 9.75 GHz [66]. Additionally, measurements are sometimes made at frequencies other than 9 GHz. Because, the linewidth of EPR spectrum depends on magnetic field so it is easy to identify unresolved hyperfine structure with interpretation of the narrower lines.

In general, field-swept instruments are used to record EPR spectra. The spectra have the conventional absorption lineshape and the first derivative of it gives EPR signal that creates the spectrum [Fig. B.8].

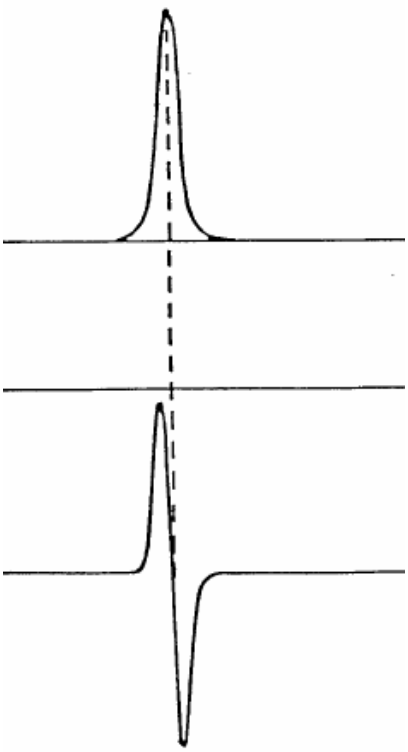

Figure B.8: Scheme of the absorption peak (top) and the derivative of it (bottom) [67].

The peak of the absorption curve, and equally the first derivative of it, is placed at the magnetic field for maximum absorption, B. υ in GHz and B in gauss (10000 gauss= 1 tesla) are inserted in the equation b.6, and thus, the operating frequency and the intensity of the magnetic field at which maximum EPR absorption occurs, lead to calculate g.

B.4.2 Instrumentation:

The determination of paramagnetic resonance in a sample is measured by EPR spectrometer. A spectrometer mainly consists of source, resonator, electromagnet, and, detector. Additionally, there are two types of spectrometer; one is a continuous wave

electron paramagnetic resonance spectrometer [Fig. B.9] and the other is an optical spectrometer (pulsed in the amplitude of B) [Fig. B.10].

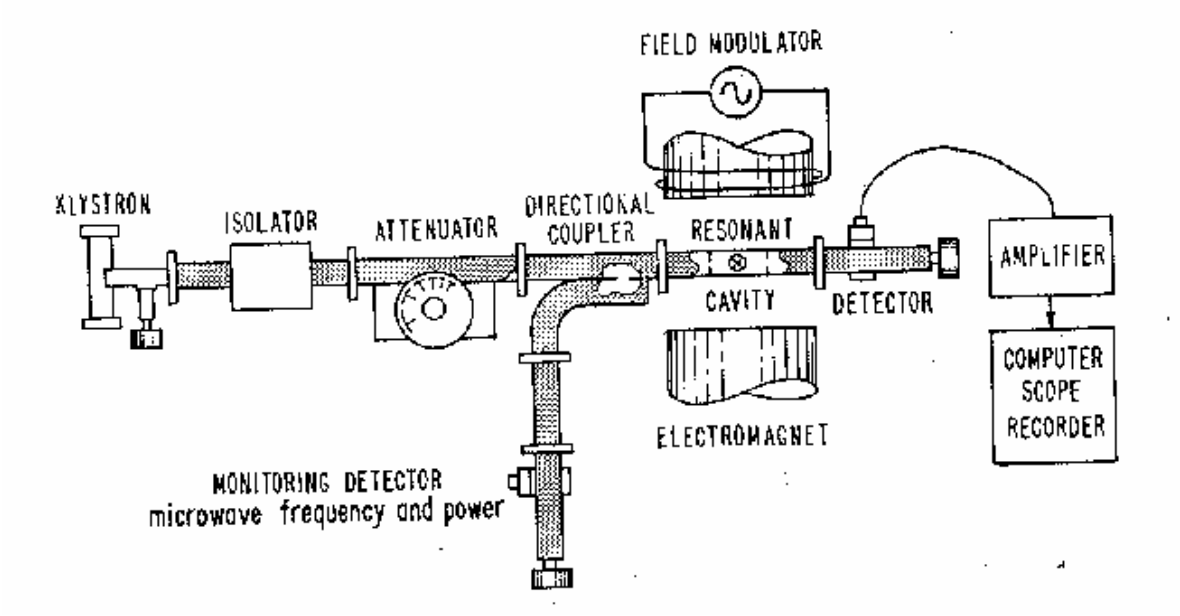

Figure B.9: Block diagram of a continuous-wave electron paramagnetic resonance spectrometer [66].

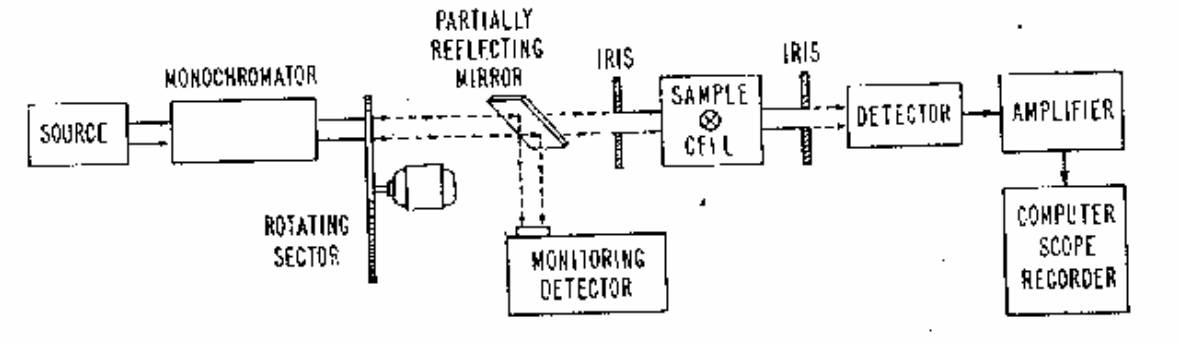

Figure B.10: Block diagram of an optical spectrometer [66].

In both cases, a sample is exposed to monochromatic radiation and the transmitted or reflected radiation is recorded by a detector. As mentioned above, the basic components of a spectrometer such as; source, resonator, electromagnet, and, detector are briefly explained below.

Source: In an EPR spectrometer, the radiant energy's frequency is generally 9.5GHz, in the medium-frequency microwave region. A klystron that is a vacuum tube is used as a microwave source for its low-noise characteristics. Additionally, the magnetic field, B, in the range of 1-100 GHz, is produced by oscillations within its own tunable cavity. Considerably, the microwave power is incident and pulsed for standard and certain modern spectrometer, respectively.

Resonator: A resonant cavity which admits microwaves through an iris is used for an EPR spectrometer. The frequency of the source is tuned to appropriate frequency of the cavity [66]. However, the resonant wavelengths depend on the dimension of cavity. When a resonant mode is operated, it maximizes B at the location of the sample.

Magnetic Field: The stability of magnetic field is a critical factor for EPR measurements. From this point of view, a Half- effect detector is used to control and operate to the magnitude of B.

Detector: There are many different types' solid-state diodes that are sensitive to microwave energy. When the energy differences is equal to the quantum energy, hυ, absorption peaks can be observed, this causes the change in detector current.

In addition to this, if samples contain high concentration of unpaired electrons, it is possible to detect absorption signals directly. But, in this case, noise to signal ratio is very high and making it detection difficult. For this reason, a light beam is commonly used for improving the signal to noise ratio in the optical spectrometer.

B.4.3 Sample Preparation:

Samples having unpaired electrons can be analyzed as solid or liquid [68]. For this purpose, The samples are placed in EPR tubes for measurement. The volume of samples alters 1-100 microliters depend on frequency of measurement.

In this research, sample preparation was done in glove-box because of the air sensitivity of the sample. Therefore, almost 150mg of the sample was put in an EPR tube and the tube was sealed to prevent air circulation during the measurement. Additionally, The X band (9.5 GHz) continous wave EPR measurements were performed using ESP 300E spectrometer (Bruker) equipped with a rectangular TE_{112} resonator. The magnetic field was read out with a NMR gauss meter (ER 035M, Bruker). All spectra were recorded at 10 K with an Oxford cryostat. Additionally, a standard field marker (polycrystalline DPPH with g= 2.0036) was used for calibration of the resonance magnetic field values and the determination of the exact g-factor of the samples.

B.5 Thermal Analysis

Thermal analysis is an analytic technique. It is used to monitor physical or chemical changes of a sample which occurs as the increasing or decreasing of sample temperature.

The basic thermoanalytical methods are differential thermal analysis, thermogravimetry, and, differential scanning calorimetry. In this research, differential thermal analysis and thermogravimetry are used as thermal analysis methods [69].

Investigation of stabilities of compounds and mixture of elevated temperature and determination of drying temperature for compounds and mixtures are easily done by thermogravimetry. In the case of differential thermal analysis, the temperature difference, T_D, between a sample and inert reference material (ex.: aluminum oxide) is monitored. They are heated, or cooled, at a predetermined rate. Commonly used temperature sensors; multijunction thermocouples and thermistors are placed in an oven. According to the temperature difference, T_D, enthalpic changes are observed. If T_D is positive, the process is exothermic, and if it is negative, the process is endothermic.

Some chemical and physical processes can be observed using differential thermal analysis as compared to thermogravimetry. Crystalline transition, fusion, vaporization, sublimation, desorption, and, adsorption can be considered as endothermic physical processes. On the other hand, endothermic chemical processes include dehydration, decomposition, gaseous reduction, redox reaction, and solid-state metathesis. In the case of exothermic processes, adsorbtion, chemisorbtion, decomposition, oxidation, redox reaction, and, solid-state metathesis reactions can be observed.

Application area of the technique can be summarized as the identification, characterization, and, quantitation of a wide variety of materials, including polymers, pharceuticals, metals, clays, minerals, and inorganic and organic compounds. Purity, heats of reaction, thermal stability, phase diagrams, catalytic properties, and, radiation damage
of compounds can be determined by the technique.

B.5.1 Instrumentation:

A differential thermal analyzer consists of a sample holder including thermocouples, sample containers, and a ceramic or metallic block, furnace, temperature program, recording system [Fig. B.11].

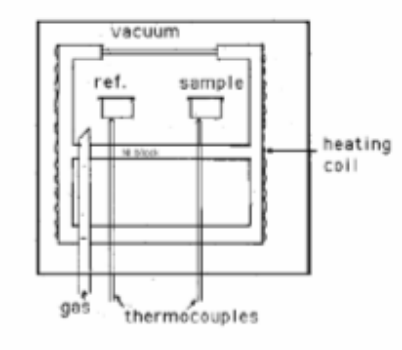

Figure B.11: Schematic illustration of a DTA cell [69].

For the thermal analysis of the samples synthesized in this research, Seiko SSC/5200 DTA/TG instrument was used. Aluminum sample holders were used for measurements and 15 mg sample was heated up to 600 ^{0}C with rate 5 ^{0}C. Empty aluminum holder was considered as references. Additionally, air, nitrogen, and, oxygen were used as an inert atmosphere.

B.5.2 Interpretation and Presentation of Data

At the end of a measurement, evaluation or absorption of heat following physical or chemical changes in sample can be observed as peaks. The area of peak; A, can be calculated according to formula b.7.

$$A = \frac{mq}{gK} \text{ (b.7)}$$

where;

m= sample mass

q=enthalpy change per unit mass

g= shape factor

K= thermal conductivity of sample

This A value is related to enthalpy changes in the sample. If the sample is porous, compacted or heaped, the gas filling the porous can change the thermal conductivity of the atmosphere surrounding the DTA container and lead to large errors in the peak area. For improved the results, DTA instrument should be calibrated by measuring peak areas on standard samples over specified temperature range [69].

BIBLIOGRAPHY

[1] A. Joannis, C.R. Hebd. Seances Acad. Sci. 13 (1891) 795.

[2] Smyth, F. h. J. Am. Chem. Soc. 1917, 39, 1299.

[3] Kraus, C. A. J. Am. Electrochem. Soc. 1924, 45, 175.

[4] Zintl, E.; Goubeau, J., Dullenkopf, W. Z. Phys. Chem., Abt. A 1931, 154, 1.

[5] Zintl, E.; Harder, A. Z. Phys. Chem., Abt. A 1931, 154, 47.

[6] Zintl, E.; Dullenkopf, W. Z. Phys. Chem., Abt. B 1932, 16, 183.

[7] Hume-Rotery, W.; J. Inst. Metals, 1926, 35, 295.

[8] Grimm, H.O.; and Sommerfeld, A.; Z. Phys., 1926, 36, 36.

[9] Diehl, L.; Khodadadeh, K.; Kummer, D.; Strahle; J., chem. Ber. 109, 1976, 3404.

[10] Belin, C.H.E.; Corbett, D. J.; Cisar, A.; J. Am. Chem. Soc. 99, 1977, 7163.

[11] Mei, E.; Popov, A. I.; Dye, J. L.; J. Phys. Chem., 1977, 81, 1677.

[12] Quéneau, V.; Sevov, S.C. Angew. Chem. Int. Ed. Engl. 36, 1997, 1754.

[13] Schnering von H. G.; Baytinger, M.; Bolle, U.; Cabrera-Carillo, W.; Curda J.; Grin, Y.; Heimann, F.; Llanos, J.; Peters, K.; Schmeding, A.; Somer, M. Z. Anorg. Allg. Chem. 623, 1997, 1037.

[14] Quéneau, V.; Todorov, T.; Sevov, S.C. J. Am. Chem. Soc. 120, 1998, 3263.

[15] Somer M.; Cabrera-Carrillo, W.; Peters, E. M.; Peters, K.; Kaupp, M.; Schnering, von H.G. Z. Anorg. All. Chem. 624, 1998, 1915.

[16] Cabrera-Carrillo, W.; Gil, C. R.; Somer, M.; Persil, Ö.; Schnering von H.G. Z. Anorg. Allg. Chem. 2003, 629, 601.

[17] Schnering, Von H. G.; Nova Acta Leop. 1985, 59, 168.

[18] Gallmeir, J.; Schakfer, H.; Weiss, A.; Z. Naturforsch, 1969, 246, 665.

[19] Amor, A.; Cros, C.; Pouchard, M.; Jaussaud, N.; Bassat, J. M.; Villeneuve, G.; Duttine, M. ; Ménétrier, M. ; Reny, E. ; Solid State Sciences 2004, 6, 393.

[20] Schnering, Von H. G.; Schwarz, M.; Chang, H. J.; Peters, K.; Peters, M. E.; Nesper, R.; Z. Kristallogr. NCS, 2005, 220, 525.

[21] Böhne, B.; Guloy, A.; Tang, Z.; Schnelle, W.; Burkhardt, U.; Baitinger, M.; Grin, Y.; J. Am. Chem. Soc. 2007, 126, 17, 5349.

[22] Guloy, M. A.; Ramlau, R.; Tang, Z.; Schnelle, W.; Baytinger, M.; Grin, Y.; Nature, 2006, 443, 320.

[23] Zintl, E. Angew. Chem. 52, 1939, 1.

[24] Klemm, W. Proc. Chem. Soc. London 1959, 329.

[25] Wade, K. Adv. Inorg. Chem. Radiochem. 18, 1976, 1.

[26] Ugrinov, A. G. Dissertation, 2004, Notre Dame, India.

[27] Housecroft, C. E.; Sharpe, A. G.; Inorganic Chemistry, 2005, Pearson Education Limited.

[28] Schnering von H. G.; Baytinger, M.; Bolle, U.; Cabrera-Carillo, W.; Curda J.; Grin, Y.; Heimann, F.; Llanos, J.; Peters, K.; Schmeding, A.; Somer, M. Z. Anorg. Allg. Chem. 623, 1997, 1037.

[29] Corbett, J.D.; Edwards, P. A. J. Am. Chem. Soc. 99, 1977, 3313.

[30] Burns, R.; Corbett, J. D. Inorg. Chem. 24, 1985, 1489.

[31] Quéneau, V.; Sevov, S.C. Inorg. Chem. 1998, 37, 1358.

[32] Todorov, E.; Sevov, S.C. Inorg. Chem. 37, 1998, 3889.

[34] Fässler, T. F; Hoffmann, R. J. Chem. Soc. Dalton Trans. 1999, 3339.

[35] Krebs, B.; Mummert, M.; Brendel, C.; Journal of Less Common Metals, 1986, 116, 1, 159.

[36] Campbell, J.; Schrobilgen, G. J. Inorg. Chem. 36, 1997, 4078.

[37] Somer M.; Cabrera-Carrillo, W.; Peters, E. M.; Peters, K.; Kaupp, M.; Schnering, von H.G. Z. Anorg. All. Chem. 625, 1999, 37.

[38] Edwars, P. A.; Corbett, J. D. Inorg. Chem. 16, 1977, 903.

[39] Belin, C. H. E.; Corbett, D. J.; Alan, C. J. Am. Chem. Soc. 1977, 99, 7163.

[40] Belin, C.; Mercier, H.; Angilella, V. New J. Chem. 1991, 15, 931-938.

[41] Fässler, T. F.; Hunziker, M. Inorg. Chem. 1994, 33, 5380-5381.

[42] Burns, C. R.; Corbett, D. J. J. Am. Chem. Soc. 1982, 104, 2804.

[43] Fässler, F. T.; Coordination Chemistry Reviews, 2001, 215, 347.

[44] Xu, L.; Sevov, C. S. J. Am. Chem. Soc. 1999, 121, 9245.

[45] Nienhaus, A.; Hoffmann, S. D.; Fässler, T. F. Z. Anorg. Allg. Chem. 2006, 632, 1752.

[46] Schentrunk, C.; Daniels, J.; Somer, M.; Carrillo- Cabrera, W.; Korber, N.; Z. Für Natur. B, 2005, 60, 277.

[47] Ugrinov, A.; Sevov, S. C.; J. Am. Chem. Soc. 2002, 124, 10990.

[48] Ugrinov, A.; Sevov, S. C.; Inorg. Chem. 2003, 42, 19, 5789.

[49] Yong, L.; Hoffmann, D. S.; Fässler, T. F. Z. Anorg. Chem. 2005, 631, 1149.

[50] Yong, L.; Hoffmann, D. S.; Fässler, T. F. Z. Anorg. Chem. 2004, 630, 1977.

[51] Downie, C.; Tang, Z.; Guloy, M. A. Angew. Chem. Int. Ed. 2000, 39, 2.

[52] Von Schnering, H. G.; Llanos, J.; Chang, J. H.; Peters, K.; Peters, E. M.; Nesper, R.; Zeitschrift für Kristallographie, 2005, 220, 3, 324.

[53] Banwell, N. C and McCash M. E.; Fundementals of molecular spectroscopy (fourth edition).

[54] Bombach, R.; Scherrer, P.; Ercoftac Summer school (notes), march 2002, Zurich, Switzerland.

[55] P. Matousek, I.P. Clark, E.R.C. Draper, M.D. Morris, A.E. Goodship, N. Everall, M. Towrie, W.F. Finney, A.W. Parker, Subsurface Probing in Diffusely Scattering Media using Spatially Offset Raman Spectroscopy, Appl. Spectrosc. 59 (2005) 393.

[56] Mark, C.; Fundamentals of Light Sources and Lasers, Wiley 2004.

[57] Gloveboxes, Innovative Technology, Inc., USA.

[58]Michette, A.; Pfauntsch, S.; X-rays; the first hundered years, John Wiley&Sons, 1996.

[59] Bragg, W. L.; The Diffraction of Short Electromagnetic Waves by a Crystal, Proceedings of the Cambridge Philosophical Society, 17 (1912), 43–57.

[60] Pecharsky, V. K.; Zavalij, P. Y.; Fundementals of powder diffraction and structural characterization of materials, 2005.

[61] Clegs, W.; Crystal Structure determination, 1998, Oxford, New York: Oxford University press.

[62] Haris, K. D. M.; Tremayne, M.; Kariuki, B. M.; Angew. Chem. Int. Ed. 2001, 40, 1626.

[63] Luger, P. Modern X-ray Analysis on Single Crystals, 1980, Berlin; New York.

[64] Farrugia, L. J.; Journal of Applied Crystallography, 1999, 32.

[65] Eaton, G. R.; Eaton, S. S.; Salikhov, K. M.; Foundations of Modern EPR, Singapore; River Edge, NJ: World Scientific, 1998.

[66] Weil, A. J.; Bolton, R. J.; Wertz, J. E.; Electron Paramagnetic Resonance, John Willey&sons, Inc. 1994.

[67] Graham, A. P.; VIII-Introduction to Electron Paramagnetic Resonance, BIOS481, Chapter 8, Rice University.

[68] Thurnauer, M.; Chemistry Division, Argonne National Labrotary, Chicago.

[69] Bhadeshia, H. K. D. H.; Metarial Science & Metallurgy, University of Cambrige.

Vita

Aslıhan Kırcalı was born in Istanbul, Turkey in 1982. She graduated form high school, Edirne Fen Lisesi in 1999. She received her B.S. degree from Department of Chemistry, Fatih University in 2004. In 2005, she started her study in the department of Material Science and Engineering, Koc University as a M.S. candidate. She will join the Department of Material Science and Engineering, Leipzig University to continue her PhD research.